University of Nebraska - Lincoln

DigitalCommons@University of Nebraska - Lincoln

NASA Publications

National Aeronautics and Space Administration

2011

The 2009 edition of the GEISA spectroscopic database

N. Jacquinet-Husson
Universite Pierre et Marie Curie (Paris VI)

L. Crepeau
Universite Pierre et Marie Curie (Paris VI)

R. Armante
Universite Pierre et Marie Curie (Paris VI)

C. Boutammine
Universite Pierre et Marie Curie (Paris VI)

A. D. Chedin
Universite Pierre et Marie Curie (Paris VI)

See next page for additional authors

Follow this and additional works at: https://digitalcommons.unl.edu/nasapub

Part of the Physical Sciences and Mathematics Commons

Authors

N. Jacquinet-Husson, L. Crepeau, R. Armante, C. Boutammine, A. D. Chedin, N.A. Scott, C. Crevoisier, V. Capelle, C. Boone, N. Poulet-Crovisier, A. Barbe, A. Campargue, D. Chris Benner, Y. Benilan, B. Bezard, V. Boudon, L.R Brown, L.H. Coudert, A. Coustenis, V. Dana, V.M. Devi, S. Fally, A. Fayt, J.-M. Flaud, A. Goldman, M. Herman, G.J. Harris, D. Jacquemart, A. Jolly, I. Kleiner, A. Kleinbohl, F. Kwabia-Tchana, N. Lavrentieva, N. Lacome, Li-Hong Xu, O.M. Lyulin, J.-Y. Mandin, A. Maki, S. Mikhailenko, C.E. Miller, T. Mishina, N. Moazzen-Ahmadi, H.S.P. Muller, A. Nikitin, J. Orphal, V. Perevalov, A. Perrin, D.T. Petkie, A. Predoi-Cross, C.P. Rinsland, J.J. Remedios, M. Rotger, M.A.H. Smith, K. Sung, S. Tashkun, J. Tennyson, R.A. Toth, A.-C. Vandaele, and J. Vander-Auwera
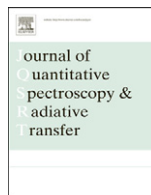
The 2009 edition of the GEISA spectroscopic database

N. Jacquinet-Husson [a,*], L. Crepeau [a], R. Armante [a], C. Boutammine [a], A. Chédin [a], N.A. Scott [a], C. Crevoisier [a], V. Capelle [a], C. Boone [b], N. Poulet-Crovisier [b], A. Barbe [c], A. Campargue [d], D. Chris Benner [e], Y. Benilan [f], B. Bézard [g], V. Boudon [h], L.R. Brown [i], L.H. Coudert [f], A. Coustenis [g], V. Dana [j], V.M. Devi [e], S. Fally [k], A. Fayt [l], J.-M. Flaud [f], A. Goldman [m], M. Herman [n], G.J. Harris [o], D. Jacquemart [p], A. Jolly [f], I. Kleiner [f], A. Kleinböhl [i], F. Kwabia-Tchana [p], N. Lavrentieva [q], N. Lacome [p], Li-Hong Xu [r], O.M. Lyulin [q], J.-Y. Mandin [j], A. Maki [s], S. Mikhailenko [q], C.E. Miller [i], T. Mishina [q], N. Moazzen-Ahmadi [t], H.S.P. Müller [u], A. Nikitin [q], J. Orphal [v], V. Perevalov [q], A. Perrin [f], D.T. Petkie [w], A. Predoi-Cross [x], C.P. Rinsland [y], J.J. Remedios [z], M. Rotger [c], M.A.H. Smith [y], K. Sung [i], S. Tashkun [q], J. Tennyson [o], R.A. Toth [i], A.-C. Vandaele [k], J. Vander Auwera [n]

[a] *Laboratoire de Météorologie Dynamique, UMR 8539, CNRS/IPSL, Université Pierre et Marie Curie, Ecole Polytechnique, 91128 Palaiseau, France*
[b] *Institut Pierre Simon Laplace, Université Pierre et Marie Curie, 75252 Paris, France*
[c] *Groupe de Spectrométrie Moléculaire et Atmosphérique, UMR 6089, CNRS, Université de Reims-Champagne-Ardenne, 51687 Reims, France*
[d] *Laboratoire de Spectrométrie Physique, Université Grenoble 1/CNRS, UMR 5588 LIPHY, 38402 Grenoble, France*
[e] *The College of William and Mary, Department of Physics, Williamsburg, VA 23187, USA*
[f] *Laboratoire Inter-Universitaire des Systèmes Atmosphériques, UMR 7583, CNRS, Universités Paris Diderot (Paris 7) et Paris EST-Créteil (UPEC), 94010 Créteil, France*
[g] *Laboratoire d'Etudes Spatiales et d'Instrumentation en Astrophysique, UMR 8109, CNRS, Universités Pierre et Marie Curie et Denis Diderot, Observatoire de Paris-Meudon, 92195 Meudon, France*
[h] *Laboratoire Interdisciplinaire Carnot de Bourgogne, UMR 5209, CNRS, Université de Bourgogne, 21078 Dijon, France*
[i] *Jet Propulsion Laboratory, California Institute of Technology, Pasadena, CA 91109, USA*
[j] *Laboratoire de Physique Moléculaire pour l'Atmosphère et l'Astrophysique, UMR 7092, CNRS, Université Pierre et Marie Curie, 75252 Paris, France*
[k] *Institut d'Aéronomie Spatiale de Belgique, B-1180 Brussels, Belgium*
[l] *Université Catholique de Louvain, Laboratoire de Spectroscopie Moléculaire, B-1348 Louvain-la-Neuve, Belgium*
[m] *University of Denver, Department of Physics, Denver, CO 80208, USA*
[n] *Université Libre de Bruxelles, Service de Chimie Quantique et Photophysique, C.P. 160/09, B-1050 Brussels, Belgium*
[o] *University College London, Department of Physics and Astronomy, London WC1E 6BT, UK*
[p] *Laboratoire de Dynamique, Interactions et Réactivité, UMR 7075, CNRS, Université Pierre et Marie Curie, 75252 Paris, France*
[q] *VE Zuev Institute of Atmospheric Optics, 634021 Tomsk, Russian Federation*
[r] *Centre for Laser, Atomic, and Molecular Sciences (CLAMS), Department of Physics, University of New Brunswick, Saint John, NB, Canada E2L 4L5*
[s] *15012 24th Ave. S.E., Mill Creek, WA 98012, USA*
[t] *Department of Physics and Astronomy, University of Calgary, Calgary, Alberta, Canada T2N 1N4*
[u] *I. Physikalisches Institut, Universität zu Köln, 50937 Köln, Germany*
[v] *Institute for Meteorology and Climate Research Research Centre Karlsruhe/University (KIT), 76021 Karlsruhe, Germany*
[w] *Department of Physics, Wright State University, Dayton, OH 45435, USA*
[x] *Department of Physics and Astronomy, University of Lethbridge, Lethbridge, AB, Canada T1K 3M4*
[y] *NASA Langley Research Center, Science Directorate, Hampton, VA 23681, USA*
[z] *EOS, Space Research Centre, Department of Physics and Astronomy, University of Leicester, Leicester LE1 7RH, UK*

* Corresponding author. Tel.: +33 169335162; fax: +33 169335218.
  E-mail address: jacquinet@lmd.polytechnique.fr (N. Jacquinet-Husson).

ARTICLE INFO

ABSTRACT

The updated 2009 edition of the spectroscopic database GEISA (Gestion et Etude des Informations Spectroscopiques Atmosphériques; Management and Study of Atmospheric Spectroscopic Information) is described in this paper. GEISA is a computer-accessible system comprising three independent sub-databases devoted, respectively, to: line parameters, infrared and ultraviolet/visible absorption cross-sections, microphysical and optical properties of atmospheric aerosols. In this edition, 50 molecules are involved in the line parameters sub-database, including 111 isotopologues, for a total of 3,807,997 entries, in the spectral range from 10^{-6} to $35,877.031 \, cm^{-1}$.

The successful performances of the new generation of hyperspectral sounders depend ultimately on the accuracy to which the spectroscopic parameters of the optically active atmospheric gases are known, since they constitute an essential input to the forward radiative transfer models that are used to interpret their observations. Currently, GEISA is involved in activities related to the assessment of the capabilities of IASI (Infrared Atmospheric Sounding Interferometer; http://smsc.cnes.fr/IASI/index.htm) on board the METOP European satellite through the GEISA/IASI database derived from GEISA. Since the Metop-A (http://www.eumetsat.int) launch (19 October 2006), GEISA is the reference spectroscopic database for the validation of the level-1 IASI data. Also, GEISA is involved in planetary research, i.e., modeling of Titan's atmosphere, in the comparison with observations performed by Voyager, or by ground-based telescopes, and by the instruments on board the Cassini–Huygens mission.

GEISA, continuously developed and maintained at LMD (Laboratoire de Météorologie Dynamique, France) since 1976, is implemented on the IPSL/CNRS (France) "Ether" Products and Services Centre WEB site (http://ether.ipsl.jussieu.fr), where all archived spectroscopic data can be handled through general and user friendly associated management software facilities. More than 350 researchers are registered for on line use of GEISA.

1. Introduction[1]

Spectroscopic remote sensing is an indispensable tool of modern meteorology. It is used to investigate climate change and provide an improved understanding of the different phenomena driving an atmospheric system in order to predict its past and future evolution. In particular, spectrally highly resolved radiances measured by powerful observational techniques such as ground-, aircraft-, balloon-, or satellite-based sensors enable global monitoring of atmospheres, provide a wealth of information about its actual state. The corresponding sensors have been improved significantly in recent years. Currently, there are many satellite-based instruments recording high quality spectra in order to understand the atmospheric state in great detail. Planetary examples include the recent Mars Express (http://www.esa.int/SPECIALS/Mars_Express/index.html), Venus Express (http://www.esa.int/esaMI/Venus_Express/) and Cassini–Huygens missions (http://www.esa.int/SPECIALS/Cassini-Huygens/index.html), studying the terrestrial planets and Jupiter, Saturn and Titan, respectively. Numerous space-based missions continually provide a very large number of spectral observations which produce new revelations in planetology.

For remote sensing of astronomical objects, an essential prerequisite is high accuracy forward radiative transfer modeling. This in turn requires extensive knowledge of both the fundamental spectroscopic parameters of atmospheric constituents and the equations governing the propagation of radiation through the atmosphere. Numerous physical phenomenon that influence the radiative transfer of a planet can be discerned and often measured from the variation of specific spectral features. As a consequence, spectroscopy is at the root of modern planetology, enabling us to determine the physical properties of planets remotely. Generally, forward models used in such studies are generated from line-by-line codes. Their accuracy is affected in many ways, and uncertainty in the spectroscopic information is one of the greatest impacts.

During second half of the 20th century, the synergy between the simultaneous development of new technologies (high speed processing with computers, high-resolution laboratory facilities, quantum-mechanical treatment in theoretical spectroscopy, etc.), provided the means to interpret a multitude of long-path atmospheric transmissions by performing radiance calculations for numerous scenarios. As a result, the first standardized spectroscopic database, the so-called "AFGL tape", oriented towards the Earth's atmosphere, was initiated in 1973, at Air Force Geophysics Laboratory USA, by McClatchey et al. [1] and Garing and McClatchey [2]. This early database was limited to the strongest infrared absorbers (H_2O, CO_2, O_3, N_2O, CO, CH_4, and O_2) in the terrestrial atmosphere. It contained approximately 100,000 transitions.

In 1976, the ARA group at LMD (http://ara.abct.lmd.polytechnique.fr) initiated a similar effort with the development of GEISA [3–8]. The initial emphasis of GEISA and HITRAN varied somewhat because HITRAN was focused on the terrestrial atmosphere while GEISA was oriented towards planetary atmospheres (in particular to support the Voyager mission to the giant planets). The GEISA archive included the

---

[1] Acronyms used in the text are documented in Appendix A.

same seven atmospheric absorbers as in HITRAN, with a dozen additional species such as: NH_3, PH_3, C_2H_4, GeH_4, C_3H_8, C_2H_2, HC_3N, $HCOOH$, C_3H_4, as well as molecules such as: NO, SO_2, NO_2. There are other notable differences:

- a specific major initial task of GEISA has been to develop software so that users of the database could easily perform various kinds of extractions for their own applications in atmospheric physics and molecular spectroscopy;
- since the very first edition of GEISA, any isotopologue of a species having symmetry properties different from that of the main isotopologue (e.g., CH_3D and CH_4, C_2HD and C_2H_2) was entered as an independent molecular species; its line intensities were given for a 100% sample rather than scaling by standard isotopic abundances (as for $^{12}CH_4$ and $^{13}CH_4$).

The ARA group has continued to develop and maintain GEISA for over three decades, responding to incorporate new species and improve the completeness and accuracies of the spectroscopic parameters. Since quality of its reference information strongly impacts applications of planetary radiative transfer, there is an acute and constant demand for validated, operational and interactive public spectroscopic databases that are comprehensive and trustworthy. In its present structure, GEISA is a computer accessible database system, which, as described previously [5–9], delivers the necessary data to interpret the terrestrial and planetary atmospheric observations. GEISA comprises three independent sub-databases devoted, respectively, to (a) line parameters, (b) infrared and ultraviolet absorption cross-sections, and (c) microphysical and optical properties of atmospheric aerosols. It is used on-line by more than 300 laboratories for studies in atmospheric physics, astronomy and astrophysics, and planetology.

The role of molecular spectroscopy in modern atmospheric research has entered a new phase with the advent of highly sophisticated spectroscopic instruments and computers. The launch of high spectral resolution vertical infrared sounders like AIRS (http://www-airs.jpl.nasa.gov/) on board EOS (http://eospso.gsfc.nasa.gov/)-Aqua (http://aqua.nasa.gov/) since May 2002, or IASI (http://smsc.cnes.fr/IASI/index.htm) on board the European polar satellite Metop-A (http://www.eumetsat.int/Home/Main/Satellites/Metop/index.htm?l=en; http://www.esa.int/export/esaLP/LPMetop.html) since October 2006, have opened promising perspectives for remote sensing applications as the improvement of temperature and water vapor profile retrieval, cloud and surface characteristics retrieval, or retrievals of greenhouse gases (CO_2 and CH_4 for example) and of various chemical species. The January 2009 launch of the GOSAT satellite (http://www.gosat.nies.go.jp/index_e.html) is another noteworthy event. The main aim of this mission is to measure the column amounts and profiles of the concentration of CO_2 and CH_4 over the globe.

Since the launch of Metop-A, GEISA has been declared as the reference basis by the international working group (ISSWG) in charge of the IASI hyperspectral sounder, through the GEISA/IASI database [10] which was derived from GEISA, as a sub-set for selected molecules, within the 599–3001 cm^{-1} spectral range. GEISA/IASI is currently and routinely used for the validation of the level-1 IASI data, using the 4A radiative transfer model [11,12]; 4A/LMD; 4A/OP co-developed by LMD and Noveltis, http://www.noveltis.fr/, with the support of CNES).

The contents of each of the three sections of GEISA in its 2009 edition (hereafter GEISA-09) will be described in this paper. Recommendations on the quality of spectroscopic line parameters required (from the conclusions of experts involved in atmospheric and planetary science) will also be summarized.

GEISA is freely accessible from Ether, the CNRS/CNES/IPSL Products and Services Center, website (http://ether.ipsl.jussieu.fr/).

It should be noted that other well known spectroscopic data compilations are available including:

- HITRAN (former "AFGL tape") for atmospheric and planetary remote sensing (see Ref. [13] for 2004 and 2008 Editions);
- MIPAS [14] specifically tied to satellite experiments in the Earth's atmosphere;
- BEAMCAT, for millimeter and submillimeter wave propagation in the Earth's atmosphere [15];
- the JPL Catalog of microwave to sub-millimeter transitions [16] which contains, for the most part, rotational transitions of a few hundred molecules which can or may be observed in the atmospheres of Earth or other planets to molecules occurring in the Inter StellarMedium (ISM) or in CircumStellar Envelopes (CSE) of late type stars. A small, but probably increasing number of entries contain infrared transitions;
- the CDMS Catalog [17] which also contains mostly rotational transitions of molecules important for the ISM or CDEs. Naturally, some of the molecules are also of relevance for Earth's atmosphere or that of other planets. Furthermore, a number of entries deal with infrared transitions of such molecules. Selected examples are low-lying vibrational modes of C_3 and C_3O_2 or selected bands of CH^+, C_2H, or CH_3CCH.

2. Line parameters GEISA-09 sub-database description

2.1. General overview

In the significant 2009 update described below, the GEISA-09 sub-database of line parameters archives, at the reference temperature of 296 K, the spectral properties of 50 molecular species (111 isotopologues) corresponding to a total of 3,807,997 entries in the spectral range from 10^{-6} to 35,877.031 cm^{-1} (10^{10} to 0.28 μm). This represents an increase of 8 molecular species, 14 isotopologues and 2,139,626 entries since the GEISA-03 [8,9] edition. This 28% increase in entries is mainly due to: extension of spectral ranges (i.e., CO_2, N_2O, etc.), addition of new vibrational bands and isotopologues (i.e., SO_2, etc.), more sophisticated theoretical and/or experimental determination of the spectroscopic parameters (i.e., CO_2, HNO_3, H_2CO, C_2H_2, HCN, C_4H_2, SF_6, etc.), and new archived molecular species (see Table 1 for details). The newly archived molecular species

Table 1

Contents of the GEISA-09 sub-database on line parameters. Details per molecule of the 2009 evolution of GEISA content since its 2003 edition. Reference temperature is 296 K.

Mol.	ID	GEISA-03				GEISA-09				Refs.
		Spectral range (cm^{-1})	# lines	Intensity exponent		Spectral range (cm^{-1})	# lines	Intensity exponent		
				Max.	Min.			Max.	Min.	
H_2O	1	0.007–22,656.465	58,726	−18	−31	0.007–25,232.004	67,789	−18	−33	[20–31]
CO_2	2	436.123–9648.007	76,826	−18	−41	5.891–12,784.053	413,619	−18	−42	[32–69]
O_3	3	0.026–4060.783	319,248	−19	−30	0.026–6395.379	389,378	−19	−30	[70–97]
N_2O	4	0.838–5131.249	26,681	−17	−27	0.838–7796.633	50,633	−17	−25	[98–102]
CO	5	3.414–8464.882	13,515	−18	−77	3.414–8464.882	13,515	−18	−77	No update
CH_4	6	0.010–9199.285	216,196	−18	−33	0.001–9199.284	240,991	−18	−38	[103–126]
O_2	7	10^{-6}–15,927.806	6290	−23	−50	10^{-6}–15,927.230	6428	−23	−50	[127–137]
NO	8	3×10^{-5}–9273.214	99,123	−19	−84	10^{-6}––9273.214	105,079	−19	−94	[133–139]
SO_2	9	0.017–4092.948	38,853	−19	−27	0.017–4092.948	68,728	−19	−28	[140–166]
NO_2	10	0.498–3074.366	104,224	−18	−27	0.498–3074.152	104,223	−18	−27	[167–168]
NH_3	11	0.058–5294.502	29,082	−18	−38	0.058–5294.501	29,082	−18	−38	[169–170]
PH_3	12	17.805–2478.765	11,740	−18	−27	17.805–3601.652	20,421	−18	−27	[171–178]
HNO_3	13	0.035–1769.982	171,504	−19	−26	0.012–1769.982	669,988	−19	−27	[179–195]
OH	14	0.005–35,877.030	42,866	−16	−84	0.005–35,877.031	42,866	−16	−84	No update
HF	15	41.110–11,535.570	107	−16	−25	41.111–11,535.570	107	−16	−25	No update
HCl	16	20.240–13,457.841	533	−18	−25	20.240–13,457.841	533	−18	−25	No update
HBR	17	16.231–9758.565	1294	−18	−32	16.231–9758.564	1294	−18	−32	No update
HI	18	12.509–8487.305	806	−19	−29	12.509–8487.305	806	−19	−29	No update
CLO	19	0.015–1207.639	7230	−20	−29	0.015–1207.639	7230	−20	−29	No update
OCS	20	0.381–4118.004	24,922	−17	−27	0.381–4199.671	33,809	−17	−27	[196–210]
H_2CO	21	3×10^{-6}–2998.527	2701	−19	−37	3×10^{-6}–3099.958	37,050	−19	−37	[211–216]
C_2H_6	22	725.603–2977.926	14,981	−20	−27	706.601–3000.486	27,644	−20	−29	[217–236]
CH_3D	23	7.760–3306.810	35,518	−22	−29	7.7602–6510.326	49,237	−22	−29	[237–245]
C_2H_2	24	604.774–4225.435	3115	−17	−26	604.774–9889.038	11,340	−17	−27	[246–255]
C_2H_4	25	701.203–3242.172	12,978	−19	−25	701.203–3242.172	18,378	−19	−36	[256–260]
GEH_4	26	1937.37–2224.570	824	−18	−21	1937.371–224.570	824	−18	−21	No update
HCN	27	2.870–18,407.973	2550	−18	−27	0.006–17,581.010	82,042	−18	−33	[261–292]
C_3H_8	28	700.015–799.930	8983	−21	−23	700.015–799.930	8983	−21	−23	[293–298]
C_2N_2	29	203.955–2181.690	2577	−19	−23	203.955–2181.690	2577	−19	−23	[299–301]
C_4H_2	30	190.588–654.425	1405	−19	−23	191.635–730.235	119,480	−18	−23	[302–315]
HC_3N	31	474.293–690.860	2027	−19	−23	463.604–759.989	179,347	−19	−23	[316–319]
$HOCl$	32	0.0236–3799.682	17,862	−19	−27	0.0236–3799.682	17,862	−19	−27	No update
N_2	33	1992.63–2625.497	120	−27	−33	1992.63–2625.497	120	−27	−33	[320–322]
CH_3Cl	34	674.143–3172.927	18,344	−19	−31	674.143–3172.927	18,344	−19	−31	[323–324]
H_2O_2	35	0.043–1499.486	100,781	−19	−28	0.043–1730.371	126,983	−19	−28	[325–327]
H_2S	36	2.985–4256.547	20,788	−18	−25	2.985–4256.547	20,788	−18	−25	[328–331]
$HCOOH$	37	1060.96–1161.251	3388	−19	−21	10.018–1889.334	62,684	−19	−25	[332–342]
COF_2	38	725.005–2001.348	83,750	−19	−23	725.005–2001.348	83,750	−19	−23	No update
SF_6	39	940.424–952.238	11,520	−19	−21	588.488–975.787	92,398	−19	−23	[343–348]
C_3H_4	40	290.274–359.995	3390	−20	−22	288.913–673.479	19,001	−19	−23	[349–357]
HO_2	41	0.173–3675.818	38,804	−19	−25	0.173–3675.819	38,804	−19	−25	No update
$ClONO_2$	42	763.641–792.488	32,199	−21	−24	0.636–797.741	356,899	−21	−27	[358–362]
CH_3BR	43	–				794.403–1705.612	36,911	−20	−26	[363–377]
CH_3OH	44	–				0.019–1407.206	19,897	−19	−34	[378–389]
NO^+	45	–				1634.83–2530.462	1206	−18	−80	[390–391]
HNC	46	–				0.217–4814.904	5619	−17	−24	[392–401]
C_6H_6	47	–				642.427–705.262	9797	−20	−23	[402–405]
C_2HD	48	–				416.785–3421.864	15,512	−22	−28	[406–409]
CF_4	49	–				594.581–1312.647	60,033	−19	−23	[410–420]
CH_3CN	50	–				890.052–1650.000	171,172	−19	−37	[428–432]
			Total # lines: 1,668,371				Total # lines: 3,807,997			

Note: "No update" in the Refs. column indicates that the contents in GEISA-09 and GEISA-03 are identical.

are: CH_3Br, CH_3OH, NO^+, HNC, C_6H_6, C_2HD, CF_4, and CH_3CN. As stated above, the molecules included in GEISA-09 (and since the database creation), are constituents, not only of the atmospheres of Earth (major permanent and trace molecules), but also of other planets (such as: C_2H_4, GeH_4, C_3H_8, C_2N_2, C_4H_2, HC_3N, H_2S, HCOOH and C_3H_4, mainly for giant planets). The evolution of the GEISA line parameters sub-database, since 1975, is presented in Fig. 1.

The parameters of each spectral line or molecular vibrational–rotational transition are stored in the new "standard format" for GEISA and GEISA/IASI as described in Ref. [10], with some newly introduced technical
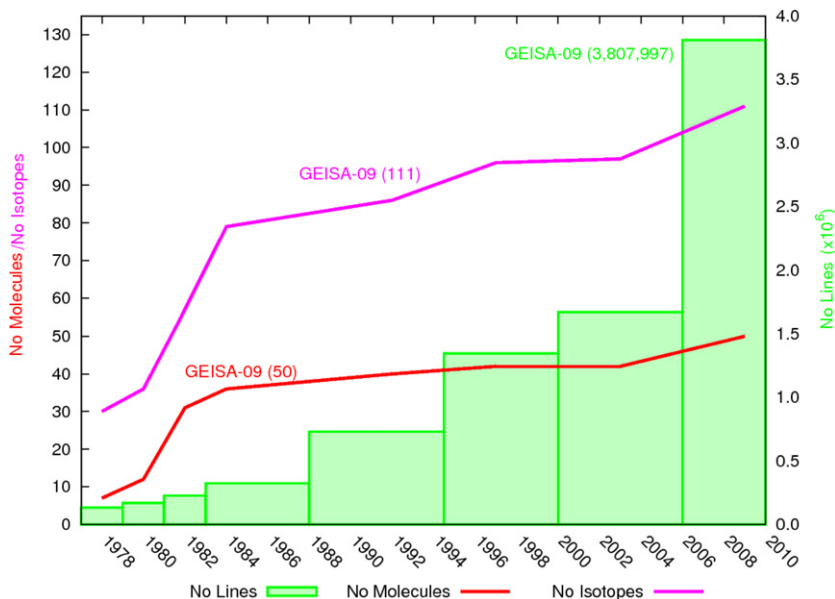
Fig. 1. Evolution of the GEISA line parameters sub-database since 1975. The year identifications are on the *X*-axis. The evolution of the number of lines is displayed as histograms (green color) with corresponding scale given on the right *Y*-axis. The total number of molecules and isotopes, included in each atlas, are color coded, as red and purple curves, respectively, with corresponding scale on the left *Y*-axis.

modifications, i.e., extended format field for quantum identifications for the lower and upper states of the transition, for self-broadened half-width and air-induced pressure shift of the line transition, corresponding, respectively, to fields of format symbols: E_i ($i=1$–4), M and N; former fields identified as P (accuracy indices for wavenumber, intensity and half-width) and Q (indices for lookup of references for wavenumber, intensity and half-width) have been removed. See Appendix B for details.

Evolution of the contents of GEISA-09 since the 2003 edition of GEISA (hereafter GEISA-03) is summarized in Table 1. Individual GEISA-09 molecule names and their corresponding identification codes (ID codes defined for the GEISA management software) are in the first two columns of the Table. The following columns give successively for GEISA-03 and for GEISA-09: the spectral range (cm^{-1}), the number of entries, the exponents of the maximum and minimum intensity values (expressed in cm^{-1}/(molecule cm^{-2}) at 296 K), for each molecule, and finally the 2009 update references. The spectroscopic line parameters of 31 of the 42 molecules included in GEISA-03 have been updated. The parameters of 11 molecules, i.e., CO, OH, HF, HCl, HBr, HI, ClO, GeH_4, HOCl, COF_2, and HO_2, are kept unchanged as in GEISA-03. The details of the GEISA-09 sub-database on line parameters are given in Table 2. The items listed in columns 3–6 for each molecular species, given in column 1, are: the number of lines, the intensity average in cm molecule^{-1} (different expression for cm^{-1}/(molecule cm^{-2})), the average half-width at half-maximum (HWHM in cm^{-1} atm^{-1}), the present isotopologue identification codes (see Table 2 of Ref. [7] for isotopic species code identifications and complementary information, in Appendix C, for new isotopic and molecular species in GEISA-09); for each isotopic species listed in

column 6, are given in columns 7–11: the number of lines with associated minimum and maximum wavenumbers (cm^{-1}) and intensities (in cm molecule^{-1}).

Table 3 summarizes the differences between the GEISA-09 and the HITRAN 2008 (hereafter HITRAN-08) [13] databases in terms of the number of lines, bands, and isotopologues. An example of quantitative comparison between H_2O intensity values in GEISA-09 and HITRAN-08 is given in Fig. 2. In the spectral range 1400–2100 cm^{-1}, 5626 transitions with common quantum identification in both databases and with intensity values larger than 10^{-23} cm^{-1}/(molecule cm^{-2}), are involved in this comparison. One can notice that 8% of the strong lines (intensities greater or equal 10^{-20} cm^{-1}/(molecule cm^{-2})) exhibit differences greater that 5%. Evaluations of impact on atmospheric radiative transfer modeling, using HITRAN or GEISA, are presented, for instance, in Jacquinet-Husson et al. [8], Matricardi [18] Newman [19]. It may be noted that the previous updates of HITRAN and GEISA databases have been finalized at nearly the same time, and include very similar data sources for many molecules. Because of its origin, certain molecules, mainly related with planetary atmospheres (especially those of the giant planets) are specific to GEISA, such as: GeH_4, C_3H_8, C_2N_2, C_4H_2, C_3H_4, HC_3N, HNC, C_6H_6, and C_2HD. On the other hand, species HOBr and O are HITRAN specific, and in HITRAN CH_3D and C_2HD are considered isotopologues of methane and acetylene, but they are independent molecules in GEISA (see Sections 1 and 2). In Table 3, molecular species formulae are listed in column 1 and their identification codes for database managements in column 2. For each molecular species and for each data base, the number of bands, isotopologues and lines, are given in columns 3, 4 and 5, respectively. The related minimum and maximum of the spectral range

Table 2
The GEISA-09 sub-database on line parameters. Spectral and intensity ranges per molecule and isotopologue.

Mol.	ID	# lines	Intensity average (cm molecule^{-1})	HWHM average (cm^{-1} atm^{-1})	Isot. ID	# lines	Minimum wavenumber (cm^{-1})	Maximum wavenumber (cm^{-1})	Minimum intensity (cm molecule^{-1})	Maximum intensity (cm molecule^{-1})
H_2O	1	67,789	1.088×10^{-21}	0.0699	161	41,147	0.401	25,224.909	9.400×10^{-33}	2.654×10^{-18}
					81	8360	6.785	14,362.151	2.005×10^{-28}	5.390×10^{-21}
					171	5468	6.471	13,909.783	2.671×10^{-31}	9.830×10^{-22}
					162	11,980	0.007	13,900.444	1.240×10^{-32}	2.700×10^{-22}
					182	659	1173.772	3824.717	2.033×10^{-27}	5.083×10^{-26}
					172	175	1234.235	1598.7655	2.033×10^{-27}	9.319×10^{-27}
CO_2	2	413,619	2.724×10^{-22}	0.0704	626	165,181	345.936	12,784.052	1.000×10^{-30}	3.520×10^{-18}
					636	66,657	433.190	12,462.048	1.000×10^{-30}	3.740×10^{-20}
					628	110,136	5.891	11,422.648	1.000×10^{-30}	6.870×10^{-21}
					627	19,064	10.600	8270.099	1.000×10^{-30}	1.260×10^{-21}
					638	39,007	449.686	6744.160	1.000×10^{-30}	7.810×10^{-23}
					637	2741	580.856	6768.643	1.000×10^{-30}	1.400×10^{-23}
					828	10,045	484.297	8162.742	1.000×10^{-30}	1.330×10^{-23}
					728	493	626.438	5031.885	1.009×10^{-28}	2.500×10^{-24}
					838	295	2115.684	2276.481	4.870×10^{-42}	3.289×10^{-24}
O_3	3	38,9378	5.247×10^{-23}	0.0698	666	233,132	0.026	6395.379	3.904×10^{-29}	4.060×10^{-20}
					668	44,302	0.921	2767.874	4.692×10^{-28}	7.760×10^{-23}
					686	24,886	1.177	2739.289	9.970×10^{-29}	7.560×10^{-23}
					667	58,171	0.289	820.380	5.135×10^{-31}	5.356×10^{-25}
					676	28,887	0.213	822.795	1.433×10^{-31}	5.827×10^{-25}
N_2O	4	50,633	1.254×10^{-21}	0.0750	446	34,468	0.838	7796.633	1.016×10^{-29}	1.003×10^{-18}
					456	4466	5.028	5088.906	5.220×10^{-26}	3.423×10^{-21}
					546	4841	4.8580	4992.236	4.720×10^{-26}	3.513×10^{-21}
					448	4412	541.342	4672.579	1.614×10^{-25}	1.930×10^{-21}
					447	1778	549.367	4429.961	1.614×10^{-25}	4.017×10^{-22}
					458	105	2121.770	2203.983	1.673×10^{-25}	6.637×10^{-24}
					548	108	2144.997	2226.290	1.675×10^{-25}	7.631×10^{-24}
					556	455	1226.536	3415.768	1.642×10^{-25}	1.210×10^{-23}
CO	5	13,515	7.543×10^{-22}	0.0467	26	5908	3.53010	8464.882	7.880×10^{-78}	4.460×10^{-19}
					36	4768	3.414	8180.219	3.610×10^{-73}	4.690×10^{-21}
					27	748	3.714	6338.061	8.190×10^{-40}	1.600×10^{-22}
					28	770	3.629	6266.577	7.610×10^{-39}	8.320×10^{-22}
					37	580	1807.871	6196.551	1.030×10^{-36}	1.680×10^{-24}
					38	741	3.462	6123.294	2.580×10^{-40}	8.700×10^{-24}
CH_4	6	240,991	8.225×10^{-23}	0.0521	211	212,115	0.010	9155.326	1.117×10^{-39}	2.099×10^{-19}
					311	28,876	0.032	6069.084	4.936×10^{-34}	2.317×10^{-21}
O_2	7	6428	3.885×10^{-26}	0.0430	66	1431	0.000	15,927.230	9.808×10^{-51}	8.762×10^{-24}
					67	4326	0.000	14,536.515	8.513×10^{-51}	3.439×10^{-27}
					68	671	1.572	15,851.213	1.186×10^{-35}	1.727×10^{-26}
NO	8	105,079	4.625×10^{-23}	0.0477	46	100,902	0.000	9273.214	1.451×10^{-95}	1.188×10^{-20}
					48	679	1601.909	2038.846	4.190×10^{-28}	1.390×10^{-22}
					56	699	1609.585	2060.462	4.430×10^{-28}	2.550×10^{-22}
SO_2	9	68,728	5.850×10^{-22}	0.0090	626	57,963	0.017	4092.948	1.020×10^{-28}	4.851×10^{-20}
					646	10,765	1060.196	2500.400	4.980×10^{-24}	4.493×10^{-23}
NO_2	10	104,223	5.980×10^{-22}	0.0742	646	104,223	0.498	3074.153	4.240×10^{-28}	1.302×10^{-19}
NH_3	11	29,082	1.639×10^{-21}	0.0827	411	27,992	0.0582	5293.578	8.086×10^{-39}	4.585×10^{-19}
					511	1090	0.375	5179.786	5.460×10^{-29}	1.992×10^{-21}
PH_3	12	20,421	1.367×10^{-21}	0.0648	131	20,421	17.805	3601.652	1.849×10^{-28}	2.520×10^{-19}
HNO_3	13	669,988	1.768×10^{-22}	0.1048	146	669,988	0.012	1769.982	3.590×10^{-28}	3.130×10^{-20}
OH	14	42,866	2.806×10^{-20}	0.0440	61	42,711	0.005	35,877.030	1.500×10^{-85}	6.450×10^{-17}
					62	90	0.010	1.824	2.090×10^{-31}	5.780×10^{-29}
					81	65	0.053	6.325	1.200×10^{-30}	1.200×10^{-26}
HF	15	107	6.773×10^{-19}	0.0407	19	107	41.111	11,535.570	1.110×10^{-26}	1.440×10^{-17}
HCl	16	533	3.189×10^{-20}	0.0403	15	284	20.270	13,457.841	1.090×10^{-26}	5.030×10^{-19}
					17	249	20.240	10,994.721	1.010×10^{-26}	1.610×10^{-19}
HBr	17	1294	4.769×10^{-21}	0.0429	11	642	16.231	9757.189	1.528×10^{-32}	1.178×10^{-19}
					19	652	16.236	9758.565	9.450×10^{-33}	1.211×10^{-19}
HI	18	806	1.361×10^{-21}	0.0500	17	806	12.5094	8487.305	1.644×10^{-30}	3.423×10^{-20}
ClO	19	7230	1.605×10^{-22}	0.0873	56	3599	0.028	1207.639	1.520×10^{-29}	3.240×10^{-21}
					76	3631	0.015	1199.840	5.090×10^{-30}	1.030×10^{-21}

Table 2 (*continued*)

Mol.	ID	# lines	Intensity average (cm molecule^{-1})	HWHM average (cm^{-1} atm^{-1})	Isot. ID	# lines	Minimum wavenumber (cm^{-1})	Maximum wavenumber (cm^{-1})	Minimum intensity (cm molecule^{-1})	Maximum intensity (cm molecule^{-1})
OCS	20	33,809	3.436×10^{-21}	0.0894	622	19,130	0.406	4199.671	8.550×10^{-20}	1.220×10^{-18}
					624	6665	0.396	4165.233	6.400×10^{-27}	4.720×10^{-20}
					632	3243	0.404	4055.090	1.720×10^{-27}	1.200×10^{-20}
					623	2788	509.007	4163.069	4.678×10^{-26}	8.430×10^{-21}
					822	1626	0.380	4045.602	2.620×10^{-28}	2.090×10^{-21}
					634	357	1972.188	2032.039	1.010×10^{-23}	5.240×10^{-22}
H$_2$CO	21	37,050	1.175×10^{-21}	0.1079	126	36,120	0.000	3099.941	1.224×10^{-38}	7.436×10^{-20}
					128	367	0.034	47.486	1.392×10^{-30}	1.332×10^{-22}
					136	563	0.037	72.744	2.424×10^{-30}	7.548×10^{-22}
C$_2$H$_6$	22	28,439	1.600×10^{-22}	0.0670	226	22,402	706.601	3000.486	5.422×10^{-29}	3.210×10^{-20}
					236	6037	725.603	918.717	1.320×10^{-28}	1.770×10^{-23}
CH$_3$D	23	49,237	1.903×10^{-25}	0.0542	212	45,024	7.760	6510.326	5.677×10^{-30}	5.714×10^{-23}
					312	4213	959.394	1694.123	2.768×10^{-29}	1.398×10^{-25}
C$_2$H$_2$	24	11,340	3.877×10^{-21}	0.0720	221	11,055	604.774	9889.0377	4.425×10^{-28}	1.187×10^{-18}
					231	285	613.536	6588.935	3.820×10^{-26}	4.942×10^{-19}
C$_2$H$_4$	25	18,378	1.081×10^{-21}	0.0861	211	18,097	701.203	3177.173	2.764×10^{-37}	8.412×10^{-20}
					311	281	2947.832	3180.238	5.061×10^{-24}	1.618×10^{-21}
GeH$_4$	26	824	4.978×10^{-20}	0.1000	411	824	1937.371	2224.570	1.960×10^{-22}	3.680×10^{-19}
HCN	27	82,042	4.201×10^{-22}	0.1002	124	79,957	0.006	17,581.009	8.057×10^{-34}	7.010×10^{-19}
					125	791	2.870	3550.842	5.156×10^{-32}	2.468×10^{-21}
					134	791	2.880	3532.252	1.431×10^{-31}	3.785×10^{-21}
					224	503	2.415	2725.192	1.801×10^{-30}	7.317×10^{-23}
C$_3$H$_8$	28	8983	4.139×10^{-23}	0.0800	221	8983	700.015	799.930	1.583×10^{-24}	1.810×10^{-22}
C$_2$N$_2$	29	2577	1.885×10^{-21}	0.1023	224	2577	203.955	2181.690	3.130×10^{-24}	1.200×10^{-20}
C$_4$H$_2$	30	119,480	2.530×10^{-22}	0.0999	211	119,480	191.635	730.235	3.024×10^{-24}	1.435×10^{-19}
HC$_3$N	31	179,347	6.982×10^{-23}	0.0998	124	179,347	463.604	759.989	1.052×10^{-24}	4.040×10^{-20}
HOCl	32	17,862	1.867×10^{-21}	0.0689	165	9293	0.023	3799.249	1.650×10^{-27}	3.590×10^{-20}
					167	8569	0.349	3799.682	7.220×10^{-28}	1.140×10^{-20}
N$_2$	33	120	5.605×10^{-29}	0.0343	44	120	1992.628	2625.497	1.590×10^{-34}	3.548×10^{-28}
CH$_3$Cl	34	18,344	4.370×10^{-22}	0.0951	215	10,039	679.050	3172.927	9.051×10^{-32}	1.128×10^{-20}
					217	8305	674.143	3161.830	4.192×10^{-26}	3.542×10^{-21}
H$_2$O$_2$	35	126,983	4.622×10^{-22}	0.0999	166	126,983	0.043	1730.371	5.064×10^{-29}	5.582×10^{-20}
H$_2$S	36	20,788	2.992×10^{-22}	0.0740	121	12,330	2.985	4256.547	1.450×10^{-26}	1.360×10^{-19}
					131	3564	5.601	4098.234	2.020×10^{-26}	5.990×10^{-21}
					141	4894	5.615	4171.176	2.020×10^{-26}	1.080×10^{-21}
HCOOH	37	62,684	1.231×10^{-21}	0.1010	261	62,684	10.018	1889.334	3.966×10^{-26}	5.068×10^{-20}
COF$_2$	38	83,750	2.105×10^{-21}	0.0845	269	83,750	725.005	2001.348	4.740×10^{-24}	3.940×10^{-20}
SF$_6$	39	92,398	5.117×10^{-22}	0.5000	29	92,398	588.488	975.787	1.000×10^{-24}	1.453×10^{-20}
C$_3$H$_4$	40	19,001	6.338×10^{-22}	(−)	341	19,001	288.912	636.482	4.230×10^{-24}	1.550×10^{-20}
HO$_2$	41	38,804	6.847×10^{-22}	0.1070	166	38,804	0.173	3675.818	1.000×10^{-26}	2.744×10^{-20}
ClONO$_2$	42	356,899	7.958×10^{-24}	0.1404	564	206,861	0.636	797.741	7.547×10^{-28}	3.850×10^{-22}
					764	150,038	0.928	790.805	7.519×10^{-28}	1.260×10^{-22}
CH$_3$br	43	36,911	1.293×10^{-22}	0.0939	79	18,692	794.403	1705.612	9.970×10^{-27}	2.580×10^{-21}
					81	18,219	795.083	1696.896	1.000×10^{-26}	2.530×10^{-21}
CH$_3$oh	44	19,897	9.181×10^{-22}	0.1000	216	19,897	0.019	1407.205	8.826×10^{-35}	3.771×10^{-20}
NO+	45	1206	2.168×10^{-21}	0.0600	46	1206	1634.831	2530.462	6.121×10^{-81}	1.186×10^{-19}
HNC	46	5619	4.201×10^{-22}	0.1002	142	5619	0.217	4814.904	1.001×10^{-25}	1.164×10^{-18}
C$_6$H$_6$	47	9797	8.394×10^{-22}	0.1014	266	9797	642.427	705.262	4.070×10^{-24}	9.490×10^{-21}
C$_2$HD	48	15,512	4.843×10^{-25}	0.0680	122	15,512	416.785	3385.564	5.194×10^{-29}	3.219×10^{-23}
CF$_4$	49	60,033	1.377×10^{-21}	0.5000	291	60,033	594.581	1312.646	7.912×10^{-24}	4.717×10^{-20}
CH$_3$CN	50	17,172	2.688×10^{-22}	0.0792	234	17,172	890.052	1650.000	1.200×10^{-38}	3.824×10^{-20}
Total		3,807,997								

Note: (−) Missing data.

Table 3
Summary of differences for molecular species cataloged in the line parameter portion of GEISA-09 (G) and HITRAN 2008 (H) [13].

Mol.	Mol ID		# bands		# isot		# lines		Spectral coverage (cm^{-1})			
									Minimum wavenumber (cm^{-1})		Maximum wavenumber (cm^{-1})	
	G	H	G	H	G	H	G	H	G	H	G	H
H_2O	1	1	245	373	6	6	67,789	69,201	0.007	0.007	25,232.004	25,232.004
CO_2	2	2	3747	2832	9	9	413,619	314,919	5.891	0.736	12,784.052	12,784.052
O_3	3	3	162	218	5	5	389,378	409,686	0.026	0.026	6395.379	5786.118
N_2O	4	4	369	351	8	5	50,633	47,843	0.838	0.838	7796.633	7796.633
CO	5	5	104	47	6	6	13,515	4477	3.414	3.462	8464.882	8464.881
CH_4	6	6	138(§)	138	2	2(§)	240,991(§)	240,854(§)	0.001	0.001	9155.326	9155.326
O_2	7	7	19	19	3	3	6428	6428	0.000	0.000	15,927.230	15,927.230
NO	8	8	293	293	3	3	105,079	105,079	0.000	0.000	9273.214	9273.214
SO_2	9	9	17	13	2	2	68,728	58,250	0.017	0.017	4092.948	4092.948
NO_2	10	10	11	11	1	1	104,223	104,223	0.498	0.498	3074.153	3074.153
NH_3	11	11	78	78	2	2	29,082	29,084	0.058	0.058	5293.578	5293.578
PH_3	12	28	19	18	1	1	20,423	20,099	17.805	770.877	3600.701	3600.701
HNO_3	13	12	26	18	1	1	669,988	487,254	0.012	0.012	1769.982	1769.982
OH	14	13	245	221	3	3	42,866	31,976	0.005	0.003	35,877.030	19,267.804
HF	15	14	6	6	1	1	107	107	41.111	41.111	11,535.570	11,535.570
HCl	16	15	17	17	2	2	533	613	20.240	20.240	13,457.841	13,458.024
HBr	17	16	16	16	2	2	1293	1293	16.232	16.231	9758.312	9758.312
HI	18	17	9	9	1	1	806	806	12.509	12.509	8487.305	8487.305
ClO	19	18	12	16	2	2	7230	11,501	0.015	0.015	1207.639	1207.639
OCS	20	19	192	164	6	5	33,809	29,361	0.381	0.381	4199.671	4199.671
H_2CO	21	20	17	17	3	3	37,050	37,050	0.000	0.000	3099.958	3099.958
C_2H_6	22	27	6	6	2	2	28,439	28,439	706.601	706.601	3000.486	3000.486
CH_3D(§)	23	(§)	26	26	2	2(§)	49,237(§)	49,237(§)	7.760	7.760	6510.326	6510.326
C_2H_2	24	26	118	118	2	2	11,340	11,340	604.774	604.774	9889.038	9889.038
C_2H_4	25	38	12	12	2	2	18,378	18,378	701.203	701.203	3177.173	3177.173
GeH_4	26	ABS	1	ABS	1	ABS	824	ABS	1937.371	ABS	2224.570	ABS
HCN	27	23	775	30	4	3	82,042	4253	0.006	0.015	17,581.009	3423.927
C_3H_8	28	ABS	1	ABS	1	ABS	8983	ABS	700.015	ABS	799.930	ABS
C_2N_2	29	ABS	7	ABS	1	ABS	2577	ABS	203.955	ABS	2181.690	ABS
C_4H_2	30	ABS	1509	ABS	1	ABS	119,480	ABS	191.635	ABS	730.2352	ABS
HC_3N	31	ABS	3302	ABS	1	ABS	179,347	ABS	463.604	ABS	755.696	ABS
HOCl	32	21	6	8	2	2	17,862	16,276	0.024	1.081	3799.682	3799.682
N_2	33	22	1	1	1	1	120	120	1992.628	1992.628	2625.497	2625.497
CH_3Cl	34	24	14	83	2	2	18,344	196,171	674.143	0.873	3172.927	3172.927
H_2O_2	35	25	130	130	1	1	126,983	126,983	0.043	0.043	1730.371	1730.371
H_2S	36	31	30	30	3	3	20,788	20,788	2.985	2.985	4256.546	4256.547
HCOOH	37	32	8	8	1	1	62,684	62,684	10.018	10.018	1889.334	1889.334
COF_2	38	29	7	7	1	1	83,750	70,601	725.005	725.005	2001.348	2001.348
SF_6(∗)	39	30	6	3	1	1	92,398	2,889,065(∗)	588.488	580.000	975.788	996.000
C_3H_4	40	ABS	22	ABS	1	ABS	19,001	ABS	288.912	ABS	673.479	ABS
HO_2	41	33	4	4	1	1	38,804	38,804	0.173	0.173	3675.818	3675.818
$ClONO_2$(∗)	42	35	7	3	2	2	356,899	32,199(∗)	0.636	763.641	797.741	797.741
CH_3Br	43	40	6	6	2	2	36,911	36,911	794.403	794.403	1705.612	1705.612
CH_3OH	44	39	16	16	1	1	19,897	19,897	0.019	0.019	1407.205	1407.205
NO^+	45	36	6	6	1	1	1206	1206	1634.831	1634.831	2530.462	2530.462
HNC	46	ABS	84	ABS	1	ABS	5619	ABS	0.217	ABS	4814.904	ABS
C_6H_6	47	ABS	1	ABS	1	ABS	9797	ABS	642.427	ABS	705.262	ABS
C_2HD	48	ABS	348	ABS	1	ABS	15,512	ABS	416.785	ABS	3385.564	ABS
CF_4	49	42	5	5	1	1	60,033	60,033	594.581	594.581	1312.647	1312.647
CH_3CN	50	41	2	2	1	1	17,172	3572	890.052	890.052	1650.000	945.655
O	ABS	34	ABS	1	ABS	1	ABS	2	ABS	68.716	ABS	158.303
HOBr	ABS	37	ABS	1	ABS	2	ABS	4358	ABS	0.155	ABS	315.908

Note: ABS stands for a molecular species not included in the actual database (HITRAN or GEISA)
(§) CH$_3$D considered as an individual molecule in GEISA; but as an isotopologue of CH$_4$ in HITRAN.
(§) For HITRAN, column 5, sub-column "H", includes:

- for CH$_4$ (Mol. "6"), total # lines of isotopologues numbered "1" and "2" (coded "211" and"311" [7], respectively, in GEISA);
- for CH$_3$D (Mol. "23"), total # lines of CH4 isotopologues numbered "3" and "4" (coded "212" and"312" [7], respectively, in GEISA).

(∗) Molecule included in HITRAN 2008 supplemental line list.

(in cm^{-1}) are in the last four columns. The parameters for molecules SF$_6$, ClONO$_2$ and CF$_4$ have been archived in the supplemental line list of HITRAN-08 whereas they are kept in the main list of GEISA-09. The format of HITRAN-08 line parameters [13] is different from that of GEISA. Among the GEISA management software capabilities a program has
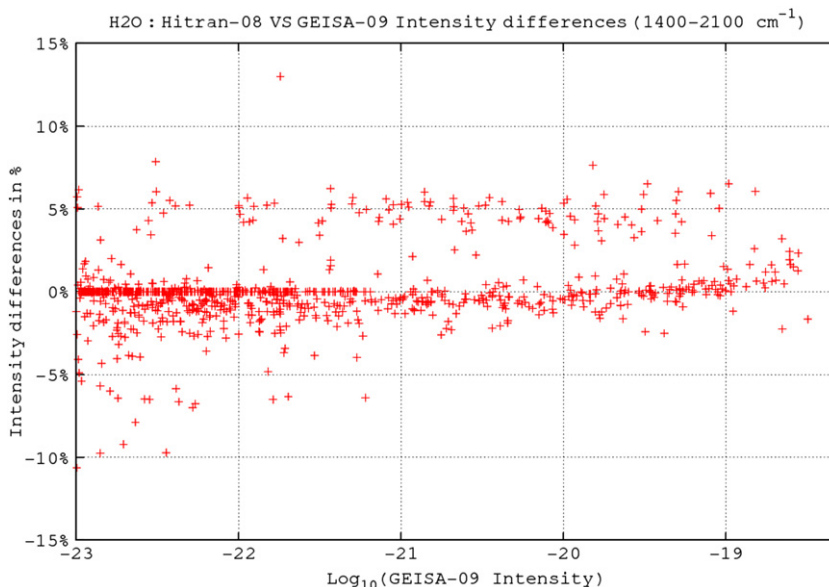
Fig. 2. Quantitative comparison between H_2O intensity values in GEISA-09 and HITRAN-08 [13]. Line intensity differences (GEISA-09 value minus HITRAN-08 value), in percent of GEISA-09 value, are on the *Y*-axis; the base 10 logarithm of GEISA-09 line intensity is on the *X*-axis. Data points are indicated by a read +.

been created which makes it possible to convert routinely the format of one database into the other database format, in their actual public release (GEISA-09 to HITRAN-08 format, or HITRAN-08 to GEISA-09 format). This has proven to be an efficient added capability for both database users especially for the purpose of easier identification and evaluation of the impact of spectroscopic content in specific applications (such as planetary atmosphere radiative transfer modeling).

2.2. Description of updates per individual molecules

2.2.1. H_2O (molecule 1)

The water molecule is of great interest both in terrestrial and in planetary studies, not the least because of its interference during ground-based observations.

The GEISA-09 H_2O update involves spectroscopic parameters from three different origins, i.e. in the spectral region 500–7973 cm^{-1}, the JPL data of Toth are available with their related description and references from the mark4sun website at http://mark4sun.jpl.nasa.gov/spec data.html. These data represent a total of 36,849 lines.

In the 10–2000 cm^{-1} spectral region, for the normal isotopologue $H_2^{16}O$, updated line parameters are computed using the results of Coudert et al. [20]. This update covers line position and line intensity analyses of data up to the second triad as well as line strength (or line intensity) measurements for ν_2 band transitions. Using the spectroscopic parameters from this reference and the theoretical approach of Lanquetin et al. [21], a line list of 5624 entries was generated with a line intensity cutoff of 10^{-27} cm^{-1}/ (molecule cm^{-2}). This calculation along with the line measurements of Ref. [20] revealed that experimental line intensity values for transitions belonging to the ν_2 band in the 1000–2000 cm^{-1} range were underestimated in previous measurements of Toth in 1998 [22], for the strongest
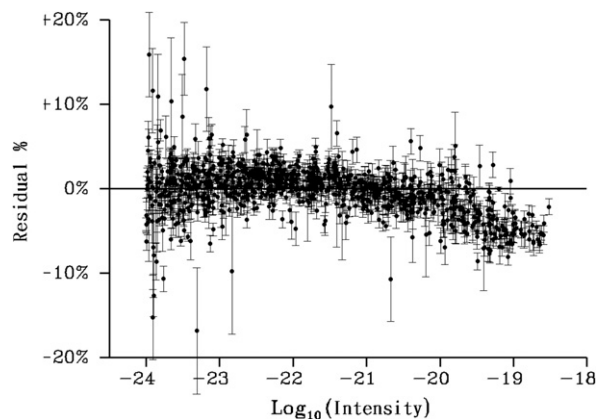
Fig. 3. Residuals of observed H_2O line intensities of Toth Ref. [22] minus those from Coudert et al. [20] (archived in GEISA-09). The *X*-axis is the base 10 logarithm of the observed line intensity in cm^{-1}/ (molecule cm^{-2}). The *Y*-axis corresponds to the residual in percent of the observed line intensities [22]. Each data point is indicated by a dot, error bars are also drawn. For clarity, the figure only displays the 967 strongest transitions from Ref. [22], belonging to the ν_2 band, with an intensity larger than 10^{-24} cm^{-1}/(molecule cm^{-2}).

transitions in this region. Fig. 3 shows the differences between the new intensity values from Coudert et al. [20] and those reported in Ref. [22]. In agreement with Ref. [20], this figure emphasizes that discrepancies of about -5% arise for strong transitions with an intensity on the order of 10^{-19} cm^{-1}/(molecule cm^{-2}).

For the spectral range 9500–14,500 cm^{-1}, line positions and intensities were taken from Tolchenov and Tennyson [23]. These data, representing 12,027 entries, came from a refit of room temperature Fourier transform absorption spectra of pure, natural abundance-water vapor by Schermaul et al. [24,25] recorded at path lengths

from 5 up to 800 m. These parameters have demonstrated [23] to give a more consistent representation of the underlying spectrum than previous studies. In this spectral region, line broadening and shifting due to N_2 and O_2 pressure effects are included from calculations which use a semi-empirical approach based on impact theory modified by introducing additional parameters to extend the use of empirical data [26]. This method was further developed by using anharmonic wavefunctions in the estimates of the line parameters. The main feature is the use of a complete set of high accuracy vibration–rotation dipole transition moments calculated for all possible transitions using wavefunctions determined from variational nuclear motion calculations and an *ab initio* dipole moment surface [27]. Full details of this approach are described in Ref. [28], the results of H_2O line parameters calculation and comparison with experimental data are presented in Refs. [29–31].

Fig. 4 exhibits the differences between H_2O lines, in the frequency range 9500–14,500 cm^{-1}, archived in GEISA-03, and those added in GEISA-09. The exponents of the intensity values (expressed in cm^{-1}/(molecule cm^{-2})) at 296 K) are on the Y-axis and the transition wavenumbers on the X-axis. Data included in each GEISA edition are identified by different colors: red triangles for GEISA-03 and blue crosses for GEISA-09.

In practice, the resulting total file the GEISA-09 update has been processed as follows: as a first step Toth's data were retained and replaced, for the main $H_2^{16}O$ isotopologue, by Coudert's data for lines with similar quantum identification; as a second step the file was finalized by adding the new data for the 9500–14,500 cm^{-1} spectral region. The GEISA-09 H_2O archive comprises 67,789 entries against 58,726 in GEISA-03.

2.2.2. CO_2 (molecule 2)

Carbon dioxide, like water, is an ubiquitous species observed in most of the solar system planets. To accommodate planetary applications, the GEISA-09 line list
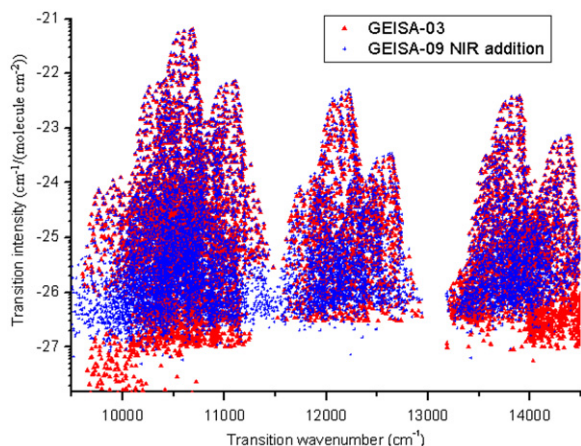
Fig. 4. H_2O intensity versus wavenumber for transitions present in GEISA-03 (▲ in red) and for those added in GEISA-09 (+ in blue), in the NIR spectral region.

update has been processed with 412,831 new transitions from seven isotopologues ($^{12}C^{16}O_2$, $^{13}C^{16}O_2$, $^{16}O^{12}C^{18}O$, $^{16}O^{12}C^{17}O$, $^{16}O^{13}C^{18}O$, $^{16}O^{13}C^{17}O$ and $^{12}C^{18}O_2$) between 5.9 and 12,784.0 cm^{-1}. It has to be noted that 788 transitions, of the two other isotopologues species: $^{13}C^{18}O_2$ and $^{17}O^{12}C^{18}O$, have been retained from GEISA-03 in the final GEISA-09 CO_2 line list. The increase in the number of transitions (from 76,826 to 413,619) compared to the GEISA-03 list (see Table 2) arises from lowering the minimum intensity to 10^{-30} cm^{-1}/(molecule cm^{-2}) at 296 K, in the seven isotopologues update entries, and merging the two compilations: the CDSD-296 databank [32] and partly the JPL near-infrared line list [33], as explained below.

The current version of the CDSD-296 databank is an extension and development of its previous 2003 version [34] which was used in GEISA/IASI [10] and GEISA-03. For the four most abundant isotopologues $^{12}C^{16}O_2$, $^{13}C^{16}O_2$, $^{16}O^{12}C^{18}O$ and $^{16}O^{12}C^{17}O$, the line positions and line intensities are calculated using new sets of effective Hamiltonian and effective dipole moment constants. These new constants are determined by including extensive new measurements in the fitting (see [35–59] and references therein); in particular, the data obtained at JPL and at the Joseph Fourier University (Grenoble, France) resulted in better accuracy and completeness for the near infrared calculations. Using Fourier transform spectroscopy experiments the first team has performed very precise measurements of both line positions and line intensities of nine isotopologues of carbon dioxide in the 4300–7000 cm^{-1} region [33,38,48,52,57]. The second team used highly sensitive CW-CRDS experiments and measured line positions and line intensities of a large number of lines including very weak lines as low as 10^{-29} cm^{-1}/(molecule cm^{-2}) of several isotopologues in the 5851–7045 cm^{-1} region [35,40,46,51,55,56,58,59]. The parameters obtained by including these weak lines belonging to high J values or to hot band transitions considerably improved the extrapolation properties of elaborated models of effective Hamiltonian and effective dipole moment operators. The theoretical approach used for global modeling of high resolution spectra of carbon dioxide is presented in Refs. [60–63]. Extension of the wavenumber region for the rare isotopologues was done using the sets of the effective dipole moment parameters belonging to the most abundant isotopologues. In order to meet the needs of the modern infrared sensors the intensity cutoff was lowered to 10^{-30} cm^{-1}/(molecule cm^{-2}) at 296 K. Because of this a large number of additional weak bands and weak lines corresponding to high values of the angular momentum quantum number of the strong bands became available in the new version of CDSD-296. The accuracy of the line parameters of these weak lines strongly relies on the extrapolation abilities of the models used. It was shown in Ref. [64] that the effective operator models, used for the generation of CDSD-296, provide reliable extrapolation properties.

On average, the residuals between CDSD calculated line positions and those observed are two times larger than measurement uncertainties. The CDSD calculated line intensities are practically always within their measurement uncertainties for all isotopologues. Air- and

self-broadening parameters were calculated using the equations from Rothman et al. [65], but the air-induced pressure shift parameter was set to zero throughout. The current atmospheric version of the databank is available on the web site of the IAO: ftp.iao.ru/pub/CDSD-2008/296.

Finally, it was determined that some of the intensities in the near infrared line list from Toth et al. were more accurate than the reanalyzed values and that the newer pressure broadening coefficients (widths and shifts) in the Toth et al. studies [66,67] better represented the measured spectra. Therefore, this line list, consisting initially of 28,530 entries, has been retained for the GEISA-09 update too, adopting the following process for its inclusion: first, 15,788 lines whose intensities were lower than 10^{-26} cm^{-1}/(molecule cm^{-2}) at 296 K for the two main isotopologues $^{12}C^{16}O_2$ and $^{13}C^{16}O_2$ and for all the isotopologues with intensities between 10^{-29} and 10^{-30} cm^{-1}/(molecule cm^{-2}) at 296 K (Brown private communication) were discarded; second, the 12,742 remaining lines were merged with the CDSD data, replacing them when the quantum identification was the same.

With this change, the choice of Toth et al. [66,67] for air-broadening, self-broadening and air-induced pressure shift of the line parameters is included in GEISA-09. These broadening parameters were replaced, for $^{12}C^{16}O_2$ lines with the same quantum numbers, by the results from the latest work of Predoi-Cross et al. [68] for the temperature dependences of air-broadened CO_2 widths, temperature dependence of air-induced pressure shift and temperature dependence of the self-broadened half-widths. The parameters from Predoi-Cross et al. were implemented for the entire line list when available. Since the database

was completed, a new effort to predict air-broadened pressure shifts has been undertaken by Hartmann [69] which will be considered for future database updates.

2.2.3. O_3 (molecule 3)

An update of the line positions and intensities has been made for the three main isotopologues of ozone, $^{16}O_3$, $^{16}O^{16}O^{18}O$, and $^{16}O^{18}O^{16}O$. For the main isotopologue $^{16}O_3$, the list of the 27 newly included bands (spectral range from 1632 to 4845 cm^{-1}) in GEISA-09 is given in the first column of Table 4 with associated spectral interval (cm^{-1}), number of lines and sum of line intensities, listed under columns 2–4, respectively. Table 5 lists the 28 updated bands with a similar display. These data cover the spectral range from 1613 to 4845 cm^{-1}. The line list is given with an intensity cutoff of 2×10^{-26} cm^{-1}/(molecule cm^{-2}) at 296 K for 100% $^{16}O_3$ abundance. These results are based on the analyses of the absorption spectra recorded in the GSMA laboratory using the FTS of the Champagne-Ardenne University (Reims, France) [70]. The calculations of the line positions were made using the Hamiltonian parameters for the lower states (0 0 0), (1 0 0) and (0 0 1) from Ref. [71], for the (0 1 0) state from Ref. [72] and for the (0 2 0) state from Ref. [73].

The line positions of three bands associated with the (0 3 1) upper state ($3\nu_2+\nu_3-2\nu_2$, $3\nu_2+\nu_3-\nu_2$, and $3\nu_2+\nu_3$) have been calculated using Hamiltonian parameters of Ref. [74]. The transition moment parameters of the $\nu_2+\nu_3$ band [75] were used for calculation of line intensities for the $3\nu_2+\nu_3-\nu_2$ band. The line intensities of two other bands were calculated with the transition moment parameters of Ref. [74].

Table 4
New ozone bands ($^{16}O_3$) in the GEISA-09 edition.

Band	Spectral region (cm^{-1})	Number of lines	Sum of line intensities (10^{-22} cm^{-1}/(molecule cm^{-2}))
031–020	1632–1711	1109	1.747
022–020	1921–2067	1046	0.740
121–020	1984–2079	1817	14.342
130–001	1991–2061	3	0.005
130–100	2040–2102	10	0.026
201–010	2281–2325	11	0.004
031–010	2333–2407	742	0.477
022–010	2603–2769	1629	1.740
131–020	2666–2741	899	0.834
031–000	3032–3111	689	0.420
130–000	3133–3249	384	0.126
022–000	3256–3511	1826	1.234
121–000	3286–3480	1764	7.481
131–010	3369–3440	910	0.694
113–100	3506–3566	466	0.197
014–001	3525–3605	992	1.316
113–010	3864–3968	1466	4.398
014–010	3875–3968	183	0.076
320–010	3888–4000	279	0.175
202–000	4034–4207	1387	1.108
131–000	4065–4145	714	0.460
301–000	4179–4264	1213	2.489
221–000	4444–4525	1066	1.041
014–000	4522–4700	1998	1.638
113–000	4562–4668	1599	8.814
320–000	4586–4700	587	0.435
212–000	4700–4845	924	0.415

Table 5
Updated ozone bands ($^{16}O_3$) in the GEISA-09 edition.

Band	Spectral region (cm^{-1})	Number of lines	Sum of line Intensities (10^{-21} cm^{-1}/(molecule cm^{-2}))
111–100	1613–1849	1271	0.269
012–001	1616–1826	1581	0.645
111–001	1629–1854	1557	0.131
012–100	1637–1706	85	0.004
210–100	1701–2051	1663	0.198
210–001	1719–2066	388	0.015
003–100	1848–2104	1920	1.183
003–001	1867–2098	2847	1.313
102–100	1869–2071	2206	0.429
012–010	1872–2120	3794	3.221
201–100	1888–2243	2831	10.979
201–001	1896–2289	2165	0.331
102–001	1901–2086	2965	15.787
111–010	1918–2220	3520	43.121
210–010	2005–2353	3050	0.844
300–001	2012–2313	1804	0.921
300–100	2021–2288	2508	0.475
003–010	2254–2396	1809	1.199
102–010	2270–2407	479	0.040
130–010	2424–2552	487	0.019
012–000	2590–3025	3886	3.293
111–000	2626–3050	3604	25.087
121–010	2678–2774	1851	1.658
210–000	2704–3156	3327	0.812
003–000	2907–3202	4512	141.143
201–000	2919–3273	2706	7.910
102–000	2925–3196	4646	13.774
300–000	2955–3398	2445	0.472

The line positions of six bands associated with the upper states (0 2 2) and (1 2 1) have been calculated using the Hamiltonian parameters for the upper states from Ref. [76]. The calculations of the line intensities of the $2\nu_2+2\nu_3$ and $\nu_1+2\nu_2+\nu_3$, $2\nu_2+2\nu_3-\nu_2$ and $\nu_1+2\nu_2+\nu_3-\nu_2$, $2\nu_2+2\nu_3-2\nu_2$ and $\nu_1+2\nu_2+\nu_3-2\nu_2$ bands were made with the transition moment parameters from Refs. [76–78], respectively.

The line positions of four bands of Table 4 and of all bands of Table 5 (except the band $\nu_1+2\nu_2+\nu_3-\nu_2$) associated with the upper states {(0 1 2), (1 1 1), (2 1 0), (0 0 3), (1 0 2), (2 0 1), (1 3 0), (3 0 0)} have been calculated using the Hamiltonian parameters for the upper states from Ref. [79]. The transition moment parameters for the cold bands (2590–3400 cm^{-1} spectral range) of these states are given in Ref. [79]. The calculations of the main part of the hot bands line intensities have been done with the transition moments given in Refs. [75,78,80]. The dipole moment transitions of the $2\nu_1+\nu_3-\nu_2$, $\nu_1+2\nu_3-\nu_2$ and $3\nu_3-\nu_1$ bands can be found at the web sites of the S&MPO system [81], similarly in Russia: http://smpo.iao.ru/1446x915/en/tran/par/1/8-2/; http://smpo.iao.ru/1446x915/en/tran/par/1/8-3/, or in France: http://ozone.univ-reims.fr/1446x915/en/tran/par/1/8-2/; http://ozone.univ-reims.fr/1446x915/en/tran/par/1/8-3/.

Three bands of the (1 3 1) upper state have been calculated with the Hamiltonian parameters [82] and the transition moment parameters [82,76,80] for the cold and hot bands, respectively.

The line positions of the eight bands associated with the upper states {(0 1 4), (1 1 3), (3 2 0)} and the line intensities of cold bands have been calculated using the Hamiltonian and the transition moments parameters from Ref. [83]. The transition moment parameters from Refs. [84,85] were used to calculate the line intensities of the $\nu_1+\nu_2+3\nu_3-\nu_1$, $\nu_2+4\nu_3-\nu_3$, and $\nu_1+\nu_2+3\nu_3-\nu_2$ hot bands. Estimates of the transitions moments of the $4\nu_3$ and $3\nu_1+\nu_2$ bands [86] were used for the calculations of the line intensities of the $\nu_2+4\nu_3-\nu_2$, and $3\nu_1+2\nu_2-\nu_2$ hot bands.

The calculations for the $2\nu_1+2\nu_3$, $3\nu_1+\nu_3$, $2\nu_1+2\nu_2+\nu_3$ and $2\nu_1+\nu_2+2\nu_3$ bands are based on the results from Refs. [87–90].

Table 6 lists 9 bands in the 5935–6394 cm^{-1} spectral region. These results were obtained by using CW–CRDS technique [91,92]. The spectra were recorded in Laboratoire de Spectrométrie Physique at the Joseph Fourier University (Grenoble, France). The analysis and theoretical modeling of these data have been reported in Refs. [92,93]. Note that the 6017–6131 and 6318–6394 cm^{-1} spectral ranges are dominated by a band labeled as $2\nu_1+2\nu_2+3\nu_3$. See Refs. [92,93] for more details.

The spectral interval 1854–2768 cm^{-1} has been updated for the two isotopologues $^{16}O^{16}O^{18}O$ and $^{16}O^{18}O^{16}O$, this region relates to the bands: $2\nu_3$, $\nu_1+\nu_2+\nu_3-\nu_2$, $\nu_1+\nu_3$, $2\nu_1$, and $\nu_1+\nu_2+\nu_3$. Bands $2\nu_3$, $\nu_1+\nu_2+\nu_3-\nu_2$, $2\nu_1$, $\nu_1+\nu_2+\nu_3$ of $^{16}O^{16}O^{18}O$ as well as bands $\nu_1+\nu_2+\nu_3$ and $\nu_1+\nu_2+\nu_3-\nu_2$ of $^{16}O^{18}O^{16}O$ have been

Table 6
New GEISA-09 ozone bands ($^{16}O_3$) from CW-CRDS spectra [91,92].

Band	Spectral region (cm^{-1})	Number of lines	Sum of line Intensities (10^{-24} cm^{-1}/(molecule cm^{-2}))
034–000	5935–6083	610	1.178
105–000	5971–6071	1006	2.456
124–000	6004–6363	1933	4.566
223$_I$–000	6017–6131	1578	13.188
510–000	6030–6139	272	0.401
025–000	6225–6311	913	7.656
430–000	6295–6395	75	0.298
501–000	6301–6366	685	6.335
223$_{II}$–000	6318–6394	717	6.758

included in the GEISA-09 database for the first time. The calculations of all bands of both isotopologues were made using the Hamiltonian parameters for the lower states for the (0 0 0) and (0 1 0) states from Ref. [94]. Hamiltonian parameters of the upper vibrational states correspond to Ref. [95] for $^{16}O^{16}O^{18}O$ and to Ref. [96] for $^{16}O^{18}O^{16}O$. The transition moment parameters of both species, given by Barbe and De Backer-Barilly [97] have been obtained from studies of Fourier-transform ozone spectra enriched in oxygen-18. The broadening parameters (both air and self) for all B-type and A-type bands were derived, respectively, from those of ν_1 and ν_3 bands. These values are originated from the S&MPO system [81] (see Ref. [54] at http://smpo.iao.ru/1280x795/en/refs/9/ therein). These parameters are different from those reported in HITRAN-08 [13].

The temperature dependence coefficient $n=0.76$ of the air pressure broadening has been attributed to all the transitions. The absolute intensities are obtained from direct experimental measurements for each band (no indirect normalization).

Line lists are given with a cutoff intensity of 1×10^{-24} cm^{-1}/(molecule cm^{-2}) at 296 K for 100% abundances of $^{16}O^{16}O^{18}O$ and $^{16}O^{18}O^{16}O$. It has to be noted that all the ozone data in GEISA-09 are given in natural abundance of isotopologues.

2.2.4. N_2O (molecule 4)

The N_2O line list has been almost completely revised. Only the rotational part: 0.83–45.263 cm^{-1} has been kept from GEISA-03 (451 entries). All 50,182 lines of Toth's data [98–101] from the website: http://mark4sun.jpl.nasa.gov/ n2o.html, which cover the spectral range 525.462272– 7796.633112 cm^{-1}, have been included in GEISA-09 line list. As a consequence, three new isotopologues have been added: $^{15}N_2^{16}O$, $^{14}N^{15}N^{18}O$ and $^{15}N^{14}N^{18}O$, representing a total of 668 entries. The source of the N_2O broadening parameters are from Ref. [101] which gives N_2 and air widths and shifts of N_2O. These data were used to generate the parameters used for the website http://mark4sun.jpl. nasa.gov in 2004 under science data.

The N_2O GEISA-09 archive now comprises 50,633 entries and eight isotopologues. This represents an increase of 23,952 entries over GEISA-03 (26,681 entries).

The JPL catalog contains new entries for the rotational transitions of N_2O in its $\nu_2=0$, 1, and 2 vibrational states as well as for the singly substituted isotopologues in their ground vibrational states. These entries are based in particular on [102]. These entries will be considered for the next update of GEISA.

2.2.5. CH_4 (molecule 6)

Many of the infrared methane line parameters of $^{12}CH_4$ were updated between 0 and 3300 cm^{-1}, but little changes were made for the $^{13}CH_4$ parameters. As noted in Sections 1 and 2, entries for methane isotopologues $^{12}CH_3D$ and $^{13}CH_3D$ are included in GEISA as an independent molecule, CH_3D, numbered "23" (see Table 2); related updates are described below. At the longer wavelengths, a minimum intensity limit of 10^{-29} cm/molecule at 296 K was applied out of planetary considerations, but the weak lines were still not included in the near-IR regions. Misaligned fields in the near-IR quantum numbers were corrected, but only a few new assignments (and thus lower state energies) were entered to existing entries. Significant changes were made for air-broadening coefficients between 5800 and 6180 cm^{-1}.

Below 3300 cm^{-1}, new calculated $^{12}CH_4$ line positions and intensities were obtained from the global analysis by Albert et al. [103] of the three lowest polyads (ground state, dyad from 900 to 1900 cm^{-1} and pentad from 1900 to 3400 cm^{-1}). In the far-IR, the intensities of ground state–ground transitions were adjusted by 16% based on Wishnow et al. [104], but no change was required for the dyad–dyad ($\nu_2 - \nu_2$, $\nu_2 - \nu_4$, $\nu_4 - \nu_4$) hotbands. Some predicted pentad ($2\nu_4$, $\nu_2 + \nu_4$, ν_1, ν_3 and $2\nu_2$) positions were recomputed using semi-empirical upper state energy levels obtained by adding observed positions to calculated lower state energies. The hot band parameters between 900 and 3500 cm^{-1} and of the Octad (3200 and 4900 cm^{-1}) were taken from GEISA-03 rather than the global study because the prior database had better accuracies for the strongest features in the interval; a minimum intensity limit for hot bands was set to 10^{-27} cm^{-1}/(molecule cm^{-2}) at 296 K.

The line list for methane near 6000 cm^{-1} was somewhat improved using new measurements of intensities, empirical lower state energies and broadening parameters of the stronger features. First, the intensities and widths for the 5860–6180 cm^{-1} region were replaced by results from Frankenberg et al. [105]. This also included implementation of the empirical lower state energies of Margolis [106,107] which were missing in GEISA-03. In addition, lower state values from Gao et al. [108]

were added. However, several thousand weak lines ($< 10^{-24}$ cm^{-1}/(molecule cm^{-2})) are still missing between 5500 and 6180 cm^{-1}. There are a number of recently published and ongoing studies which will help to improve the near infrared (4800–7700 cm^{-1}) line parameters [109–118].

For broadening, relatively few (< 3000) direct measurements of widths and pressure shifts are available for methane transitions so that default values for self- and air-broadened widths, air-induced pressure shifts and temperature dependences are applied (similar to those used in earlier versions of GEISA see [119,120]. For the 7.5 μm region of the Dyad, new measurements of ~ 500 transitions from Smith et al. [121] were inserted for self- and air-broadening widths, shifts and temperature dependence of widths. For the 3.3 μm region of the Pentad, ~ 3800 theoretically predicted broadening coefficients (air-widths, pressure shifts and temperature dependences) from Antony et al. [122] and ~ 500 prior measurements [119] were inserted for ν_3. At 2.3 μm (the Octad), the self- and air-broadening parameters of Predoi-Cross et al. [123,124] were retained in the list carried over from the GEISA-03 database.

In the 1.66 μm region (the Tetradecad) over 480 air-broadened widths and shifts and some temperature dependence were inserted between 5560 to 5860 cm^{-1} [111], while the scaled N$_2$-broadening reported by Frankenberg et al. [105] were used from 5860 to 6184 cm^{-1}. Otherwise, defaults constants of 0.75 below 5860 cm^{-1} or 0.85 above 5860 cm^{-1} were set for the temperature dependence.

Lastly, the current methane database is customized to interpret atmospheric remote sensing of the Earth. Further near-IR analyses will be needed for planetary and stellar applications. (e.g., [125]). Calculations of partition functions [126] and much weaker transitions can be found at http://www.iao.ru/mirs or http://icb.u-bourgogne.fr/JSP/TIPS.jsp. However, extrapolations to higher values of quanta provide less accurate parameters, particularly for the intensities.

2.2.6. O$_2$ (molecule 7)

Line parameters for the oxygen A-band ($b^1\Sigma_g^+ \leftarrow X^3\Sigma_g^-$) were revised for ^{16}O$_2$ and ^{16}O^{18}O, and those of ^{16}O^{17}O were added in the 0.76 μm region. The line positions, intensities, air- and self-broadened half-widths and air-induced pressure shifts were taken from the work of Robichaud et al. [127–130] who performed CW-CRDS of the P branch. The positions now have accuracies of 0.00006 cm^{-1} or better for ^{16}O$_2$ and ^{16}O^{18}O and 0.00050 cm^{-1} for ^{16}O^{17}O through calibration against atomic potassium calibration standards [131]. The differences between the old and new positions are on average 0.0007 cm^{-1} [127] for ^{16}O$_2$ and 0.002 cm^{-1} [129] for ^{16}O^{17}O, but much larger for ^{16}O^{18}O (up to 0.20 cm^{-1}) because the latter were based on 60-year-old results [132].

Line intensities changed only slightly for the first two isotopologues: -0.8% for ^{16}O$_2$, $+1\%$ for ^{16}O^{18}O, but $\pm 5\%$ for ^{16}O^{17}O (depending on the rotational quanta). The

accuracies are thought to be $\pm 1\%$ or better for the first two species, but more study is needed for ^{16}O^{17}O.

For all three species, the widths are computed via an expression from Yang et al. [133]

$$HWHM = A + \frac{B}{1 + c_1 J' + c_2 J'^2 + c_3 J'^4} \tag{1}$$

by using the ^{16}O$_2$ constants from Table 6 of Robichaud et al. [128] based on retrievals done with Galatry (not Voigt) profiles. For the widths, the values at high quantum numbers ($J > 22$), previously in error by more than 40% near $J = 30$, are now thought to be accurate to $\pm 2\%$.

Pressure-induced shifts are still rather uncertain (± 0.003 cm^{-1}) with different studies in poor agreement (e.g., [129,134,135]). For the interim, the measured A-band pressure shifts of Robichaud et al. [127] for the P branch and the averages of shifts from Predoi-Cross et al. [134,135] for the R branch were inserted, along with the temperature dependence of widths from Brown and Plymate [136].

Finally, it should be emphasized that even with these improvements, the line parameters are not sufficient to reproduce atmospheric observations at 13,100 cm^{-1} because Voigt line shapes are inadequate. The combined analyses of Tran and Hartmann [137], Predoi-Cross et al. [134,135] and Robichaud et al. [128–130] have demonstrated the need to consider line mixing, Galatry and/or speed dependence line shapes in order to model the oxygen A-band properly.

It has to be noted that the revised O$_2$ GEISA-09 line list does not derive from the GEISA-03 line list, but from the HITRAN 2004 [13] one. The major difference between the two line lists is for the intensity values, especially in the 1.27 μm spectral region (Ref. [32] of Ref. [8]). As an unfortunate consequence of this alternate line list inclusion (due to a final mis-manipulation among different generated test files for data validation studies), the two lines closest to the γ band head (at 15,927.701 and 15,927.805 cm^{-1}), present in GEISA-03, are now detrimentally missing in GEISA-09, propagating a technical error occurring in HITRAN 2004. This must be fixed in the next GEISA edition.

2.2.7. NO (molecule 8)

The GEISA-03 NO line list has been totally replaced by a new one provided by Goldman [138]. The new line list is partially based on the work described by Goldman et al. [139], and is equivalent to the updated NO in HITRAN-08 [13]. The updates mainly consist of: including, for the first time, Einstein-A coefficients to replace, in format field M, the former GEISA-03 transition probabilities (see Table 11) and the implementation of hyperfine splitting for the microwave and far infrared lines. Magnetic dipole satellite transitions between spin components of the electronic ground state have also been added, and are further identified by the letter "m" in the first field for the upper state quantum numbers. When lines with resolved hyperfine structure were not available from Ref. [139], they were taken from the JPL catalog [16].

These updates have increased the total number of NO transitions in GEISA from 99,123 to 105,079 (293 bands).

2.2.8. SO_2 (molecule 9)

Sulfur dioxide, SO_2, is well known to be both of astrophysical and planetary importance. SO_2 is an important constituent on Venus [140–144] and Io [145–148], where it actively participates in the photochemistry of their atmospheres. It has also been observed in comets [149–152]. In the terrestrial atmosphere, SO_2 is a trace species produced by both anthropogenic and natural sources; mainly present in the troposphere [153–155], it is a primary pollutant emitted by fuel combustion and responsible for the production of acid rain. The most important natural sources of SO_2 are the oxidation of sulfur compounds from oceans and marshes and from volcanic eruptions and outgassing. Most volcanic SO_2 emissions remain in the troposphere where the lifetime of the species strongly depends on the meteorological conditions. After major volcano eruptions, SO_2 is also present in the stratosphere [156–157] in high concentrations, where it is converted into sulfate aerosols which affect both stratospheric chemistry and climate. SO_2 has been detected on Io in the microwave and more recently at 19 μm [158]; this is of high relevance to the studies of exchanges between the atmosphere and the surface of the satellite.

The GEISA-03 database provided SO_2 parameters in seven different spectral regions, which correspond to transitions in the microwave region and the 19.3, 8.6, 7.3, 4, 3.7 and 2.5 μm spectral regions. However in the 19.3, 8.6 and 7.3 μm spectral regions new studies [159–162] have been performed improving the corresponding spectral parameters. These three spectral regions are important for SO_2 measurements in atmospheres. The 7.3 μm which is the strongest SO_2 infrared region unfortunately cannot be used for ground measurements of SO_2 since it is severely overlapped with the strong v_2 band of water vapor. On the other hand, the v_1 band, although about nine times weaker corresponds to a rather clear atmospheric window. Finally the rather weak 19.3 μm region can be used for retrieving SO_2 in the atmosphere of planets [158].

Based on the new studies an improved line list including line positions, intensities, transition assignments and lower state energy levels has been generated. It includes not only, for the main isotopologue $^{32}SO_2$, the cold bands v_2, v_1 and v_3, but also the corresponding hot bands $2v_2 - v_2$, $3v_2 - 2v_2$, $v_1 + v_2 - v_2$ and $v_3 + v_2 - v_2$, as well as the v_1, v_3, $v_1 + v_2 - v_2$, $v_2 + v_3 - v_2$, $v_1 + v_3$ bands of $^{34}SO_2$, from the results of a series of papers [163–165] devoted to the high resolution study of the absorption of the $^{34}SO_2$ species in the infrared. The resulting newly archived $^{34}SO_2$ spectral line parameters are much better than the previous ones, related only to the $v_1 + v_3$ band. The accuracy for line positions is estimated to be better than 0.001 cm^{-1}. For line intensities the accuracy is estimated to be of the order of 2–3% degrading up to about 15% for high J or K_a transitions. Finally, the GEISA-09 SO_2 line list comprises a total of 68,728 lines among which 43,941 are new or updated entries. From GEISA-03 have been kept 24,787 entries of the main isotopologue $^{32}SO_2$, in two distinct spectral regions, i.e., 0.017394–256.241135 cm^{-1} (9622 rotational lines) and 2433.192300–4092.948220 cm^{-1} (15,165 lines).

As far as the pressure broadening coefficients are concerned the situation is different for air-broadening and self-broadening coefficients.
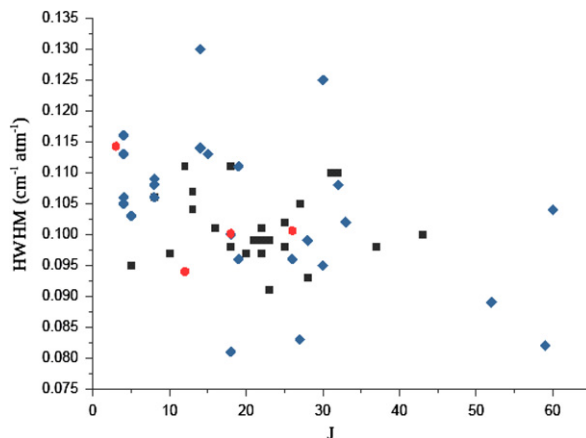

Fig. 5. $^{32}SO_2$ Lorentz air-broadened half-width parameters (at 296 K) (● Microwave, ◆ v_3 band, ■ v_1 band) versus the quantum number J of the lower level of the transition.

For the air-broadened half-width coefficients (HWHM) it turns out that it was only possible to estimate an average value for this parameter. In fact no variation of this parameter with respect to the lower quantum numbers J or K_a of the transitions could be determined. As an example, Fig. 5 presents the measured parameters (Y-axis) with respect to the lower quantum numbers J of the transitions (X-axis), for the microwave and the v_3 and v_1 bands spectral regions. It appears not possible to derive any clear variation (the same is true when these parameters are plotted versus the quantum number K_a) so only an average value of 0.1025 cm^{-1} atm^{-1} could be determined. This value has been used for all the updated lines of isotopologue $^{32}SO_2$; in the case of isotopologue $^{34}SO_2$, the value 0.1000 cm^{-1} atm^{-1} has been attributed to the lines of $v_1 + v_3$ The GEISA-09 missing value -0.9999 cm^{-1} atm^{-1} has been given to the lines of $v_2 + v_3 - v_2$ for both isotopologues. Related with the entries remaining from GEISA-03, the average value is 0.1000 cm^{-1} atm^{-1} for the 9622 rotational lines and 0.1100 cm^{-1} atm^{-1} for the other 15,165 lines.

The situation is quite different for the self-broadening parameters. It was possible indeed to observe a clear variation of these parameters with respect to the K_a quantum number of the lower state of the transitions (see illustration in Fig. 6 for the v_1, v_2, and v_3 bands, with a display similar to Fig. 5). On the other hand no variation with respect to the quantum number J could be observed.

Based upon these results, it was decided to include in the database the following values for the self-broadened half-width coefficients:

$HWHM_{self} = 0.4$ cm^{-1}/atm for $K_a \leq 5$
$HWHM_{self} = 0.156$ cm^{-1}/atm for $K_a \geq 21$
$HWHM_{self}$ is calculated through a linear interpolation for $6 \leq K_a \leq 20$

For the updated transitions, these new parameters have been used for all the lines of main isotopologue $^{32}SO_2$ except for those of band $v_2 + v_3 - v_2$ for which the GEISA-09 missing value -9.9999 cm^{-1} atm^{-1} has been
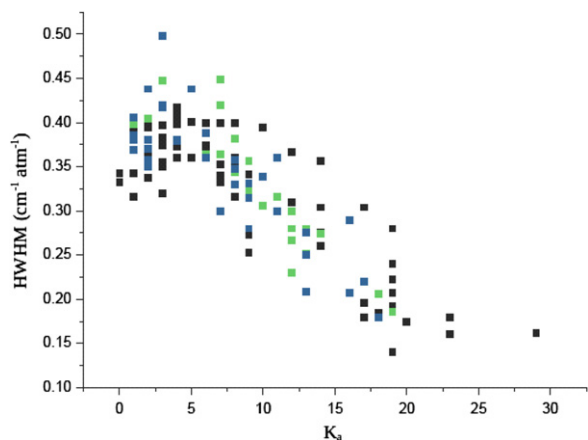
Fig. 6. $^{32}SO_2$ Lorentz self-broadened half-width parameters (■ ν_2, ■ ν_3 band, ■ ν_1 band) versus the quantum number K_a of the lower level of the transition.

given to both isotopologues, as well as to 83 lines of isotopologue $^{34}SO_2$ in the spectral region 1165.402–1379.267 cm^{-1}.

For the GEISA-03 retained transitions, the missing value has been attributed to the rotational transitions and the default value 0.39 cm^{-1} atm^{-1} to all the other ones

As a consequence, an accuracy of 10–15% for the newly updated air-broadening and self-broadening parameters seems reasonable.

Finally, a "standard" default value of 0.75 has been used for the temperature dependence coefficient n of the air-broadening halfwidth.

It is worthwhile mentioning that the CDMS catalog provides an entry for ν_2 which is based on extensive rotational transitions in its $\nu_2=0$ and 1 states [166] along with previous IR data. This entry may be the basis for a GEISA entry in the next update.

2.2.9. NO₂ (molecule 10)

The study by Perrin et al. [167] provided accurate line positions and absolute intensities for several NO₂ bands, including the ν_2 and ν_3 fundamentals and their associated hot bands. Benner et al. [168] obtained precise line positions and relative intensities for the ν_3 band including accurate determinations of position differences for a large number of spin-splittings. In addition, air-broadened half-width and air-induced pressure shift coefficients and their variations with temperature were also determined for over 1000 transitions. These two studies [167,168] were combined to form an updated NO₂ line list at 6 μm. The positions and absolute line intensities are retained to values from Ref. [167] for the ν_3 band transitions, while the measured values of half-width, pressure-induced shift and the temperature dependence exponents of half-width coefficients were inserted line-by-line.

For all other transitions the values calculated using the empirical expressions of Ref. [168] were applied for the half-width, pressure shift and their temperature dependences. Values for higher K_a quantum numbers were constrained to the highest measured K_a ($K_a=9$ for half-width and $K_a=7$ for pressure-induced shift coefficients).

No pattern was discerned for the air-broadening temperature dependence exponents, and a simple linear equation in m ($m=N''$ for P and Q branch transitions and $N''+1$ for R-branch transitions) was fit to the measurements. For selected widths, the RMS deviation was 2.5%. In GEISA-03, the air-broadened half-width coefficients of all transitions were set to a default value of 0.067 cm^{-1} atm^{-1} at 296 K, the self-broadened half-width coefficients to 0.095 cm^{-1} atm^{-1} at 296 K, air induced pressure-shift coefficients were set to zero and the temperature dependence exponents of air-broadened half-width coefficients were set to a default value of one. In the new database at 6 μm, only the self-broadened half-width coefficients remain as default values (0.095 cm^{-1} atm^{-1} at 296 K), as was done in [8,9]. The NO₂ line lists are similar in GEISA-09 and HITRAN-08 [13].

2.2.10. NH₃ (molecule 11)

The line parameters given in GEISA-03 for the spectral interval 0.058–5294.502 cm^{-1} from Kleiner and Brown [169] and described in Kleiner et al. [170] have been slightly revised in GEISA-09, on the basis of an updated line list issued soon after the final completion of GEISA-03 final process. The NH₃ line lists are similar in GEISA-09 and HITRAN-08 [13] except for duplication of two lines in HITRAN, at 4561.037254 cm^{-1} and 4568.372254 cm^{-1}.

2.2.11. PH₃ (molecule 12)

Phosphine has been detected in the atmosphere of both Jupiter and Saturn [171,172] and is a significant absorber in the 5 μm window in Jupiter where it was used to probe the deeper atmosphere [173]. Features of PH₃ near 3425 cm^{-1} are clearly seen in ground-based spectra of Saturn [174,175], and line parameters for these bands are needed for the interpretation of data recorded by VIMS on the Cassini spacecraft [176].

Based on the work of Butler et al. [177], 9 new bands have been added in the region from 2724 to 3602 cm^{-1}, representing an increase of 8359 entries since GEISA-03 PH₃ archive. The collision-broadened parameters of the 770 to 2472 cm^{-1} spectral range have been updated using the results in Ref. [177]. Over 8000 line positions and intensities of phosphine, between 2724.477 and 3601.652 cm^{-1}, were measured at 0.0115 cm^{-1} resolution.

Quantum assignments were made to most of the eight interacting vibrational states: $3\nu_2$ (2940.8 cm^{-1}), $2\nu_2+\nu_4$ (3085.6 cm^{-1}), $\nu_2+2\nu_4$ (3214.9 cm^{-1}), $\nu_1+\nu_2$ (3307.6 cm^{-1}), $\nu_2+\nu_3$ (3310.5 cm^{-1}), $3\nu_4$ ($\sim$ 3345 cm^{-1}), $\nu_1+\nu_4$ (3426.9 cm^{-1}), and $\nu_3+\nu_4$ (3432.9 cm^{-1}). However, a recent global study of PH₃ by Nikitin et al. [178] demonstrated the complexities of modeling this region and revealed the need to investigate the consistencies between band intensities at 5 and 3 μm.

2.2.12. HNO₃ (molecule 13)

A very important improvement has been brought to the entire list of lines of HNO₃. The entire GEISA-03 content (171,504 entries in the spectral range 0.035141–1769.982240 cm^{-1}) has been replaced with data originating from two different sources, i.e., from Perrin [179], in the

spectral range 0.011922–769.982240 cm^{-1}, and from Petkie [180] in the spectral range 0.155640–527.247646 cm^{-1}.

In Perrin's work, an improved set of line positions, line intensities and line broadening parameters was generated in the infrared spectral region, using new and accurate experimental results concerning line positions and line intensities as well as sophisticated theoretical methods. The present update was performed in two steps, described in Refs. [181,182], respectively.

The first study [181] was performed in the 820–1770 cm^{-1} spectral range covered by the MIPAS instrument and the results of this first update are summarized in Table 5 of Ref. [181]. The line positions have been improved for the ν_5 and $2\nu_9$ cold bands and $\nu_5+\nu_9-\nu_9$ hot band around 11.2 μm and for the $\nu_8+\nu_9$ and $\nu_6+\nu_7$ bands around 8.3 μm (see details in Refs. [181,183] and in Refs. therein). In addition, the line intensities were updated in the 11.3, 8.3 and 7.6 μm spectral ranges by making use of the cross-sections measurements performed in Ref. [184].

The results of the second update are described in Table 1 of Ref. [182]. The intensities for the ν_6 and ν_8 bands centered at 646.826 and 763.154 cm^{-1}, respectively, were decreased by about 20–30% as compared to GEISA-03. Near 11.3 μm approximate parameters for the $\nu_5+\nu_7-\nu_7$ and $\nu_5+\nu_6-\nu_6$ hot bands have been added to the line list for the first time. Also a complete update of the air-broadening parameters was performed in the 11 μm region following recent line-broadening calculations [185]. It should be noted that the air-broadening parameters implemented in the narrow Q branches of the ν_8 and $\nu_5+\nu_9-\nu_9$ bands at 763.154 and 885.425 cm^{-1}, respectively, account empirically for line mixing effects as evidenced by laboratory measurements.

The validation of these updates in the new line list was performed during several ground based, balloon borne or satellite measurements of atmospheric HNO$_3$ [181,185,186].

Future studies should concentrate to the improvements of HNO$_3$ line parameters in the 7.6 μm region. Indeed this region which corresponds to the ν_3 and ν_4 bands located at 1325.7354 and 1303.5182 cm^{-1}, respectively, needs major updates in term of line positions and intensities. Also, the previous studies in this region [188] did not consider resonances due to several dark states which perturb the 3^1 and 4^1 energy levels.

The cataloged spectral parameters of nitric acid have been updated in the millimeter/sub-millimeter-wave and 22 μm far-infrared regions. The calculated line parameters are based on the spectroscopic constants derived from the analyses of millimeter and sub-millimeter wave rotational spectra found in Refs. [189–191]. All predictions were calculated using the SPCAT program package [192]; (http://spec.jpl.nasa.gov/ftp/pub/calpgm/spinv.pdf) for a temperature of 296 K, an isotopic abundance of 0.989, a rotational partition function of 27,343, and a vibrational partition function of 1.304 [193].

In the mm/sub-mm-wave region, the pure rotational transitions from the vibrational states with band origins below 1000 cm^{-1} have been included in this update. These vibrational states account for about 97% of the thermally populated molecules at 296 K. This includes transitions in the ground state, $\nu_9=1$, $\nu_7=1$, $\nu_6=1$, $\nu_8=1$, and the interacting $\nu_5=1/\nu_9=2$ dyad. The details of the analyses and measurements can be found in Refs. [189,190] and the set of references contained therein.

In the 22 μm far-infrared spectral region, line parameters for the fundamental ν_9 band as well as the two hot band $\nu_9-\nu_9$ and $\nu_5-\nu_9$, have been updated. Line positions for the bands were calculated from the rotational analyses in Refs. [189,190] and the band origins determined in Refs. [183,194]. The high-resolution far-infrared spectrum in Ref. [195] was used both as a stringent test of the predicted far-infrared transition frequencies and to determine the relative intensities of the hot bands referenced to the intensity of the fundamental ν_9 band determined in Ref. [193]. Details of the far-infrared simulation can be found in Ref. [191].

The new HNO$_3$ GEISA-09 line list has been processed as the following: starting from Perrin's line list [179], Petkie's data have been included [180], replacing the Perrin's values for transitions with same quantum identifications. The final GEISA-09 HNO$_3$ line list comprises 669,988 entries in the spectral range 0.011922–1769.982240 cm^{-1}.

2.2.13. OCS (molecule 20)

Substantial revisions involving five isotopologues $^{16}O^{12}C^{32}S$, $^{16}O^{12}C^{34}S$, $^{16}O^{13}C^{32}S$, $^{16}O^{12}C^{33}S$, and $^{18}O^{12}C^{32}S$ provide new parameters for some 50 bands between 3800 and 4200 cm^{-1}; 13 allowed and two forbidden bands arise from the ground state while the remainders are hot bands. The number of transitions increases from ∼1100 transitions (for $2\nu_3$ of five isotopologues and the $\nu_2+2\nu_3-\nu_2$ of $^{16}O^{12}C^{32}S$ and $^{16}O^{12}C^{34}S$) to 10,425 lines. Most of the line positions are calculated using the effective rovibrational energy constants based on a global analysis [196–200] whose line position accuracy was reported to be 5×10^{-5} cm^{-1} [196]. The calculated line intensities are taken from analyses of new FTIR measurements [201–202] performed at JPL to support Venus studies. Sung et al. [201] reported line intensities of the $2\nu_3$ band at 4101.387 cm^{-1}, $\nu_1+2\nu_2+\nu_3$ at 3937.427 cm^{-1}, and $4\nu_2+\nu_3$ at 4141.212 cm^{-1} of $^{16}O^{12}C^{32}S$. The new band strengths are in good agreement (1.3%) with the prior studies by Bermejo et al. [203] and Naim et al. [196]. Intensities of all the other bands are determined by Toth et al. [202] with many bands being measured for the first time, and their uncertainties range from 1% to 6% depending on bands. The line intensities vary through five orders of magnitude, but very weak unassigned features are omitted from the database pending further analysis.

The air- and self-broadened half-widths are computed, respectively, using Refs. [204–207]. The self-broadened temperature dependence exponents of ν_1 from Bouanich et al. [207] are also applied for the broadened half-width coefficients in this region. For the transitions whose J values are greater than 65 and 75, their air- and self-broadened half-widths coefficients at 296 K are set to 0.12 and 0.0817 cm^{-1}/atm, respectively [208]. Air-induced pressure shift coefficients for $2\nu_3$ band of OCS reported by Domenech et al. [209] are inserted for the first time. In a separate parameter file, the air-broadened OCS
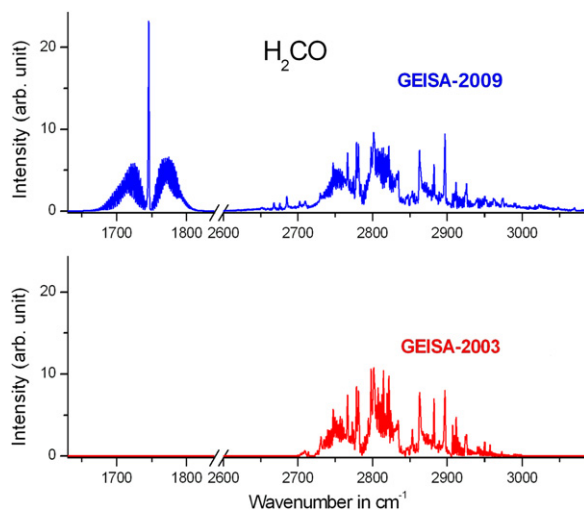
Fig. 7. Overview of the H_2CO line parameters in the 5.7 μm and 3.6 μm spectral regions. Lower and upper traces describe the status in GEISA-03 [8,9] and in GEISA-09, respectively.

half-width coefficients are replaced by CO_2-broadened half-width coefficients, using the measurements of Bouanich et al. [210] in the ν_1 band of OCS. This second database is intended to support remote sensing of Venus at 2.4 μm and is archived in a GEISA-09 complementary files line list.

2.2.14. H_2CO (molecule 21)

Formaldehyde (H_2CO) in the atmosphere can be retrieved in the 5.7 μm region by MIPAS aboard the ENVISAT satellite [211] and by the ACE-FTS instrument on board the Canadian satellite SCISAT-1 at 3.6 μm [212]. For this reason the major update for H_2CO in the infrared region which consists of the complete replacement of the line positions and line intensity parameters near 3.6 μm and the addition of a line list in the 5.7 μm region [213].

The line positions were generated using the models and the parameters described in details in Refs. [214,215] for the 5.7 and 3.6 μm, respectively. The 5.7 μm corresponds to the ν_2 band together with three dark bands. In the 3.6 μm region the lines belong to the ν_1 and ν_5 bands together with nine dark bands. In addition, a consistent set of line intensity parameters was generated for both the 5.7 and 3.6 μm spectral regions [213] from analyzing high-resolution Fourier transform spectra recorded in the 1600–3200 cm^{-1} spectral range.

The calculated band intensities derived for the 5.7 and 3.6 μm bands are in excellent agreement with the values achieved recently by medium resolution band intensity measurements.

Compared to the GEISA-03 database which contains only 1161 lines near 3.6 μm, the quality of the line parameters in GEISA-09 is significantly improved in terms of both the positions and intensities. Details giving the description of the new database which involves 3713 and 31,796 transitions at 5.7 and 3.6 μm, respectively, are given in Table 9 of Ref. [213]. A subsequent and complementary study dealing with measurements and calculations

of formaldehyde pressure induced self- and N_2-broadened half-width coefficients is in progress [216].

Fig. 7 illustrates the extended H_2CO line parameter information included in GEISA-09. Comparative absorptions as synthetic spectra (intensity, in similar arbitrary unit, along the Y-axis, versus wavenumber along the X-axis), are displayed in the 5.7 μm and 3.6 μm spectral regions, corresponding, respectively, to GEISA-03 (red curve) and GEISA-09 (blue curve) archives.

2.2.15. C_2H_6 (molecule 22)

The GEISA-03 line list for the 12 μm region of ethane contained data for the ν_9 fundamental band of $^{12}C_2H_6$, from a 1992 analysis by Daunt et al. [217], and the ν_{12} fundamental band of $^{13}CH_3^{12}CH_3$, from a high-resolution work by Weber et al. [218,219]. In the updated 2009 edition, only the line list for the ν_{12} band of $^{13}CH_3^{12}CH_3$ has been kept; the data for the ν_9 band of $^{12}C_2H_6$ has been replaced with a new list which includes a total of 21,607 lines belonging to the ν_9, $3\nu_4$, $\nu_9+\nu_4-\nu_4$, and $\nu_9+2\nu_4-2\nu_4$ bands (ν_4 is the torsional mode near 289.3 cm^{-1}). It was generated by Vander Auwera et al. [220] using a spectrum of the ν_9 band recorded at the PNNL [221], results from a global analysis of data involving the four lowest vibrational states of ethane [222] and measurements of pressure-broadening parameters [223,224]. Details can be found in [220]. As a result, the sum of the line intensities and wavenumber coverage in the 12 μm region are increased from 5.881×10^{-19} to 1.011×10^{-18} cm^{-1}/(molecule cm^{-2}) at 296 K (natural abundance) and from 725.6–918.7 cm^{-1} to 706.6–961.2 cm^{-1}, respectively. As shown by Nixon et al. [225] and Coustenis et al. [226] based on Cassini CIRS (http://cirs.gsfc.nasa.gov/) data, the new list for the 12 μm spectral region of $^{12}C_2H_6$ constitutes a significant improvement over the previously available data, leading to the first measurement of $^{12}C/^{13}C$ isotopic ratio of C_2H_6 in the atmosphere of Titan. It can be mentioned that C_2H_6 acts as the main catalyst in photosensitized

dissociation in Titan's stratosphere, as shown by Wilson and Atreya [227].

Note that the quantum number notation for representing rotation–torsion states has evolved since the GEISA-03 edition. In [220], the levels are identified by J, the quantum number for the total angular momentum of the molecule, K, the quantum number for its component along the symmetry axis, ℓ, the quantum number associated with the vibrational angular momentum of the degenerate mode ν_9, and $\sigma = 0$–3 which labels the torsional sublevels. In the new line list archived in GEISA-09, the latter is replaced by the symmetry species A_{1s}, A_{2s}, A_{3s}, A_{4s}, E_{1s}, E_{2s}, E_{3s}, E_{4s} and G_s in the G_{36}^+ extended permutation-inversion group. Because all the allowed species are s-species, the letter 's' is omitted: for instance, E_{1s} symmetry is given as 'E1' and $A_{1s}+A_{2s}$ is given as 'A12'. The symmetry of the vibration–rotation–torsion levels of $^{12}C_2H_6$ corresponding to the excitation of ν_9 and ν_4 is given in Table 7. This new notation is common to GEISA-09 and HITRAN-08 [13]. In GEISA-09, the former notation has been kept for the not updated ν_{12} fundamental band of $^{13}CH_3^{12}CH_3$.

Vander Auwera et al. [220] determined absolute line intensity information by matching to low-resolution cross-sections. They indicated that the best match between high-resolution spectra of the ν_9 band of pure ethane and spectra calculated at the same experimental conditions using the generated line list could be obtained

Table 7
Symmetry in the G_{36}^+ extended permutation-inversion group of vibration–rotation–torsional levels of $^{12}C_2H_6$ involving the excitation of the ν_9 bending and ν_4 torsional modes of vibration.

(a) $\nu_9=$even, $\nu_4=$even

K	J	$\sigma=0$	$\sigma=1$	$\sigma=2$	$\sigma=3$
0	Even	A_{1s} (6)		E_{3s} (2)	
	Odd	A_{2s} (10)		E_{4s} (6)	
$6n\pm1$			G_s (16)		E_{1s} (4)
$6n\pm2$		E_{1s} (4)		G_s (16)	
$6n+3$			$E_{3s}+E_{4s}$ (8)		$A_{1s}+A_{2s}$ (16)
$6n\neq0$		$A_{1s}+A_{2s}$ (16)		$E_{3s}+E_{4s}$ (8)	

(b) $\nu_9=$even, $\nu_4=$odd

K	J	$\sigma=0$	$\sigma=1$	$\sigma=2$	$\sigma=3$
0	Even	A_{3s} (6)		E_{3s} (2)	
	Odd	A_{4s} (10)		E_{4s} (6)	
$6n\pm1$			G_s (16)		E_{2s} (4)
$6n\pm2$		E_{2s} (4)		G_s (16)	
$6n+3$			$E_{3s}+E_{4s}$ (8)		$A_{3s}+A_{4s}$ (16)
$6n\neq0$		$A_{3s}+A_{4s}$ (16)		$E_{3s}+E_{4s}$ (8)	

(c) $\nu_9=$odd, $\nu_4=$even

G	K	J	$\sigma=0$	$\sigma=1$	$\sigma=2$	$\sigma=3$
0	≥0	Even	A_{3s} (6)		E_{3s} (2)	
		Odd	A_{4s} (10)		E_{4s} (6)	
	<0	Even	A_{4s} (10)		E_{4s} (6)	
		Odd	A_{3s} (6)		E_{3s} (2)	
$6n\pm1$				G_s (16)		E_{2s} (4)
$6n\pm2$			E_{2s} (4)		G_s (16)	
$6n+3$				$E_{3s}+E_{4s}$ (8)		$A_{3s}+A_{4s}$ (16)
$6n\neq0$			$A_{3s}+A_{4s}$ (16)		$E_{3s}+E_{4s}$ (8)	

(d) $\nu_9=$odd, $\nu_4=$odd

G	K	J	$\sigma=0$	$\sigma=1$	$\sigma=2$	$\sigma=3$
0	≥0	Even	A_{1s} (6)		E_{3s} (2)	
		Odd	A_{2s} (10)		E_{4s} (6)	
	<0	Even	A_{2s} (10)		E_{4s} (6)	
		Odd	A_{1s} (6)		E_{3s} (2)	
$6n\pm1$				G_s (16)		E_{1s} (4)
$6n\pm2$			E_{1s} (4)		G_s (16)	
$6n+3$				$E_{3s}+E_{4s}$ (8)		$A_{1s}+A_{2s}$ (16)
$6n\neq0$			$A_{1s}+A_{2s}$ (16)		$E_{3s}+E_{4s}$ (8)	

J and K are, respectively, the quantum numbers associated to the total angular momentum of the molecule and its projection along the molecule top 3-fold symmetry axis, $\sigma=0$–3 is the torsional index and $G=K-\ell\geq0$ with $\ell=\pm1$ the vibrational angular momentum quantum number associated to ν_9. $n\geq0$. The nuclear spin statistical weights are given in parentheses [218]. Empty cells correspond to non-existing levels.

provided the line intensities were reduced by about 9%. Very recently, Devi et al. [229] carried out extensive measurements of spectral line parameters in the ν_9 band of $^{12}C_2H_6$. They showed that their high-resolution line intensities were 10–15% lower than those in the line list of Ref. [220]. These observations seem to indicate that the line intensities in GEISA-09, and also in HITRAN-08 [13], are probably 10–15% too high. Note that the Devi et al [229] work also provides improved characterization of the temperature dependence of the N_2- and self-broadening parameters, which will be applied in future editions of databases.

In the 3.3 μm region, the ν_7 fundamental band of $^{12}C_2H_6$ exhibits a number of strong unresolved Q-branches ($^PQ_4$ to $^rQ_4$), observed between 2973 and 3001 cm^{-1}. GEISA contained a list of 421 lines belonging to the $^PQ_3$ branch observed near 2976 cm^{-1}, generated by Pine and Rinsland [230]. To complement this rather limited information, the line positions and intensities determined for the other strong Q-branches by Goldman et al. [231,232] have been added to this edition, even though the data are now quite dated and only allow a rather approximate modeling of the observed structure of the branches. The other line parameters have been set to the same values as for the ν_9 band. The quantum number labeling of all the levels and the symmetry of torsionally split levels are also defined as for the ν_9 band. The symmetry of levels involving unresolved torsional components is expressed using the species of the D_{3d} group, i.e., A_{1g} (8), A_{1u} (8), A_{2g} (16), A_{2u} (16), E_g (20) and E_u (20) (the numbers between parentheses are the nuclear spin statistical weights [228]). Recent studies [233,234–236] are becoming available for infrared ethane. For the important atmospheric region at 3.3 μm, Harrison et al. [233] measured absorption cross-sections for both pure ethane and mixtures with synthetic dry air at a number of temperatures and pressures appropriate for atmospheric conditions. These data were later converted to line-by-line parameters by Toon [234] with lower state energies estimated from the recorded spectra [233]. Two theoretical analyses interpreted high resolution spectra and modeled the observed positions. Di Lauro et al. [235] predicted positions and relative intensities of seven bands at 7 μm while Lattanzi et al. [236] extended assignments in four bands at 3.3 μm and modeled those line positions. Both studies are reporting new databases applicable to atmospheric remote sensing with the caveat that the intensities must be studied further and that unassigned observed features are not yet included.

2.2.16. CH_3D (molecule 23)

This GEISA independent molecule (see the section Introduction and Table 2) involves methane isotopologues $^{12}CH_3D$ and $^{13}CH_3D$. For the GEISA-09 modifications, nine new infrared bands were added at three different wavelengths (8, 2.9 and 1.56 μm). In addition, a far-IR prediction (version 1) from the CDMS database [17], based on frequencies reported by Lattanzi et al. [237], was included. The $^{13}CH_3D$ species was added to the database for the first time because the isotopologue $^{13}CH_3D$ was recently detected in Titan's stratosphere [238], using

Cassini/CIRS infrared spectrum near 8.7 μm. Fitting simultaneously the ν_6 band of both $^{13}CH_3D$ and $^{12}CH_3D$ and the ν_4 band of CH_4, this detection allowed a precise determination of the D/H ratio in methane and yielded a $^{12}C/^{13}C$ ratio in $^{13}CH_3D$ consistent with that measured in normal methane.

A prediction of the $^{13}CH_3D$ triad (ν_6, ν_3 and ν_5) between 952 and 1694 cm^{-1} was based on the line positions and energy levels analysis by Ulenikov et al. [239]. The intensities were calculated using the transition dipole moment parameters of the $^{12}CH_3D$ from Brown et al. [240]. The calculations were limited to $J=K=18$ as they are the maximum quantum numbers covered by the experimental rovibrational term values published in Ref. [239].

Titan and Saturn observations [241,242] also revealed the need for additional parameters at 2.9 μm. Six new $^{12}CH_3D$ vibrational bands ($\nu_2+\nu_3$, $\nu_2+\nu_5$, $\nu_2+\nu_6$, $\nu_3+2\nu_6$ and $3\nu_6$) were included for the first time from the analysis of positions and line intensities of by Nikitin et al. [243]. Finally, the Boussin et al. [244] empirical line list in the $3\nu_2$ region at 1.56 μm was included. The self- and air-broadened widths were generally applied using empirical formula obtained from $^{12}CH_3D$ triad measurements [245]; however, self- and air-broadened widths and shifts observed by Boussin et al. [244] were used for $3\nu_2$. For temperature dependence of widths, CH_4 values averaged by J [119] were used as a rough estimate. Additional laboratory and theoretical studies are needed to complete and improve the new mid- and near-IR parameters.

2.2.17. C_2H_2 (molecule 24)

Acetylene has been identified in some of the giant planets and Titan since the mid-1940s, and recently has been quantified by the Galileo (http://nssdc.gsfc.nasa.gov/planetary/galileo.html) and Cassini–Huygens missions. Up to now, the data available in GEISA for acetylene isotopologues, namely $^{12}C_2H_2$ and $^{12}C^{13}CH_2$, were limited to the lower energy region of the spectrum, up to 3 μm (note that the C_2HD molecule has a different code, i.e., "48", than the one of C_2H_2, i.e., "24"; see Table 1). This new edition sees the extension of data into the near infrared range for these two isotopologues, with the inclusion of a list of line parameters generated by El Hachtouki and Vander Auwera [246] and Jacquemart et al. [247,248]. In the 1.5 μm region, corresponding to the simultaneous excitation of the symmetric and anti-symmetric C–H stretching modes ν_1 and ν_3, respectively, the line list was created following the high-resolution intensity study [246]. The identification of the lines, their positions and lower state energies are from Kou et al. [249], and the line intensities are calculated using the parameters of Table 7 of [246]. Note that there is a mistake in [246]: the isotopic abundance used for $^{12}C^{13}CH_2$ is a factor 2 too small; it should read 0.02176 instead of 0.01088. As a result, the vibrational transition dipole moments of $^{12}C^{13}CH_2$ listed in Tables 6 and 7, and in Fig. 7 of [246] are a factor 2 too large. The list included in GEISA-09 contains the corrected values. Also, a large update has been performed for the $^{12}C_2H_2$ isotopologue and led to new data in nine spectral regions, namely, in the regions around 3.8, 3, 2.5, 2.2, 1.9, 1.7, 1.5, 1.4, 1.3, 1.2,

and 1 μm. The new line lists are described in details in Refs. [247,248]. Corrections of the 2.5 and 3.8 μm spectral regions of $^{12}C_2H_2$ have also been performed [250,251] and are described in Ref. [247]. Table 8 summarizes the number of new bands (cold/hot in column 2) and transitions (column 3) of the spectral regions added in GEISA-09, together with the intensity ranges (in cm^{-1}/(molecule cm^{-2})) and spectral domains involved (in μm in the first column and in cm^{-1} in the fourth column). It has to be noted that no transitions are unidentified so that the lower state energies are calculated using the spectroscopic constants from Kabbadj et al. [252].

Fig. 8 illustrates the noticeable improvements brought to GEISA-09. The information is displayed as the following: spectral regions corresponding to existing (or in project) C_2H_2 spectroscopic data are identified by vertical rectangles perpendicular to 3 horizontal axes, with spectral region mean value given at the center of each figure; on the 3 horizontal axes are given, downwards: the spectral range extend in two units, μm (top axis) and

cm^{-1} (middle axis); the ΔP polyad series values (bottom third axis; see [247] and Refs. therein for definition) associated with each of the spectral regions mean values identified along the above two axes.

These data improve and summarize the current experimental spectroscopic knowledge on acetylene. Several of the spectral regions involved are of atmospheric, planetary, astrophysical, or meteorological interest, e.g., at 3, 2.2, 1.5, and 1 μm. The study of the region at 7.7 μm, very useful for several applications, is in progress [253]. In this spectral region, intensity measurements were undertaken because the knowledge of C_2H_2 line intensities is important for several applications, especially for astrophysical interest. For example, the acetylene molecule has been observed in the circumstellar envelopes of carbon-rich stars. Using IRS on board the SST telescope, Matsuura et al. [254] detected acetylene bands at 7 and 14 μm in carbon-rich asymptotic giant branch stars in the Large Magellanic Cloud. Around 7 μm, GEISA-09 only contains line positions and intensities that Vander Auwera calculated from his absolute intensity measurements in the $(\nu_4+\nu_5)^0_+$ band [255], for the rotational quantum number J up to 35. But intensities measured in [255] for some lines of the $(\nu_4+\nu_5)^2$ band are not reported in the databases. The temperature of interest for applications being around 500 K [254], the knowledge of intensities in the remaining hot bands is also important. In Ref. [254], Matsuura et al. could not reproduce the shapes that they observed in their IRS-SST spectra around 7 μm because of the lack of data available in the databases.

The GEISA-09 C_2H_2 line list involves 11,340 entries and 118 vibrational transitions against 3115 entries and 29 vibrational transitions in GEISA-03.

2.2.18. C_2H_4 (molecule 25)

Ethylene has been identified in the atmospheres of some of the giant planets and Titan. The spectroscopic information available for this molecule in GEISA-03 dates back to the 1997 edition [7]. It includes the 10 and 3.3 μm spectral regions of the main isotopologue and the 3.3 μm region of $^{12}C^{13}CH_4$ [7]. The 10 μm region of $^{12}C_2H_4$ involves the ν_{10}, ν_7, ν_4 and ν_{12} bands observed near 826, 949, 1027 and 1442 cm^{-1}, respectively. The first

Table 8
Summary of the bands and transitions added for the $^{12}C_2H_2$ molecule in the GEISA-09 database. Reference temperature is 296 K.

| Spectral region (μm)	Number of bands[a] (cold/hot)	Number of transitions[a] (cold/hot)	Spectral domain (cm^{-1})	Intensity range (cm^{-1}/ (molecule cm^{-2}))
3.8[b]	2/3	90/331	2499–2769	10^{-21}–10^{-25}
3[c]	0/18	77 [e]/1971	3139–3398	10^{-20}–10^{-26}
2.5[b]	4/5	450/720	3762–4226	10^{-21}–10^{-27}
2.2[c]	4/4	254/392	4421–4798	10^{-22}–10^{-25}
1.9[c]	7/0	539/0	5032–5567	10^{-24}–10^{-26}
1.7[c]	2/4	175/350	5692–6032	10^{-23}–10^{-26}
1.5[e]	2/2	129/224	6448–6685	10^{-20}–10^{-24}
1.5[c]	4/16	200/1443	6277–6865	10^{-23}–10^{-28}
1.4[c]	4/0	347/0	7042–7476	10^{-22}–10^{-25}
1.3[d]	1/0	51/0	7671–7791	10^{-25}–10^{-24}
1.2[d]	2/0	132/0	8407–8612	10^{-26}–10^{-23}
1.0[d]	3/1	193/108	9516–9890	10^{-25}–10^{-22}

[a] A $^{12}C^{13}CH_2$ data are not mentioned.
[b] New data from Refs. [246,249].
[c] New data from Refs. [247,248].
[d] New data from Ref. [248].
[e] New data from Ref. [246].
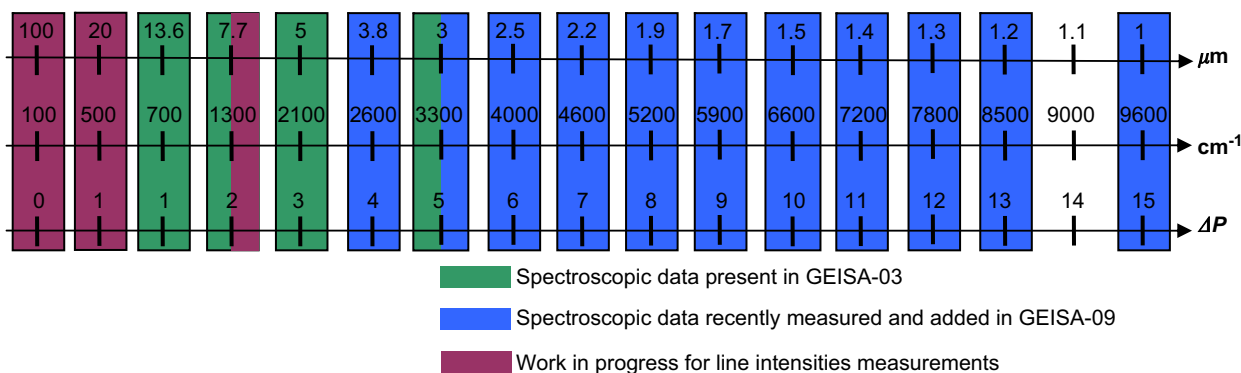
Fig. 8. Improvement of data available in GEISA-09 for the $^{12}C_2H_2$ isotopologue of acetylene. P is the pseudo-quantum number defined for acetylene as: $P=5\nu_1+3\nu_2+5\nu_3+\nu_4+\nu_5$, where ν_1, ν_2, ν_3, ν_4, and ν_5 are the quantum numbers associated with the normal modes of vibration of the molecule in the ground electronic state. Note that the thickness of each box does not represent the frequency span.

three bands are already in GEISA [8], while the ν_{12} band is absent. Recently, Rotger et al. [256] carried out an experimental and theoretical study of line positions and intensities in the ν_{12} band of $^{12}C_2H_4$. 1240 line positions and 871 intensities, measured in a set of Fourier transform spectra recorded at ULB, were fitted using the tensorial formalism developed at ICB with global root mean square deviations of 1.6×10^{-4} cm^{-1} and 1.88%, respectively [256]. Using the refined model thus obtained, the positions, intensities and lower state energies of 5400 lines in the ν_{12} band were calculated. These lines correspond to transitions from levels with $J \leq 40$, and lower and upper state rotational energies up to 1380 and 1510 cm^{-1}, respectively. This initial list of line parameters was complemented with the self- and air-broadening parameters, and the temperature dependence of the air-broadening parameter based on literature [257–260] (see [256] for details). This ν_{12} band line list (5400 entries), whose content is summarized in Table 9, has been added to the present 2009 edition of GEISA.

2.2.19. HCN (molecule 27)

In planetary atmospheres, HCN is an important nitrile, of astrobiological interest in many cases and whose abundance and its variations has been thoroughly studied (see for example Coustenis et al. [226] in the case of Titan). A major improvement has been accomplished on the entire list of lines of HCN. The entire GEISA-03 content (2550 entries in the spectral range 2.870484–18,407.972700 cm^{-1}) has been replaced, in GEISA-09, with new data originating from two different sources, i.e., from Harris [261] and from Maki [262]. The new line list comprises 82,042 entries in the spectral range 0.00636–17,581.009367 cm^{-1}.

Harris's [261] data are related to the main isotopologue H^{12}C^{14}N. Among a total of 108,402 entries 28,624 have been implemented in a supplemental line list because they did not have upper vibrational state identifications. The HCN archive has been obtained from a combination of experimental and theoretical data. The theoretical data were taken exclusively from the line list of Harris et al. [263]. Experimental data were used in preference to the *ab initio* data where they were available. The line list covers the spectral region 0.011561–17,943 cm^{-1}. Hot bands, with a lower vibrational state of 3 quanta of bend, are given for many of the lower

energy transitions. Data are included for transitions up to the (5001) stretching combination bands. The HCN line list was constructed in the following stages:

- *Construction of a list of laboratory determined energy levels*: The available laboratory line measurements [264–270]; for line positions were gathered. From these line position data, a list of HCN energy levels was determined. This was done by using a technique that deviates only slightly from that of Harris et al. [271]; the rotational constants are used to compute energy levels up to an angular momentum quantum number of 60.

- *Construction of a list of laboratory determined line positions*: Using the laboratory determined energy levels it is straight forward to compute a list of line frequencies for dipole allowed transitions. The well known selection rules for dipole transitions require a change in symmetry and allow a change in angular momentum of 0, ± 1. When applied to HCN the allowed transitions form two groups. The first has a change in parity of the vibrational angular momentum with no change in total angular momentum. The second group has no change in the parity of the vibrational angular momentum, but a change of plus or minus one in total angular momentum. For all the dipole allowed transitions between laboratory determined energy levels, line positions were computed by subtracting the lower state energy from upper state energy.

- *Construction of a list of laboratory determined line intensities*: A list of line intensities were computed from laboratory data [272,273,268–270]. These data are usually given in the form of band strengths or dipole moments that are often supplemented with Herman–Wallis factors. From this data, the line intensities of individual lines were computed by using the relevant Höln–London factor and the equation given by Maki et al. [272].

- *Construction of laboratory determined line list*: Experimentally measured line intensities were inserted into the list of laboratory determined energy levels. In this way, a HCN line list is created that is based upon laboratory measurements.

- *Augmentation of the laboratory determined line list with ab initio line intensities*: Many of the intensities for the

Table 9
Summary of the content of the line list for the ν_{12} band of $^{12}C_2H_4$. The intensities are given at 296 K for an isotopologue abundance of 0.9773.

	Value		Value
F-min (cm^{-1})	1380.0239	Int-min (cm^{-1}/(molecule cm^{-2}))	2.764×10^{-37}
F-max (cm^{-1})	1509.9819	Int-max (cm^{-1}/(molecule cm^{-2}))	6.948×10^{-21}
J''_{max}	40	Int-sum (cm^{-1}/(molecule cm^{-2}))	1.549×10^{-18}
$K''_{a\,max}$	20	HWHM$_{air}$ min (cm^{-1} atm^{-1})	0.0813
# lines	5400	HWHM$_{air}$ max (cm^{-1} atm^{-1})	0.0989
n	0.82	HWHM$_{self}$ (cm^{-1} atm^{-1})	0.125

'min' and 'max' represent the minimum and maximum values of the corresponding quantity, respectively; 'F' is the wavenumber; 'J''' and 'K_a''' are rotational quantum numbers; '# lines' is the total number of lines; 'n' is the temperature dependence exponent of the air-broadening parameter; 'Int' is the line intensity; 'Int-sum' is the sum of all the line intensities; 'HWHM$_{air}$' and 'HWHM$_{self}$' are, respectively, the air- and self-broadening parameters.

dipole allowed bands have not been measured. The resulting gap in the laboratory determined line list may only be filled by *ab initio* data.

Many of the transitions in the *ab initio* line list of Harris et al. [263] have been assigned an approximate vibrational quantum number. It has been therefore possible to insert the line strengths from the Harris et al. [263] line list into the GEISA-09 line lists, creating a more complete list of lines.

- *Augmentation with ab initio data and truncation*: The upper and lower energy levels for many strong room temperature lines have not been determined. In order to account for these strong lines, the GEISA-09 line lists for HCN were augmented with purely *ab initio* line position and intensity data from Harris et al. [263]. Finally, to reduce the size of the final line list, a minimum line intensity of 10^{-30} cm^{-1}/(molecule cm^{-2}) was chosen. Lines with intensities below this level were removed from the final line lists.

Maki's data [262] include the isotopologues: H^{12}C^{14}N, H^{12}C^{15}N, H^{13}C^{14}N and a new isotopologue species for GEISA-09, i.e., D^{12}C^{14}N and comprise 5 files in the spectral ranges: 0.014975–175.672283 cm^{-1} (408 entries); 533.819433–895.585448 cm^{-1} (981 entries); 1241.392310–1591.111005 cm^{-1} (709 entries); 2428.365681–3609.137515 cm^{-1} (1710 entries) and 452.016228–2725.191923 cm^{-1}) (452 entries) and 452.016228–2725.191923 cm^{-1} (452 entries) for DCN. Note that DCN is considered as an isotopologue of HCN and not as an independent molecule, because it has the same symmetry as HCN (see Sections 1 and 2).

The origin of the spectroscopic parameters is as the following:

- The values of line positions and their uncertainties were based on a large body of data that included many very accurate microwave and mm-wave measurements [264–281] and also several infrared measurements [265,266,282,283]. For each isotopologue all the wavenumber data were included in a least-squares analysis that made it possible to calculate all the transition wavenumbers, and their uncertainties, given in the GEISA-09 line list. These uncertainties are twice the standard deviation.
- The intensities of the far-infrared transitions are assumed to be well represented by the dipole moment measured for each vibrational state. The best dipole moment measurements are those given by Tomasevich [284] and by DeLeon and Muenter [285] and Ebenstein and Muenter [286]. The dipole moment is very large and any Coriolis-type mixing of intensity with other vibrational states would probably have a very small effect because the vibrational transition moments are small compared to the dipole moment. For that reason it was assumed that the intensities of the far-infrared transitions could be calculated by using the same dipole moment for all values of *J*. The intensities for the ν_2 transitions for H^{12}C^{14}N, H^{12}C^{15}N, and H^{13}C^{14}N were taken from the work of Devi et al. [287]. The same intensity constants were used for the hot bands that

accompany ν_2. For transitions that involve $\nu_2 > 1$, the effects of l-type resonance were included as described by Maki et al. [272]. The intensities of the $2\nu_2$ band and hot band are based on the measurements of Devi et al. [288] and Maki et al. [272,289]. For these transitions the effects of l-type resonance were taken into account [272,289]. The intensities of the ν_1 transition for HCN, H^{13}CN, and HC^{15}N were taken from the work of Devi et al. [290]. The hot bands were assumed to require the same intensity constants, as was verified by the agreement with the measurements of Devi et al. [290]. For the $\nu_1 - \nu_2$ transitions near 2600 cm^{-1} the intensity constants were taken from the measurements of Maki et al. [272]. The intensities of the $\nu_2 + \nu_3$ band near 2800 cm^{-1} came from the work of Maki et al. [289] and the intensities of the $2\nu_2 + \nu_3$ transitions near 3520 cm^{-1} were taken from that same work. In all cases the GEISA-09 archived line intensities of HCN could be used to calculate the intensities for other conditions such as temperature or isotopic composition.

- Except for the regions 2428–2720 cm^{-1} and 3089–3450 cm^{-1}, the air-broadened half-width and air-induced pressure shift coefficients of HCN, and their temperature dependences, were based on the data given by Devi et al. [287] for the ν_2 band of HCN. Except for some transitions that did not include states with $v_1 > 0$, the line parameters for the regions 2428–2720 cm^{-1} and 3089–3450 cm^{-1} were based on the measurements by Rinsland et al. [291]. Their earlier work on the $2\nu_2$ and ν_1 bands of HCN indicated that, aside from the wavenumbers of the transitions and the intensities, there is very little vibrational dependence of the Lorentz pressure-broadened half-width coefficients for HCN. The only parameters that seemed to be dependent on the vibrational state were the air-induced shift coefficients and their temperature dependences. In GEISA-09 those parameters were assumed to have the same values given by Rinsland et al. [291] for all transitions with $v_1 = 1$ in the upper state. The air-induced pressure shift parameters for all transitions with $v_1 = 0$ were assumed to be the same as those measured by Devi et al. [287] for ν_2. Devi et al. [287,288] believed that the parameters were the same, within experimental error, for both ν_2 and for $2\nu_2$ and probably would be the same for the ground state as well. Since GEISA-09 includes transitions involving much higher rotational states, to $J = 60$, than those measured by Malathy Devi et al. [287,288,290] and Rinsland et al. [291] ($J < 34$), the trends in the various line shape parameters were extrapolated beyond reasonable bounds and the uncertainties in the parameters were increased to attempt to encompass reasonable values. All of the broadening and shift parameters for H^{13}C^{14}N and H^{12}C^{15}N were assumed to be the same as for the most common isotopologue, H^{12}C^{14}N. Within experimental error, this assumption was based on a number of measurements made on the $2\nu_2$ band of H^{12}C^{14}N [288].

The air induced pressure shifts for DCN were given values that were 70% of those for HCN in agreement with

a private communication from Smith [292]. That estimate was not based on any real measurements of DCN but rather was based on the trend shown by HCl and DCl. The other parameters for DCN were the same as for HCN, but again that was not based on any measurements.

In a supplementary file (Table S1), the uncertainties in the various parameters are summarized and given along with many other parameters used for processing Maki's new HCN data.

The HCN GEISA-09 line list has been processed as follows: starting from Harris's line list [261], Maki's data [262] have been included, replacing those of Harris's with the same quantum number identifications.

The HCN GEISA-09 line list includes 82,042 entries (775 transitions) against 2550 entries (41 transitions) in GEISA-03.

2.2.20. C_3H_8 (molecule 28)

The intensities of the ν_{26} band transitions were corrected in GEISA-03 line list which includes only the cold band. A PNNL spectrum at 298 K and 0.11 cm^{-1} resolution yields an intensity of 4.27×10^{-19} cm^{-1}/(molecule cm^{-2}) for the whole band, including cold and hot bands [293], a value $(4.33 \times 10^{-19}$ cm^{-1}/(molecule cm^{-2})) that agrees with the earlier measurement of Giver et al. [294] at lower resolution. The vibrational partition function at 296 K is 2.71, so that the intensity of the fundamental cold band should be about $4.27/2.71 = 1.58 \times 10^{-19}$ cm^{-1}/(molecule cm^{-2}). In the GEISA-03 line list, an intensity of 3.76×10^{-19} cm^{-1}/(molecule cm^{-2}) had been set for the cold band, based on some low-resolution spectra that include the hot bands, which is incorrect. The GEISA-03 intensities have thus been multiplied by a factor of $1.58/3.76 = 0.420$ in the GEISA-09 edition (see Nixon et al. [295]). This scaling factor yields an intensity of 1.58×10^{-19} cm^{-1}/(molecule cm^{-2}) at 296 K for the fundamental band, as estimated from the integrated intensity of the whole region in the PNNL spectrum, 4.27×10^{-19} cm^{-1}/(molecule cm^{-2}) including hot bands, divided by the vibrational partition function at 296 K (2.71).

For all bands, a Lorentz half-width coefficient of 0.12 cm^{-1} atm^{-1} at 296 K and a temperature dependence exponent of 0.50 was assumed for all transitions, following N_2-broadening measurements by Nadler and Jennings [296] and Hillman et al. [297]. Propane has been identified in the atmospheres of some of the giant planets and of Titan. New propane data from Flaud et al. [298] including hot bands will be archived in the next version of the GEISA database. The total number of entries (8983) has not been altered since GEISA-03.

2.2.21. C_2N_2 (molecule 29)

A mistake was found in the relative intensities of the hot sub-bands of the ν_5 band listed in GEISA-03 (and in previous versions). More precisely, the intensities of the $(02)^2 \leftarrow (02)^1$, $(03)^1 \leftarrow (02)^2$ and $(03)^3 \leftarrow (02)^2$ sub-bands were two times too big; they have been corrected accordingly in GEISA-09. Following this correction, the total band intensity has been updated by multiplying all line intensities by 0.95, a factor that yields the best agreement with Grecu et al. [299] absolute intensity measurements in the $(01)^1 \leftarrow (00)^0$ cold band, as listed in Table 3 (data for 8 mbar of N_2 pressure) of Ref. [299]. Note that this determination slightly disagrees with the older measurement of the integrated band intensity by Kim and King [300], which would yield intensities 15% larger. For the Lorentz broadening parameter (HWHM), we used the expression "0.12–0.00035m" at 296 K, derived from a fit of the data points in Fig. 5 of Grecu et al. [301]. We arbitrarily assumed a temperature dependence exponent of 0.75 for all transitions listed in GEISA-09. This updated line list will be used for planetary studies in the case of Titan. The total number of entries (2577) has not been altered since GEISA-03.

2.2.22. C_4H_2 (molecule 30)

The diacetylene line list (issued 1982, 1986 [3,4]) still included in GEISA-03 (1405 entries; 5 bands) has been replaced in GEISA-09 by a new line list (119,480 entries; 1509 bands) based on experimental and theoretical studies by Jolly et al. [302]. The lines included belong to the ν_8 and ν_9 bands in the range between 581–730 cm^{-1} and 191–257 cm^{-1}, respectively. The number of lines has been increased from 1405 to 119,480. Due to low energy vibrational modes, the vibrational partition function of C_4H_2 is large ($Q_v = 61$ at 300 K). This means that only 28 % of the molecules are in the ground state at room temperature. In the previous GEISA-03 line list, hot band transitions from three different excited levels were present in the ν_9 band complex but none in the strong ν_8 band complex. The new line list includes hot band transitions with lower vibrational levels up to about 1300 cm^{-1} for the ν_8 band complex and up to about 900 cm^{-1} for the weaker ν_9 band. This was necessary to allow for the inclusion of the contributions of all the hot band transitions with a non negligible intensity at room temperature. The minimum intensity of the lines is 3×10^{-24} cm^{-1}/(molecule cm^{-2}) at 296 K. It was also necessary to extend the quantum identification, in particular the vibrational quantum numbers of both upper and lower levels. All ν values for the nine vibration modes of C_4H_2 have been included in the assignment together with the four ℓ values corresponding to all bending modes (ν_1, ν_2, ν_3, ν_4, ν_5, ν_6, ν_7, ν_8, ν_9, ℓ_6, ℓ_7, ℓ_8, ℓ_9). The new line list is based on a global analysis study as described by Fayt et al. [303]. High resolution data from Arié and Johns [304] were fitted together with other experimental data in the infrared [305,306] and in the microwave domain [307]. Since no new intensity measurements were available, band intensity measurements by Koops et al. [308] were chosen to infer the absolute intensities of the lines.

The improvement of the data is very important in particular for the study of planetary atmospheres. Diacetylene was first detected in Titan's atmosphere by the IRIS [309] spectrograph on board the Voyager spacecraft [310] and is now under close scrutiny by the CIRS spectrometer on board Cassini [226,311,312]. Using the new line list Jolly et al. [302] were able to obtain a new fit of the diacetylene contribution in Titan's atmosphere recorded by Cassini–CIRS resulting in very precise abundance determination and the first detection of the ^{13}C isotopologues of diacetylene in Titan's atmosphere. Recently

detection of the main isotopologue occurred in the atmospheres of both Uranus and Neptune using the Spitzer space telescope [313,314]. Outside the solar system, detection of diacetylene was achieved in the post-AGB object CRL2688 and in the proto-planetary nebulae CRL618 [315]. All detections so far where obtained thanks to the strong ν_8 bending mode centered at 628 cm^{-1}, but the weaker ν_9 bending mode at 220 cm^{-1} was also detected by IRIS and CIRS in Titan's atmosphere.

2.2.23. HC$_3$N (molecule 31)

A line list for cyanoacetylene has been included in GEISA since its first editions [3,4] thanks to Goldman's data [316]. It was already modified in 1990 following a new analysis by Arié et al. [317]. In GEISA-09 a completely new line list, based on experimental and theoretical studies by Jolly et al. [318], replaces the previous version. Lines included belong to the ν_5 and ν_6 band in the range between 463 and 760 cm^{-1}. The number of entries has increased from 2027 (20 bands) in the 1990 version to 179,347 (3302 bands) in GEISA-09. This considerable increase was necessary to take into account all hot band transitions with a minimum intensity of 10^{-24} cm^{-1}/(molecule cm^{-2}) at 296 K. Transitions with lower vibrational levels up to about 1500 cm^{-1} had to be included to take into account all the intensity of the bands. Only few lines belonging to hot band transitions where included [318] in the previous line list. To obtain this new line list, a global analysis was performed fitting simultaneously high resolution data from Arié et al. [317] together with all available experimental data including microwave and infrared measurements. As a result, positions and relative intensities of lines belonging to 123 excited sub-states could be obtained. As for C$_4$H$_2$, the assignment code needed to be modified to take into account levels with high vibrational quanta numbers (ν, ℓ). HC$_3$N possess four stretching and three bending modes. A complete vibrational assignment includes all seven ν values and three ℓ values (ν_1, ν_2, ν_3, ν_4, ν_5, ν_6, ν_7, ℓ_5, ℓ_6, ℓ_7). The absolute intensities of the lines have were derived from a new measurement of the integrated band intensities of ν_5 and ν_6 at 0.5 cm^{-1} resolution as described in Jolly et al. [318].

Cyanoacetylene is a molecule of great interest for planetary atmospheres and in particular for Titan's atmosphere where it has been detected by IRIS [309] during the Voyager mission [310]. The presence of HC$_3$N was confirmed by the ISO space telescope [311] and has been observed in details since 2004 by the CIRS spectrometer on board the Cassini spacecraft. The quality of the new observations by CIRS improves greatly in terms of spectral and spatial resolution on the previous observations. Recently, Jennings et al. [319] used the new line list proposed by Jolly et al. [318] to obtain a good fit of the HC$_3$N feature at 663 cm^{-1} in Titan's spectrum. The contribution of hot bands where clearly observed as a large shoulder on the high energy side of the main feature. The quality of the fit enabled small contributions due to ^{13}C isotopologues of HC$_3$N to be observed, for the first time in the solar system. The contribution of hot bands a cold environment such as Titan' atmosphere is not surprising given that the partition function equals to 1.69 at 200 K, which means that about 40 % of the molecules are still in an excited state.

2.2.24. N$_2$ (molecule 33)

The whole of the line parameters of N$_2$ has been replaced by a new line list provided by Goldman [320]. Improvements to the line parameters mainly include intensities and half-widths. The new intensities are obtained by the use of two works: the work by Goldman et al. [321], where a semi-empirical Herman–Wallis formulation of the vibration–rotation effects on the intensities associated with a final scaling based on observed spectra, and the work by Li and Le Roy [322] based on *ab initio* methods. Values derived by both, Goldman et al. [321] and Li and Le Roy, methods are very similar. However, the *ab initio* matrix elements of Ref. [322] have been adopted for the GEISA-09 line list, because it can be expected that the Herman–Wallis formulation of Goldman et al. yields less accurate values with increasing J. Presently, the GEISA-09 N$_2$ line list is restricted to only the (1–0) N$_2$ band. It should be noted that Li and Le Roy method makes it possible to derive additional line parameters for other bands that may be of atmospheric importance. The absolute accuracy of the Li and Le Roy intensities is estimated to be about 1% by the authors; these new values are still being validated. As described in Ref. [321], the new half-widths are based on available experimental and theoretical studies. As stated in Ref. [321], further extensions are expected in the near future. The total number of entries (120) has not been altered since GEISA-03.

2.2.25. CH$_3$Cl (molecule 34)

The GEISA-03 line list for CH$_3$Cl, which was based on Ref. [323], has been revised using data from Ref. [324]. In particular, previously unassigned vibrational transitions have been identified as belong to $2\nu_3$ and the self-broadened half-widths have also been revised for both isotopologues. The total number of entries (18,344) has not been altered since GEISA-03.

2.2.26. H$_2$O$_2$ (molecule 35)

The H$_2$O$_2$ (hydrogen peroxide) data previously archived in GEISA-03 (100,781 entries; 2 bands), for the ν_6 band in the 7.9-μm region, have been completely replaced, leading to improved line positions and intensities in GEISA-09 (126,983 entries; 130 bands). Indeed, this new list is more complete as it includes several hot torsional-vibration sub-bands of the ν_6 band (up to the $n=2$ torsional quantum number), instead of only the two main torsional components of the ν_6 band (in the $n=0$, $\tau=1$ and $n=0$, $\tau=3$ torsional quantum numbers). In addition the new line positions are more accurate since the vibration–torsion–rotation coupling the energy levels from the 6^1 state with those from the 2^1, 3^1 and ground vibrational states were accounted for. The line intensities are also more accurate as these parameters are based on new line intensity measurements and on a sophisticated theoretical treatment which account for the torsional effects. The sources of the new data are Perrin et al. [325] and Klee et al. [326].

2.2.27. H$_2$S (molecule 36)

No new line list has been implemented in GEISA-09 for hydrogen sulfide, but updates occurred for air- and self-broadened pressure half-widths. Where available, measured values have been adopted – those from Sumpf et al. [327], Kissel et al. [328,329] and Waschull et al. [330], for air-broadened half-widths and those from Refs. [327,330] and from Sumpf [331] for self-broadened half-widths. Otherwise, default values of 0.074 and 0.1580 have been assigned to air- and self-broadened half-widths, respectively. These values have been obtained as averages of the ones previous quoted in the above reference. The total number of entries (20,788) has not been altered since GEISA-03.

2.2.28. HCOOH (molecule 37)

GEISA-09 contains a complete replacement and enhancement of the spectroscopic information provided for formic acid (62,684 entries; 8 bands). Indeed, until GEISA-03, only parameters for 3388 lines of the ν_6 band of trans-H^{12}C^{16}O^{16}OH near 9 μm were available. They originated from the work of Goldman and Gillis [332]. The sum of the line intensities was equal to 1.757×10^{-17} cm^2/(molecule cm^{-1}) at 296 K, determined using a Fourier transform laboratory spectrum recorded at the University of Denver.

GEISA-09 provides spectroscopic information for trans-H^{12}C^{16}O^{16}OH in three spectral regions: the pure rotation spectrum in the far infrared, the ν_6 and ν_8 bands near 9 μm, and the ν_3 band around 5.6 μm.

Far-infrared Fourier transform spectra of the pure rotation spectrum of formic acid were recorded in the range from 20 to 130 cm^{-1} and analyzed by Vander Auwera [333]. To provide an accurate set of parameters describing the rotational structure of the ground state of trans-H^{12}C^{16}O^{16}OH, 592 far-infrared line positions were fitted together with 372 microwave lines [334–336]. The resulting constants and known dipole moment [337] were then used to calculate the positions, intensities and lower state energies of 6808 a- and b-type pure rotation lines observed between 10 and 100 cm^{-1}, originating from J/K_a levels ranging from 0/0 to 70/17, corresponding to $\Delta K_a=0, \pm 1$ and $\Delta K_c= \pm 1, \pm 3$, and being stronger than 4.0×10^{-26} cm^{-1}/(molecule cm^{-2}) at 296 K. The line positions have been substantiated by a study of Winnewisser et al. [338]. Note that the intensities listed in GEISA-09 are a factor 4 larger than those listed in Table II of [333], because of the oversight of the nuclear spin degeneracy of the hydrogen in the latter. To complement these data, the self- and air-broadening parameters, and temperature dependence exponent of the air-broadening parameter of all the lines were set to the same values as applied to the ν_6 and ν_8 bands (see here below).

The 9 μm spectral region was updated according to the recent work by Vander Auwera et al. [339]. They reported absolute line intensities measurements for the ν_6 and ν_8 bands using Fourier transform spectroscopy, taking the existing dimer (HCOOH)$_2$ into account in the analysis. They showed that the intensities reported by Goldman and Gillis [332], and therefore in GEISA-03, were a factor of about 2 lower than the average of the other existing laboratory measurements, and than theoretical calculations. Relying on results of that work, Perrin and Vander Auwera [340] generated a new set of 49,625 line positions, intensities and lower state energies covering the range from 940.20 to 1244.41 cm^{-1}. To complete these data, the self- and air-broadening parameters, and the temperature dependence exponent of the air-broadening parameter of all the lines were set to 0.32 cm^{-1} atm^{-1} [339], 0.101 cm^{-1} atm^{-1} [341] at 296 K, and $n=0.75$, respectively. With a sum of the line intensities equal to 3.51×10^{-17} cm^{-1}/(molecule cm^{-2}) at 296 K and a three-fold increase of the wavenumber coverage, this new list was shown to provide a significantly improved modeling of the ν_6 spectral region of formic acid [340].

Using high-resolution Fourier transform spectra of trans-HCOOH recorded at 5.6 μm, Perrin et al. [342] carried out an extensive analysis of the strong ν_3 fundamental band at 1776.83 cm^{-1}, starting from results of a previous analysis [337]. As pointed out in the literature, the ν_3 band is significantly perturbed by resonances with numerous dark bands. Perrin et al. [342] were able to assign series belonging to the $\nu_5+\nu_7$, $\nu_5+\nu_9$, $\nu_6+\nu_7$ and $\nu_6+\nu_9$ dark bands, located at 1843.48, 1792.63, 1737.96 and 1726.40 cm^{-1}, respectively. The model used to calculate energy levels accounted partly for the observed resonances, and reproduced most of the observed line positions, within experimental uncertainties. Absolute line intensities were also determined in that work with an accuracy estimated to 15% [342]. From these results, the first database for the 5.6 μm region of the formic acid spectrum was built. It includes 6251 lines belonging to the ν_3, $\nu_5+\nu_7$, $\nu_5+\nu_9$, $\nu_6+\nu_7$ and $\nu_6+\nu_9$ bands of trans-H^{12}C^{16}O^{16}OH with $J \leq 66$, $K_a \leq 18$, and lower and upper states energies up to 2700 and 3600 cm^{-1}, respectively. Table 6 of Ref. [342] details the contents of the line list.

2.2.29. SF$_6$ (molecule 39)

Sulfur hexafluoride is a strong greenhouse gas whose concentration in the atmosphere should be monitored and limited, according to the Kyoto protocol [343]. The spectrum of SF$_6$ is, however, poorly characterized, (at least for atmospheric purposes). The main reason is that this molecule is heavy, which has two important consequences for its spectrum: (i) there are low-lying bending vibrational modes producing a lot of hot bands and (ii) the spectrum is very dense so that even at high resolution there is virtually no isolated line, each line being a cluster of many overlapping transitions. The second point renders the determination of line intensities and, thus, of dipole moment derivatives, very difficult.

Although at lot of work remains to be done on this molecule, many vibrational bands have been investigated in the past years at ICB [344]. A new line list for the ν_3 stretching and the ν_4 bending fundamental regions has been produced. The only partial knowledge of the inactive ν_6 lowest fundamental still prevents a full hot band analysis, especially for $\nu_3+\nu_6-\nu_6$. However, the lower spectral density in the ν_4 region has allowed the detailed investigation of $\nu_4+\nu_6-\nu_6$ [345]. In the case of ν_3 itself, which is the strongest absorption band, a very detailed line position analysis exists, based on various

high-precision experimental data (FTIR but also saturated absorption and IR–IR double resonance). In this case, the resulting accuracy for line positions is estimated to be better than 0.001 cm^{-1} up to $J=100$. For the ν_4 fundamental, the accuracy for line positions is around 0.001 cm^{-1} up to $J=100$ and for the $\nu_4+\nu_6-\nu_6$ hot band it is *ca.* 0.002 cm^{-1} up to $J=65$. The J values given above correspond to the highest values for the assigned lines. The accuracy may decrease quickly when extrapolating to higher J values, although this is difficult to estimate in a quantitative manner.

As mentioned above, the question of line intensities in the case of SF_6 is a difficult problem. To generate the present list, we used the best-known dipole moment derivative values found in the literature [346,347]. We checked with the previous list for ν_3 from GEISA-03 that we obtain exactly the same intensities in this case. However, we globally estimate the line intensity accuracy to be no better than 20 %, in the absence of precise intensity measurements on isolated lines.

Analyses and calculations have been performed with the HTDS software [348]. The whole original ICB line list contains 30,106,484 entries. It has been reduced by applying intensity cutoff in suitable for SF_6 impact signatures in most atmospheric radiative transfer calculation. The applied intensity cutoff, in cm^{-1}/(molecule cm^{-2}) at 296 K, had the value 10^{-24} for band ν_3 (46,031 lines retained among 2,826,164 in the original list) and 10^{-23} for bands ν_4 (10,986 lines retained among 2,657,543) and $\nu_4+\nu_6-\nu_6$ (35,381 lines retained among 24,622,777). As a consequence, the new line list for SF_6 in GEISA-09 (spectral range 580 to 996 cm^{-1}) contains a total number of entries reduced to 92,398 lines (6 bands). For the whole line list, a default value of 0.50 cm^{-1} atm^{-1} has been given to the air-broadening pressure half-widths and of 0.65 to the associated temperature dependence coefficient n.

2.2.30. C_3H_4 (molecule 40)

Line parameters for two CH_3C_2H (C_3H_4) bands (the ν_{10} at 331 cm^{-1} and the ν_9 at 639 cm^{-1}) were provided by Graner (private communication), based on constants of Pekkala et al. [349] for the frequency calculations and Blanquet et al. [350] for intensities of individual lines. For the ν_{10} band, the study of a first spectrum at a resolution of 0.0056 cm^{-1} by Horneman et al. [351] was followed by the analysis of a 0.002 cm^{-1} resolution spectrum by Graner and Wagner [352]. The description of the ν_{10} was accomplished and, in addition, two main hot bands were also provided [352,349]. In the 16-μm region, the ν_9 fundamental band was recorded at 0.003 cm^{-1} resolution and a full analysis was completed by Pekkala et al. [349] and Pekkala [353].

The extraction of intensities from these high resolution spectra was not an easy task. As a consequence, global intensities from the literature were used to predict individual line intensities, as explained by Horneman et al. [351].

This dataset was first applied to Titan in Coustenis et al. [354]; see Fig. 11a therein. Both propyne bands were detected on Titan and the more accurate spectroscopic parameters are presented GEISA-09 which is updated for the first time since the 1992 edition. These parameters

allow for a better determination of the molecule abundance since it can now be separated from the nearby C_4H_2 band [312]. The C_3H_4 GEISA-09 line list includes 19,001 entries (22 transitions) against 3390 entries (1 transition) in GEISA-03.

The CDMS catalog contains entries for $\nu=0$, $\nu_{10}=1$, ν_{10} and ν_9 based on [355,356]. A future update of GEISA shall consider these entries or may even be based on [357].

2.2.31. $ClONO_2$ (molecule 42)

The rotational transitions from 0 to 45 cm^{-1} for the ground and $\nu_9=1$ vibrational states have been included in the GEISA database for the first time.

The predicted transitions for each isotopologue are based on the spectroscopic constants derived from the analyses of millimeter and submillimeter wave rotational spectra in Refs. [358–360]. All predictions were calculated using the SPCAT program package ([192]; http://spec.jpl.nasa.gov/ftp/pub/calpgm/spinv.pdf) for a temperature of 296 K.

From Ref. [361], isotopic abundances of 0.74957 and 0.23969 and rotational partition functions of 4,788,362 and 4,910,202 were used in the predictions for the 35 and 37 chlorine isotopologues, respectively. A vibrational partition function of 4.02 [362] was used that includes the ν_9 vibrational mode that has a band origin near 121 cm^{-1}. The rotational spectra from the ground and $\nu_9=1$ states account for about 39% of the thermally populated states. Future updates will include the addition of pure rotational spectra from higher lying vibrational states and the infrared simulation of the ν_6 fundamental band and the first two associated hot bands for each isotopologue in the 22 μm region. Due to the low lying ν_9 mode, there will be significant hot band intensity contributions to each infrared band.

The $ClONO_2$ GEISA-09 line list includes 356,899 entries (7 bands) against 32,199 entries (3 bands) in GEISA-03.

2.2.32. CH_3Br (molecule 43)

CH_3Br contributes significantly to ozone depletion since it is dissociated by UV radiation producing Br radicals who catalyze the destruction of ozone [363]. This molecule is the major contributor to bromine in the stratosphere and the main organobromide in the lower atmosphere. The bromine atoms are 50 to 60 times more destructive of ozone than the chlorine atoms coming from the chlorofluorocarbons compounds (CFCs) [364].

Methyl bromide spectroscopic line parameters are present for the first time in GEISA-09 (36,911 entries; 6 bands). Two line lists of both isotopologues have been generated: one around 10 μm for the ν_6 band [365], and the other around 7 μm for the interacting ν_2 and ν_5 bands [365–367]. In natural abundances, methyl bromide is composed of 50.54% of $CH_3^{79}Br$ and 49.46% of $CH_3^{81}Br$. Note that the broadening coefficients and its temperature dependence obtained in Refs. [365,366] around 10 μm have been used for the 7μm spectral region. Air-broadening coefficients have been deduced from nitrogen-broadening coefficients using a constant scaling as for the H_2O molecule, for which air-broadening coefficients could be obtained by multiplying N_2-broadening coefficients by the value 0.9 as suggested in Refs. [369–371].

Since CH_3Br is chemically and structurally related to CH_3Cl, we proposed to use the ratio $HWHM_{air}/HWHM_{N_2}=0.96$ in order to convert the N_2-broadening to the air-broadening. This value comes from the ratio $HWHM_{N_2}/HWHM_{O_2}=1.25$ obtained by averaging measurements of CH_3Cl from Refs. [372,373]. Note that this result is quite similar to what has been proposed for ozone in Ref. [374]. This procedure is approximate since $HWHM_{N_2}/HWHM_{O_2}$ varies from line to line. However it is expected to be accurate within a few percent which is sufficient in view of the experimental uncertainties and the accuracy of the calculations. Also, the air-width temperature dependence has been added in both spectral regions, using the same values as those obtained for the N_2-width temperature dependence (see Eq. (5) and text in Ref. [366]). Accuracies and details of the line parameter calculation can be found in Refs. [366,368]. In the absence of experimental or theoretical results for air-pressure shifts for CH_3Br, the GEISA standard missing value of $-9.999999\ cm^{-1}\ atm^{-1}$ has been used for all transitions. Note also that line mixing effects have been observed and modeled in the strong Q-branches between 220 and 300 K [375,376]. Line mixing parameters (for direct calculation or Rosenkranz profile [377]) are available upon request to the authors.

2.2.33. CH_3OH (molecule 44)

The importance of methanol microwave, millimeter wave, sub-millimeter wave and terahertz spectroscopy to space science and astrophysics can be traced back to several decades ago when methanol was first discovered in interstellar clouds and star forming regions [378]. The rich variety of torsion–rotational methanol transitions falling in the frequency bands accessible to most radio and sub-millimeter wave telescopes and notably the new Herschel (http://www.esa.int/SPECIALS/Herschel/SEMB M00YUFF_0.html), ALMA (http://www.eso.org/sci/facil ities/alma/) and SOPHIA (http://www.sofia.usra.edu/) observatories, leads to a dense and detailed interstellar spectrum and demands an accurate knowledge of the methanol energy levels so that the interstellar "methanol weeds" can be removed. The infrared spectroscopy of methanol has also acquired renewed importance in wide areas of application in recent years, such as the recent observations of the 10 μm feature in forest fire [379], the influence of biogenic emissions on upper-tropospheric methanol as revealed from space [380], observations in the terrestrial atmosphere [381], the 3 μm features in several comets and the icy mantles of interstellar dust grains [382–385]. These applications require reliable simulation of the absorption band profiles at any prescribed conditions of temperature and density. Achieving reliable calculations in turn requires detailed understanding of the vibration–torsion–rotation structures of the bands, in terms of both the line positions and intensities.

A methanol line list (19,897 entries; 16 bands) is included for the first time in the GEISA database; it consists of two regions, 0.019265–$33.336958\ cm^{-1}$ and 911.608420–$1407.205540\ cm^{-1}$. The first region is based on a global analysis of the first two torsional states of $v_{12}=0$, and 1 and $J_{max}=20$ [386] which led to a prediction

list to $J_{max}=26$ at a frequency cutoff of 1 THz [387]. Line strengths in that list were calculated using permanent dipole moment values of $\mu_a=2.999 \times 10^{-30}\ C\ m\ (0.899\ D)$ and $\mu_b=-4.803 \times 10^{-30}\ C\ m\ (-1.44\ D)$. The list was originally designed at that time to assist the radio astronomy community. More recently, an expanded global analysis with $v_{12}=0, 1, 2$ and $J_{max}=30$ has been published [388]. The second region was built on extensive Fourier transform spectroscopic analyses of methanol spectra in the 10 μm region ([389] and references therein). Due to strong vibration–torsion and rotational interactions, the transitions observed in the 10 μm region arise not only from the v_8 CO-stretch fundamental band, but also from v_8 hot bands and nearby vibrations such as v_5, v_6 and v_7 entering in the region with different v_{12} torsional combinations. Within the limits of the isolated vibration–torsion–rotation band model, the predicted positions and intensities unfortunately did not reproduce the spectrum within experimental uncertainties for v_8 and v_8+v_{12}. In addition to strong and medium intensity transitions of the v_8 and v_8+v_{12} bands, there are many additional transitions appearing with visible intensity in the spectral window; these were identified as belonging to the $v_8+2v_{12}-2v_{12}$, v_7—ground, $v_7+v_{12}-v_{12}$, v_6-v_{12}, v_6-2v_{12}, $v_6+v_{12}-v_{12}$, v_5-2v_{12}, $3v_{12}$—ground and $4v_{12}$—ground bands. Many of these transitions are perturbation-induced, gaining intensity via anharmonic and Coriolis interactions with the strong v_8 vibration in the region. Thus, with an isolated-band approach, these transitions cannot be modeled in either position or intensity. Therefore, it has been chosen simply to include empirical positions and intensities of these features whenever available in our database.

Arriving at the ultimate 10 μm region database, several steps were taken to ensure that the contents reflected the best knowledge of the molecule at the present time (i.e., with observed positions and intensities substituted for predictions whenever available). More specifically, (i) line positions (for 95% of the transitions) were replaced with observed values from the NRC FT spectra except for the congested Q-branch region, in which Q transitions were recomputed from the corresponding observed R- and P-transitions using averaged upper-state term values; (ii) intensities were replaced with measured intensity retrievals from the highest density Kitt Peak spectrum (1.95 Torr, 10 cm). With the predicted database as the input, over 13,500 new intensities were retrieved between 970 and $1085\ cm^{-1}$, including a few lines not currently assigned. Weak lines in the prediction that could not be discerned in the new effort were added to the database with a "default intensity" in order to maintain a complete record of known assignment; the very low intensity value of $10^{-26}\ cm^{-1}/$ (molecule cm^{-2}) was chosen so that these unmeasured transitions would not contribute extra absorption in the radiative transfer calculations for most applications.

The lower state transition energy is referenced to $128.1069\ cm^{-1}$ for the $K=0$ *a* level, the temperature dependence of width have been attributed the 0.75 default value and the air pressure shift of the line transition has the GEISA-09 standard missing value (i.e., -9.999999). The vibrational index are: Ground, v_{12}, $2v_{12}$, $3v_{12}$, $4v_{12}$, v_8,

$\nu_8+\nu_{12}$, $\nu_8+2\nu_{12}$, ν_7, $\nu_7+\nu_{12}$, ν_6, $\nu_6+\nu_{12}$, ν_5 for upper and lower states and the torsional symmetry A, E_1 or E_2; the overall rotational angular momentum J involves component K along the molecular a-axis. Resolved K-doublets of A symmetry have an additional $\pm$ to distinguish the A^+ or A^- component of the doublet.

2.2.34. NO$^+$ (molecule 45)

The data on the nitric oxide molecular ion NO$^+$ are debuting in GEISA-09.

The line positions of the GEISA-09 NO$^+$ line list are issued of a paper by Lopez Puertas et al. [391] and associated subsequent publications: using high resolution (0.035 cm^{-1} unapodized) spectra of the Earth's atmosphere, recorded by the MIPAS experiment, line positions of rovibrational NO$^+$ transitions have been obtained with an unprecedented accuracy. As a consequence, comparisons with the HITRAN 1996 line list [390] have shown that the spectral line positions of the NO$^+$ (1–0) and of the NO$^+$ (2–1) rovibrational bands are shifted by about 0.15 cm^{-1} and approximately 0.05–0.1 cm^{-1}, respectively.

For $J'' \leq 40$, the archived line positions have been derived from a set of Hamiltonian constants for NO$^+$ obtained from a fit of the MIPAS data together with the existing microwave and infrared data (see [391] for details). Accurate frequencies for high-J values cannot be predicted with the use of those constants; consequently, for J'' greater than 40, line positions have been derived from the former HITRAN 1996 archive [390].

It has to be noted that the newly generated NO$^+$ GEISA-09 line list by Flaud [391] (1206 entries; 6 bands, in the spectral range 1634.831–2530.462 cm^{-1}), is similar with the HITRAN-08 one [13]; this includes, in particular, the intensities, kept from Werner and Rosmus [390], and the default value 0.06 cm^{-1} chosen for the air-broadened half-widths, as well.

It is clear that new high resolution spectra of the NO$^+$ species are needed in order to improve its spectral parameters.

2.2.35. HNC (molecule 46)

Although HCN and HNC actually lie on a single potential energy surface, they are separated by a significant barrier [392]. Within GEISA-09 they are treated as separate species and HNC is a new molecular species for this new edition of GEISA. HNC is the less stable isomer but is known to be overabundant compared to HCN in the interstellar medium (e.g., [393]). Furthermore the partition function of HNC increases much more rapidly with temperature than that of HCN meaning that at temperatures of about 2500 K, the equilibrium abundance of HNC should be about 20% of HCN [394]. The spectrum of HNC has been identified in carbon stars Harris et al. [395].

The GEISA-09 HNC line list was compiled by Harris [261] for the main isotopologue H^{14}N^{12}C. Among an initial total of 9117 entries, in the spectral range 0.216955–12,594.316928 cm^{-1}, 3498 are included only in a supplemental line list because they did not have upper vibrational states identification. Consequently, the final GEISA-09 archived HNC data comprises 5619 lines (84 bands) in the spectral range 0.216955–4814.904168 cm^{-1}.

As for HCN, the GEISA-09 HNC line list was constructed from a combination of experimental and theoretical data. The theoretical data are taken exclusively from the line list of Harris et al. [263]. Experimental data are used in preference to the *ab initio* data when they are available. The GEISA-09 HNC line list is less extensive than that for HCN; it is also less accurate since there is substantially less laboratory data to base it on. The spectral region covered for HNC is 0.217–12,594 cm^{-1}. Hot bands with a lower vibrational state of 2 quanta of bend, are given for most of the transitions.

The GEISA-09 HNC line list was constructed in the following stages:

- *Construction of a list of laboratory determined energy levels*: The laboratory line frequency measurements of Northrup et al. [396] were used to determine a set of experimental HNC energy levels. This was done by using a technique that deviates only slightly from that of Harris et al. [271]; the rotational constants are used to compute energy levels up to an angular momentum quantum number of 60.

- *Construction of a list of laboratory determined line positions*: Using the laboratory determined energy levels it is straight forward to compute a list of line positions for dipole moments allowed transitions. The well known selection rules for dipole moments transitions require a change in symmetry and allow a change in angular momentum of 0, ± 1. When applied to HNC the allowed transitions form two groups. The first has a change in parity of the vibrational angular momentum with no change in total angular momentum. The second group has no change in the parity of the vibrational angular momentum, but a change of plus or minus one in total angular momentum. For all the dipole moments allowed transitions between laboratory determined energy levels, line positions were computed by subtracting lower state energy from upper state energy.

- *Construction of a list of laboratory determined line intensities*: A list of line intensities was computed from laboratory data given by Nezu et al. [397]. These data are given in the form of band dipoles that are supplemented with Hermann–Wallis factors. From these data, the intensities of individual lines were computed by using the relevant Höln-London factor and the equation given by Maki et al. [272].

- *Construction of laboratory determined line list*: Experimentally measured line intensities were inserted into the list of laboratory determined energy levels. In this way, an HNC line list based upon laboratory measurements was created.

- *Augmentation of the laboratory determined line list with ab initio line intensities*: Many of the intensities for the dipole allowed bands have not been measured. The resulting gap in the laboratory determined line list may only be filled by *ab initio* data.

  Many of the transitions in the *ab initio* line list of Ref. [263] have been assigned an approximate vibrational quantum number. We were therefore able to

insert the line strengths from Ref. [263] line list into the GEISA-09 final HNC file, creating a more complete list of lines.

- *Augmentation with ab initio data and truncation*: The upper and lower energy levels for many strong room temperature lines have not been determined. In order to account for these strong lines the HNC GEISA-09 line list was augmented with purely *ab initio* line frequency and intensity data from Ref. [263]. Finally, 3498 entries have been suppressed from the original file because of lack of upper vibrational quanta identification.

Recent reports on emission spectra of HNC [398,399] not only provide many more experimental lines, but also used in the analyses comparatively recent pure rotational data [400,401]. These results will be used in updated CDMS entries and may also be used in future GEISA updates.

2.2.36. C_6H_6 (molecule 47)

Benzene (C_6H_6) (benzol, benzin) is an aromatic hydrocarbon produced in the Earth's atmosphere and is found in air due to emissions from the burning of coal and oil and also from gas stations, and from motor vehicle exhaust. Benzene is also of importance for astronomical studies. The high abundances of N_2 and CH_4 in the atmosphere of Titan, Saturn's largest moon lead to high abundances of nitrogen and carbon compounds, and its atmosphere and smog-like haze are of particular interest because of its similarity to the atmosphere that may have existed on Earth before life began. Polycyclic Aromatic Hydrocarbons (PAHs) are important interstellar species, and their precursor benzene (C_6H_6) has been detected in our solar system, in particular on Titan. Benzene was identified on Titan through ISO and Cassini/CIRS data [312]. It has also been measured in the upper atmospheres of Jupiter at midlatitudes and Saturn (disk average) [402].

Benzene is introduced in GEISA-09 for the first time. Line parameters for the ν_4 band of benzene near 678 cm^{-1} were provided by Dang-Nhu (private communication) and generated from the molecular constants and band strength compiled in Dang-Nhu and Plíva [403].

Two approaches were used to determine the absolute intensities. Dang-Nhu et al. [404] made a line-by-line study, using a very high resolution tunable diode laser which yielded 30 individual intensities, from which a vibrational strength was derived (see also [403]). At the same time, a study at medium resolution (1 cm^{-1}) performed on spectra recorded at LISA by Raulin et al. [405] provided the integrated band intensity of benzene in the spectral region which was related to the previous one through the vibrational partition function.

This dataset (9797 lines) was first applied to modeling of the Titan spectrum in Coustenis et al. [354,318]; see Figs. 5, 6, 8, 9 and 11a therein.

2.2.37. C_2HD (molecule 48)

The line list of monodeuterated acetylene is new in the GEISA database. The need for a line list of deuterated acetylene arose following the recent detection of this isotopologue in the atmosphere of Titan by Coustenis et al. [406]. The line list has been assembled by a joint effort of several laboratories [407]. It is based on new band intensity measurements performed at a resolution of 0.5 cm^{-1} in France (LISA) and a new analysis done in Belgium (ULB, UCL) of the high resolution spectra of C_2HD recorded in Italy (University of Bologna) [407]. The new global fit was obtained by using the computer package developed in UCL and dedicated to both energy and intensity treatments [408,409]. Included lines belong to both bending modes ν_4 and ν_5 which could be detected on Titan thanks to their strong Q-branch at 519 and 678 cm^{-1}, respectively. Lines belonging to both strong stretching modes ν_1 and ν_3 centered at 3335.6 and 2583.6 cm^{-1}, respectively, are also present in the new line list. A total of 15,512 lines (348 bands) are present in the list with a minimum intensity of 1.6 10^{-25} cm^{-1}/ (molecule cm^{-2}) at 296 K. All five vibrational modes and both ℓ values are used in the vibrational assignment of the upper and the lower level of each transition (ν_1, ν_2, ν_3, ν_4, ν_5, ℓ_4, ℓ_5). The line broadening parameters of C_2HD have been assumed to be equal to those of the most abundant C_2H_2 isotopologue.

The study of deuterated acetylene in planetary atmospheres is of great importance and in particular the determination of D/H isotopic ratios. The recent detection of $^{12}C_2HD$ in Titan allowed a value of D/H [406] to be determined. This could be compared to the values obtain for CH_4 (CH_3D) and H_2 (HD) as C_2HD is the third deuterated molecule to be detected in Titan's atmosphere.

2.2.38. CF_4 (molecule 49)

In the previous editions of GEISA, tetrafluorocarbon (CF_4) was referred to as CFC-14 and was only included in the cross-sections part [410], with no line list. It is, however, a strong greenhouse gas of both anthropogenic and natural origin [411,412]. Its concentration is increasing in the atmosphere [413,414]. Although it has been identified and measured from balloon-borne measurements [415], its spectroscopy remains only very patchily investigated, for much the same reasons as for SF_6 (presence of many hot bands, dense spectrum with clustered lines). Its infrared spectrum is dominated by the strong ν_3 stretching fundamental band at 1282 cm^{-1} [415], this band being strongly coupled with the first overtone of the ν_4 bending mode.

The ν_4 (around 15.8 μm) and $2\nu_4/\nu_3$ regions (around 7.3 μm) have been recently reinvestigated, thanks to several new Fourier transform infrared spectra recorded at a resolution of 0.003 cm^{-1}. Just as in the previous work of Gabard et al. [416], a simultaneous analysis of the ground state, ν_4, ν_3, $2\nu_4$ and $\nu_3 - \nu_3$ bands was performed, thanks to the XTDS and SPVIEW programs [417] developed by the ICB group. Compared to Ref. [416], the present work extends the analysis to much higher J values (70 instead of 40 for ν_4 and 63 instead of 32 for the $2\nu_4/\nu_3$ dyad). As for absorption intensities, it was possible to go a bit further than for SF_6. By calculating synthetic spectra for exactly the same physical conditions as for the experiment, it was possible to fit the ν_4 and ν_3 dipole-moment derivatives. The results compare very

well to the literature values of Papoušek et al. [418]. The details of this new analysis will be given in a forthcoming paper [419].

This analysis allowed to generate the first reliable line list for $^{12}CF_4$ that covers the spectral ranges 600 to 670 cm^{-1} (ν_4) and 1276 to 1290 cm^{-1} ($2\nu_4/\nu_3$). Tetra-fluorocarbon becomes GEISA-09 molecule number 49. The precision for line positions is estimated to be around 0.001 cm^{-1}, up to $J=60$. The intensity accuracy, however, may not be better than 20%, especially for the high-J regions. Line-broadening coefficients were taken from Ref. [420]. The newly archived CF_4 line list comprises 60,033 entries (5 bands) in the spectral range 594-1312 cm^{-1}.

2.2.39. CH_3CN (molecule 50)

CH_3CN (methyl cyanide, acetonitrile, ethanenitrile), a molecule of astronomical and atmospheric importance, is a new entry in GEISA-09. Line parameters of CH_3CN are needed for planetary studies because this species has been observed, by heterodyne millimeter wave spectro-scopy from the ground [421], on Titan. The dissociation of N_2 leads to the formation of nitriles such as HCN, HC_3N and C_2N_2, identified for the first time by the Voyager probes in the earlier 1980s. One of the goals of the Cassini–Huygens mission, investigating the Saturn system between 2004 and 2008, was to map all the photochemi-cal compounds, hydrocarbons and nitriles, in order to better understand the photochemical cycle of Titan and its coupling with the dynamics and the production of organic aerosols [312,422]. CH_3CN spectra have been observed in comets [423], and in interstellar molecular clouds [424], as well.

CH_3CN is also a gas present in the Earth's atmos-phere with a lifetime of several months, mainly emitted through forest fires and then probably deposited in the oceans. Since 1993, this molecule has been classified as an atmospheric pollutant and is the object of a number of varied chemical, biological and atmospheric [425–428] studies.

The GEISA-09 CH_3CN line list consists of spectroscopic parameters for two different regions.

Region 1: as the result of a multispectrum nonlinear least squares fitting technique applied to measure accu-rate zero-pressure line center positions, Lorentz self- and N_2-broadening coefficients and self- and N_2-pressure-induced shift coefficients, 3571 features have been archived in the ν_4 parallel band region between 890 and 946 cm^{-1}. Published line positions and intensities from Rinsland et al. [429] have been supplemented by unpub-lished measurements from the same dataset, as well as selected values from preliminary Hamiltonian calcula-tions. Only lines with intensities greater than 10^{-24} $(cm^{-1}/(molecule\ cm^{-2}))$ at 296 K are included. The spec-tral region from 918.5 to 920.3 cm^{-1} (containing the Q branch and the P1 and P2 manifolds) proved too dense to measure directly and so these parameters are represented by 326 calculated transitions of ν_4. Some 2243 lines are given without quantum identifications; many are thought to be hot band lines involving yet unanalyzed upper state levels of $\nu_4+\nu_8$. The lower state energy of these uniden-tified lines is set to the GEISA-09 standard missing value,

i.e., -0.9999. It should be noted that a number of hot-band lines are not included in the list; this is most noticeable at the hot band Q branch near 924 cm^{-1}. Measured self-broadening coefficients were available, and identified lines with the same K quantum number and the same or very close m were assigned approxi-mately the same or interpolated values. The total number of lines with self-broadening assigned in this manner is 2185. For the lines lacking measured or estimated Lorentz half-width coefficients for air- and self-broadening, default values of 0.14 and 1.5 $cm^{-1}\,atm^{-1}$ at 296 K were used, respectively (obtained as an approximate average of measured values). The measured N_2 shifts [429], where available, were inserted for air shifts. Unmeasured pres-sure shifts are set to zero, the approximate average of the measured values. There are no measurements of the temperature dependence of the Lorentz half-width in air and only one in N_2 [430], so the default n is set to the single measured N_2 value of 0.72.

Region 2: an excerpt in the spectral range of 970–1650 cm^{-1} of an empirical "pseudo-line-list" (total extent 870–1650 cm^{-1}), where the ν_7 band around 1050 cm^{-1} and the ν_3, ν_6, $\nu_7+\nu_8$ bands around 1450 cm^{-1} are located. This represents a total of 13,601 entries. A pseudo-line list, typically derived by fitting equally spaced "pseudo-lines" to laboratory spectra, is not intended to supplant any proper quantum-mechanically based line list. However, it provides a convenient means for radiative transfer calculations in case quantum-mechanically derived line lists are unavailable or unreli-able. In the process of building up the GEISA-09 CH_3CN line list, the mixing of quantum-mechanically derived lines and pseudo-lines has been avoided, as one cannot expect to get realistic results in a radiative transfer calculation if the quantum-mechanically derived lines have not been taken into account during the derivation of the pseudo-lines. The pseudo-line-list for CH_3CN has been successfully used to identify and quantify CH_3CN in the Earth's atmosphere from balloon-borne solar occulta-tion Fourier-Transform infrared measurements [428] and to attempt its detection on Titan from Cassini CIRS infrared data.

The CH_3CN pseudo-line-list [431] was created based on 29 laboratory spectra taken at PNNL. The measure-ments and the absorption cross-sections, including assignments of major bands, are described by Rinsland et al. [432]. The cross-sections were converted back into transmittance spectra from knowledge of the cell length and gas concentrations. The resulting laboratory trans-mittance spectra were then simultaneously fitted by iteratively adjusting the strengths and ground-state ener-gies of the pseudo-lines. At each line frequency, an effective strength and ground-state energy was derived by simultaneous non-linear least squares fitting to the 29 spectra. The air-broadened half-width was calculated from the ground-state energy using a simple parameter-ization that results in air-broadened half-widths between 0.04 and 0.08 cm^{-1}/atm and gives the most appropriate fit to the narrowest features in the considered frequency region. The self-broadened half-width, the temperature dependency of the air-broadened half-width, and the

pressure shift were chosen to be values that are typical for heavy molecules.

Due to the resolution of the laboratory spectra of 0.1125 cm^{-1} and their spectral point spacing of 0.0603 cm^{-1}, a pseudo-line spacing of 0.05 cm^{-1} was considered to be appropriate. Note that when the pseudo-line-list is used in radiative transfer calculations, it is recommended that the Doppler-width of the lines is set to the value of the pseudo-line spacing. Otherwise calculations for low pressures will lead to unrealistic spikes at the positions of the individual pseudo-lines.

2.2.40. Non updated molecules

Since GEISA-03 no update occurs for the following molecules: CO (molecule 5), OH (molecule 14), HF (molecule 15), HCl (molecule 16), HBr (molecule 17), HI (molecule 18), ClO (molecule 19), GeH_4 (molecule 26), HOCl (molecule 32), COF_2 (molecule 38) and HO_2 (molecule 38). For HO_2, a technical error in the GEISA-03 rotational quantum number identification is corrected in GEISA-09.

3. GEISA-09 infrared absorption cross-sections sub-database

The infrared absorption cross-section sub-database of GEISA-03 contents has been extensively described in Refs. [8,9] (see Table 2.5 of Ref. [9]). In the spectral range from 200 cm^{-1} to 2000 cm^{-1}, 35 molecular species have been already archived, i.e., CFC-13, CFC-113, CFC-114, CFC-115, CFC-11, CFC-12, CFC-14, HCFC-22, HCFC-123, HCFC-124, HFC-125, HFC-134a, HCFC-141b, HCFC-142b, HFC-152a, HCFC-225ca, HCFC-225cb, HFC-32, HFC-143a, HFC-134, N_2O_5, SF_6, $ClONO_2$; HFC-143, HCFC-21, CCl_4, C_2F_6, C_2H_2, C_2H_4, C_2H_6, C_3H_8, C_4H_8, HNO_4, SF_5CF_3, HCH-365mfc. Note that in this list, many of the molecular species are identified by their common name (i.e., CFC-14 for CF_4).

3.1. Complementary data for species already implemented in GEISA-03

3.1.1. SF_5CF_3 (trifluoromethyl sulfur pentafluoride)

SF_5CF_3 IR absorption cross-sections from M. Hurley were implemented in GEISA-03. The absorption cross-sections measured by Rinsland et al. [433], at five temperatures between 213 and 323 K in the infrared bands of SF_5CF_3 are newly added to GEISA-09. The spectra were recorded at a resolution of 0.112 cm^{-1} using a commercial Fourier transform infrared spectrometer and a 20 cm temperature-controlled sample cell. The full spectral range of the measurements was $520–6500 \text{ cm}^{-1}$, with only weak bands observed beyond 1400 cm^{-1}. Absorption of thermal radiation in the 8–12 μm atmospheric window region being important for climate change, the measured integrated cross-sections of the significant absorption bands in that spectral region have been added to the GEISA archive as summarized in Table 10. It has to be noted that the SF_5CF_3 atmospheric growth has closely paralleled the rise of SF_6 during the past three decades, with an estimated radiative forcing of $0.57 \text{ W m}^{-2} \text{ ppb}^{-1}$, slightly higher than for SF_6 [434].

3.2. Molecular species added since GEISA-03 edition

3.2.1. C_6H_6 (benzene)

To provide a database for both Earth's and planetary atmosphere studies (as an example, benzene has recently been detected in the atmosphere of Titan as the first PAH of this kind [312]), integrated band intensities of benzene at temperatures of 278, 298, and 323 K, in the spectral range $600–6500 \text{ cm}^{-1}$ by Rinsland et al. [435], have been added to GEISA-09 IR cross-sections archive. These data derived from pressure broadened (1 atm N_2) laboratory spectra of benzene vapor (in natural abundance) recorded at PNNL with a 0.112 cm^{-1} resolution Bruker-66 V Fourier transform spectrometer configured to operate in the mid-infrared. Using very high precision capacitance nanometers, over nine sample pressures were recorded for each of the three temperatures. Hard-mounted into the spectrometer, a temperature-stabilized static cell (19.94 cm path length), was used for support of the samples introduced into it. Two-hundred fifty-six interferograms were averaged for each sample spectrum. A composite spectrum was calculated for each cell temperature from the individual absorbance spectra recorded at that temperature. The average uncertainty (NIST type-A) is, respectively: 0.40%, 0.38% and 0.54% for the 278, 298, and 323 K spectra. The number density for the three composite spectra was normalized to 296 K. The spectra give the absorption IR cross-sections ($\text{cm}^2 \text{ molecule}^{-1}$, naperian units) of benzene as a function of wavenumber, as summarized in Table 10 for GEISA-09 contents.

3.2.2. CH_3CN (acetonitrile, – methyl cyanide)

Infrared cross-sections were measured at the Pacific Northwest National Laboratory by Rinsland et al. [432]. These 29 spectra covered 600 and 6500 cm^{-1} with a resolution of 0.1125 cm^{-1} and were measured at three different temperatures (276 K, 299 K, and 324 K). They were recorded with different CH_3CN volume mixing ratios at 1 atm pressure using N_2 as pressure broadening gas. Table 10 summarizes the related GEISA-09 contents.

3.2.3. $C_2H_3NO_5$ (peroxyacetyl nitrate, – PAN)

PAN is an interesting molecule, linking carbon and nitrogen chemistry, which has recently gained a new importance for remote sensing. The terrestrial spectroscopic signature of PAN in the thermal infra-red was first observed in Los Angeles smog [436] but the ability to observe PAN concentrations more widely has been revolutionized by recent detections in high resolution spectra obtained in balloon-borne [437] and space-borne experiments [438,439]. New spectroscopic data for PAN, in the form of cross-sections, have therefore been included in the GEISA database for the first time, based on the measurements of Allen et al. [440,441]. The cross-sections cover the spectral range between 560 and 1400 cm^{-1} at three temperature (295, 273, 250 K), and between 1686 and 2000 cm^{-1} at two temperatures (295 and 250 K). The data include all bands from ν_4 to ν_{19}, except for ν_{16} centered at 1653 cm^{-1} which is detected in the original measurements at 295 K but is not included here because of weakness of the band and residual water vapor

Table 10
Summary of GEISA-09 update and additions for infrared cross-sections.

Molecule	Temperature (K)	Spectral range (cm^{-1})	Foreign broadening pressure[a] (Pa)	Refs.
Trifluoromethyl sulfur pentafluoride, SF_5CF_3	213 243 278 298 323	600–2600	101,324.72	[433,434]
Benzene, C_6H_6	278 298 323	600–6500	101,324.72	[435]
Acetonitrile, CH_3CN	276.1 298.7 324.1	624–4574	101,324.72	[429,432]
PAN, $C_2H_3NO_5$	250 273 295	560–2000 560–1400 560–2000	0	[436–443]
Acetone, $(CH_3)_2CO$	214.0 223.4 223.5 223.5 223.6 233.4 233.4 233.4 233.5 253.3 253.3 253.4 253.8 272.3 272.3 272.3 272.6 297.4 297.5 297.5 297.8	600–1800	0 0 20,811.60 80,260.10 50,902.50 19,985.00 50,022.50 80,113.40 0 50,089.20 79,886.80 20,051.70 0 20,025.00 49,915.90 92,765.70 0 20,718.30 50,062.50 93,325.60 0	[444–447]

[a] Pressure=0.0 Pa: spectra measured for pure gas.

contamination. The band assignments are based on those reported in Gaffney et al. [442] and Bruckmann and Wilner [443]. The five main bands are ν_4, ν_5, ν_9, ν_{10} and ν_{16} centered at 1842, 1741, 1302, 1161.5 and 791.5 cm^{-1}, respectively; a small shift of 1 cm^{-1} was observed in the peak of the ν_4 band at 1842 cm^{-1} with temperature [441]. Uncertainties in the cross-sections were estimated to be 5% at 250 K [441] rising to 7% at 295 K [440]. See Table 10 for details.

3.2.4. $(CH_3)_2CO$ (acetone)

Acetone is a fundamental molecule in volatile organic chemistry which evaporates rapidly, even from water and soil. Once in the atmosphere, it is degraded by UV light with a 22-day half-life. Acetone dissipates slowly in soil, animals, or waterways since it is sometimes consumed by microorganisms, but it is a significant groundwater contaminant due to its high solubility in water. Acetone may pose a significant risk of oxygen depletion in aquatic systems due to the microbial activity consuming it.

The spectroscopic signature of acetone in spectra of the terrestrial atmosphere has been reported first in the ν_{19}/ν_{23} band complex centered at 530 cm^{-1} (citation in [444]) and in the ν_{17} band at 1220 cm^{-1} [445,437] and in the ν_{16} Q-branch at 1365 cm^{-1} [439]. Hence it has been important to include new spectroscopic data for acetone, under the form of cross-sections, in the GEISA database for the first time, based on the measurements of Waterfall [446]. The cross-sections, at spectral resolution of 0.03 cm^{-1}, cover the spectral range between 600 and 1800 cm^{-1} around six temperature series (214, 223, 233, 253, 272 and 297 K); see Table 10 for precise details. The data include the ν_{18} band centered at 830 cm^{-1}, the ν_{17} at 1218 cm^{-1}, the ν_{16}/ν_5 bands close to 1360 cm^{-1} overlapping with the unresolved bands of $\nu_{15}, -\nu_4$ and ν_{21} centered between 1430 and 1460 cm^{-1}, and the ν_3 band centered at 1738 cm^{-1}; band assignments are taken from Wang et al. [447]. The ν_7 band, centered at 777 cm^{-1}, and the ν_{22}/ν_6 near 1093 cm^{-1} are only very weakly present in the measured cross-sections. The main cross-section influence is for the strongest bands observed between 1200 and 1800 cm^{-1} for which uncertainties range from 5% (7% for the center of the ν_3, 1738 cm^{-1} band) at the strongest parts of the band to 10% towards the edges. For the 830 cm^{-1} band, errors are approximately 12% at band center rising to greater than 20% at the band edges.

4. GEISA-09 absorption cross-sections sub-database in UV/visible regions

For molecules absorbing in the UV and visible spectral regions, except for O_2, H_2O, NO and OH, there are no individual line lists available, since most molecules and radicals show rather broad-band absorption features due to repulsive potential curves or surfaces in the upper electronic states of the relevant transitions, or due to pre-dissociation. Therefore, absorption cross-sections at all relevant temperatures (and in some cases, pressures), have to be used.

The requirements for the accuracy of molecular absorption cross-sections in this spectral range are most important for strong absorbers, especially for O_3, but it is also important to highlight the need of very accurate spectral calibration (hence reference data derived from FTS are usually recommended) and for a high dynamic range and absolute consistency between different spectral regions (e.g., between the ultraviolet and visible bands for O_3, or the consistency with respect to the mid-infrared bands). The latter requirements are especially important when the retrieved atmospheric data are used for photo-chemical modeling or for chemical budget calculations, where uncharacterized biases between different spectral regions may lead to difficult problems.

In the GEISA database, only UV–visible reference spectra of such molecules that have already been detected in the Earth's or planetary atmospheres are presented, i.e., contrary to other databases which focus on photochemical data (e.g., the NASA-JPL, NIST or IUPAC recommendations) or offer a complete coverage of all absorption spectra (e.g., the MPI Mainz and SoftCon databases). It is also important to note that, in contrast to the HITRAN database, for the sake of coherence of future studies, and to facilitate the comparison with previous work, the GEISA database contains different sets of relevant absorption cross-sections, i.e., multiple data sources and data sets for the same species; however recommendations are made for each molecule.

The GEISA database contains UV–visible absorption cross-sections for the following molecules and radicals: NO_2, CS_2, O_3, SO_2, O_2–O_2 (O_4), OClO, H_2CO, OBrO, BrO, NO_3, HONO, IO, OIO, and aromatic hydrocarbons (i.e., C_6H_6, C_7H_8 and the three isomers of $(C_6H_4(CH_3)_2$ as well). Here below, each molecule and the relevant reference data in the new GEISA-09 edition will be discussed individually.

4.1. NO_2 (nitrogen dioxide)

For NO_2, there is quite a variety of different laboratory measurements of ultraviolet–visible absorption cross-sections. For atmospheric applications, the currently recommended data set by Orphal [448] is the one of Vandaele et al. [449], but it is important to stress that also the data of Voigt et al. [450], Yoshino et al. [451], Harder et al. [452] and Frost et al. [453] are of high quality and show excellent agreement with each other. The cross-section of Harder et al. may contain a slight contamination by HONO, however. For applications where a very high signal-to-noise ratio is required or in spectral regions where the previously mentioned NO_2 absorption cross-sections are limited, the data recorded with GOME by Burrows et al. [454] or with SCIAMACHY by Bogumil et al. [455] are recommended (again, it is important to note that these data are limited by the spectral resolution of the instruments). It has to be recalled that, in general, the cross-sections recorded by an FTS have a wavelength calibration of better than 0.01 nm [448] which is an important advantage for atmospheric applications, in particular when retrieving several absorbers simultaneously.

4.2. CS_2 (carbon disulfide)

Small amounts of carbon disulfide CS_2 are released by volcanic eruptions and marshes. The absorption cross-sections, recorded with an FTS at 294 K covering the 290–350 nm spectral range are from Vandaele et al. [456].

4.3. O_3 (ozone)

As for NO_2, there exist many laboratory measurements of UV–visible absorption cross-sections at atmospheric temperatures (see [448]). However, only a few of them cover the entire spectral range from the ultraviolet to the near-infrared. Therefore, it is difficult to recommend one single data set that would be best suited for all applications. For the Huggins bands (300–360 nm), the recommended reference data are those of Brion et al. [457] and those of Bass and Paur [458], since both data sets cover most relevant temperatures (note however that the data of Brion et al. are not available below 218 K) and have been recorded at high resolution. While the data of Bass and Paur were used as some kind of standard during the past 20 years, more recent studies tend to recommend the data of Brion et al. for atmospheric remote-sensing applications (since they show better wavelength calibration, wavelength sampling, less noise and less inconsistencies concerning the temperature dependence of the cross-sections). For applications where absorption cross-sections over a broader spectral range are needed (in particular in the visible and near-infrared, i.e., the Chappuis and Wulf bands, the O_3 cross-sections recorded with GOME [454] or with SCIAMACHY [455] are recommended. These absorption cross-sections show also a very high signal-to-noise ratio, but are partly limited by the spectral resolution of the instruments. If O_3 cross-sections at very high spectral resolution are needed, then the data of Voigt et al. [459] are recommended.

4.4. SO_2 (sulfur dioxide)

SO_2 presents three main regions of absorption in the near ultraviolet domain. The strongest band lies in the 45,000 cm^{-1} (220 nm) region and corresponds to the $\hat{C}^1B_2$–X^1A_1 electronic transition. A strong absorption structure extends between 29,000 and 40,000 cm^{-1}, which can be ascribed to at least two electronic transitions. Underlying the structured bands of the A^1A_2–X^1A_1 [460], the 'continuous' absorption has been attributed to the B^1B_1–X^1A_1 transition, which has been predicted by theory [461] and measured by Brand et al. [462]. The

A^1A_2–X^1A_1 transition is forbidden but is observed because of strong vibrational interactions through the ν_3 vibration mode and is strongly perturbed by the $^1B_1$ state. The allowed transition B^1B_1–X^1A_1 is so perturbed that no rotational or vibrational analysis is possible. It forms a continuum due to the density of weak absorptions. A weak absorption feature arises in the 25,000–29,000 cm^{-1} region (345–400 nm). It has been assigned to the a^3B_1–X^1A_1 electronic transition and is a spin-forbidden transition.

In the previous edition of GEISA [8,9] the UV/vis data set for SO_2 consisted in cross-sections recorded with the SCIAMACHY spectrometer [455], covering five temperatures between 203 and 293 K and interesting for planetary science application. The 2009 update consists in recently obtained absorption cross-sections, at high resolution and at high temperatures, in support to planetary applications [463,464]. They were recorded in the 24,000–44,000 cm^{-1} spectral range (227–420 nm) with a Fourier Transform spectrometer at a resolution of 2 cm^{-1} (0.45 cm MOPD and boxcar apodization). Pure SO_2 samples were used and measurements were performed at room temperature (298 K) as well as at 318, 338 and 358 K. Temperature effects were investigated and were found in favorable agreement with existing studies in the literature. Comparison of the absorption cross-sections at room temperature [465,466] shows good agreement in intensity with most of the literature data, but shows that most of the latter suffer from inaccurate wavelength scale definition. Moreover, literature data are often given only on restricted spectral intervals, whereas this new data set offers the considerable advantage of covering the large spectral interval extending from 24,000 to 44,000 cm^{-1}, at the four temperatures investigated. These data are also available in digital form from the website of the Belgian Institute for Space Aeronomy (http://www.aeronomie.be/spectrolab/).

4.5. O_2–O_2 (O_4) (the so-called oxygen "dimer")

These broad features are mainly used for air mass determination in atmospheric remote-sensing applications. It is rather difficult to recommend one particular set of data since the differences between the available cross-sections are still not well understood. Therefore, the data of Greenblatt et al. [467], of Newnham and Ballard [468], and of Vandaele et al. [456] are all available in the archive.

4.6. OClO (chlorine dioxide)

OClO is involved in polar stratospheric chemistry, linking the catalytic cycles of ClO and BrO, and has been observed in ultraviolet–visible spectra from ground, airborne platforms and satellites. It is important to monitor stratospheric OClO in order to validate the quantitative understanding of ozone destruction in polar winter. As in the previous edition of GEISA, the UV–visible absorption cross-sections of Kromminga et al. [469] that were recorded at different temperatures using high-resolution Fourier-transform spectroscopy are recommended. For the sake of coherence with previous studies, GEISA also contains the OClO cross-sections of Wahner et al. [470].

4.7. H_2CO (formaldehyde, also called CH_2O or $HCHO$)

Formaldehyde is another important source of OH radicals in the troposphere, and one of the smallest organic molecules in the atmosphere. Gratien et al. [471] have demonstrated that the high-resolution H_2CO absorption cross-sections of Meller and Moortgat [472] are in excellent agreement with the available infrared cross-sections. For applications requiring a very high signal-to-noise ratio, the data recorded with SCIAMACHY [455] may also be of interest.

4.8. OBrO

Only cross-sections recorded by an FTS were selected. For OBrO (385–616 nm spectral range) cross-sections are available only at room temperature [473].

4.9. BrO (bromine monoxide)

BrO is observed in the stratosphere but also in the marine troposphere and in volcanic plumes. There are two sets of data which have been recorded using high-resolution Fourier-transform spectroscopy and cover all relevant atmospheric temperatures: Wilmouth et al. [474] and Fleischmann et al. [475]; both show very good agreement. As for OClO, for the sake of coherence with previous studies, GEISA also contains the BrO absorption cross-sections of Wahner et al. [476] that were used as reference spectra, before the new data became available.

4.10. NO_3 (nitrogen trioxide; the nitrate radical)

For NO_3, the main night-time oxidant in the troposphere, but also strongly occurring in the stratosphere, the recommended data set for all atmospheric temperatures is the one of Yokelson et al. [477]; note however that there exists a room-temperature spectrum that was recorded using high-resolution Fourier-transform spectroscopy [448]. The latter paper also provides an accurate theoretical model for the temperature dependence of the strong peak at 662 nm, which is based on the molecular symmetry and structure of the radical.

4.11. HONO (nitrous acid)

Nitrous acid is an atmospheric species that has received a lot of attention in the past decades, since it is a source of OH radicals in the troposphere, while its sources are still not well understood. A recent study by Gratien et al. [478] has shown that the HONO absorption cross-sections of Bongartz et al. [479] and of Stutz et al. [480] are in very good agreement with each other and with the available infrared cross-sections. Therefore, both data sets are recommended.

4.12. CHOCHO (glyoxal)

Glyoxal is a small organic molecule involved in tropospheric chemistry and aerosol formation. It has only recently been measured for the first time in the Earth's atmosphere using optical methods. Its sources are still not fully understood, especially since some CHOCHO is also observed over the Pacific Ocean. The recommended absorption cross-sections for CHOCHO are those of Volkamer et al. [481] recorded using high-resolution Fourier-transform spectroscopy.

4.13. IO (iodine monoxide)

IO has been observed only in the marine troposphere, and an upper limit of less than 1 pptv has been established for stratospheric IO. The reference data in GEISA are the cross-sections of Spietz et al. [482] which have an excellent signal-to-noise ratio, rather high resolution, and are in good agreement with other studies and with photochemical models of IO chemistry following flash photolysis of suitable precursors.

4.14. OIO (iodine dioxide)

As for IO, the OIO radical has been observed only in the marine troposphere. Its atmospheric relevance has been established only as late as 1996 when it was observed for the first time in flash-photolysis experiments by Himmelmann et al. [483]. The reference data in GEISA are the absorption cross-sections of Gomez-Martin et al. [484].

4.15. Aromatic hydrocarbons

UV absorption cross-sections (cm^2 molecule^{-1}) of five gaseous aromatic hydrocarbons have been measured with a FTS Bruker IFS120M at the resolution of 1 cm^{-1} (0.9 cm MOPD and boxcar apodization) over the 30,000–42,000 cm^{-1} spectral range (238–333 nm). The molecules, benzene (C_6H_6), toluene or methylbenzene (C_7H_8), and the three isomers of dimethyl-benzene ($C_6H_4(CH_3)_2$) also called meta-, ortho-, and para-xylene, were chosen for their importance in the chemistry of tropospheric ozone [485], in urban air quality problems [486] and in astronomical studies [317,318,402,487].

The recordings were carried out under different pressure and temperature conditions with pure samples. The complete dataset is composed of absorption cross-sections for: (i) benzene at 253, 263, 273, 283 and 293 K, (ii) toluene at 263, 273, 283 and 293 K, and (iii) the three isomers of xylene at 273, 283 and 293 K. Wavenumbers are given by increments of 0.2 cm^{-1}. Systematic and non-systematic errors are given separately, a value of 8% being estimated for the former and individual values being reported in a separate column for the latter. The experimental set-up and the procedure of analysis are given in details in [488].

Comparisons with recent studies in the same UV region [488–491] show that large discrepancies are present in some cases which are largely attributed to the experimental difficulties and to a resolution effect. Compared to these studies, a better spectral resolution, an accurate wavelength scale, and several atmospheric temperatures are provided. A linear parameterization for the temperature effect is also proposed for benzene and toluene in support of remote sensing atmospheric studies both on Earth and on other planets. These data are also available in digital form from the website of the Belgian Institute for Space Aeronomy (http://www.aeronomie.be/spectrolab/).

5. GEISA-09 sub-database on microphysical and optical properties of atmospheric aerosols

Besides the molecular species which define the gaseous infrared opacity in the Earth's atmosphere, aerosol particles also contribute to this opacity. Consequently, a GEISA aerosols sub-database has been constructed. It gathers the micro-physical and optical properties from four published aerosol data catalogs, i.e., Massie [492–494], Rublev [495], Hess et al. [496], Köpke et al. [497], the overall content of which deals with the archive of complex refractive indices and possibly computed optical related properties, for selected basic aerosol components. Softwares for data management and user-selected aerosol mixtures elaboration are available as well.

The GEISA-09 aerosols sub-database contains data on microphysical and optical properties of basic aerosol components. The following 4 sub-databases are included:

5.1. A database on refractive indices of basic atmospheric aerosol components

This database by Massie [492–494] comprises an extensive archive of complex refractive indices, determined both in situ and in laboratory, from spectral transmission and reflection measurements (over 40 references), of various aerosol components, i.e.,

- Solid substances (0.33–50,000 cm^{-1})
- Water ice (0.–22,570 cm^{-1})
- Water droplets (0.33–15,000 cm^{-1})
- Water soluble components (250–50,000 cm^{-1})
- H_2SO_4 solutions (0.–50,000 cm^{-1})
- HNO_3 solutions (0.–16,382 cm^{-1})
- Thin films (482–7000 cm^{-1})
- Ternary $H_2SO_4/HNO_3/H_2O$ solution droplets (2.000–12.1126 cm^{-1}).

5.2. The aerosols database from LITMS

The first part of the archive [495] consists in complex indices of refraction of aerosol components, which have been used for the computation of archived aerosol integrated optical properties (extinction coefficient, single scattering albedo, asymmetry factor). In the second part, the so-called AERCOMP (FORTRAN code) software package, allowing the determination of optical properties for user-defined aerosol mixtures, has been included with its

associated files for basic aerosol constituent optical properties and related scattering phase functions, as well.

5.3. The database and associated software package OPAC

The first part of this archive [496] is a data set of microphysical properties and the associated optical properties of:

- *Ten basic aerosol components*: Insoluble, soot, water soluble, two sea salt modes (various kinds of salt contained in seawater), three mineral modes (mixtures of quartz and clay minerals), mineral transported, sulfate droplets.
- *Six water clouds*: Stratus (continental and maritime), cumulus (continental (clean and polluted) and maritime), fog, and three kinds of cirrus ice clouds, both in the solar and terrestrial spectral range.

The second part is a FORTRAN program making it possible to extract data from the above archive and allowing for the calculation of any user-defined mixtures of these components. A set of computed typical mixtures is archived, as well.

5.4. The Global Aerosol Data Set GADS

Global fields of all optical parameters necessary for an estimate of the radiative forcing by aerosol particles and to quantify the resulting climate effects are not available from measurements due to the multiple influence parameters. Therefore, using the OPAC aerosol archive, GADS (Köpke et al. [497]), provides the related global aerosol distribution as climatologically averaged values both for the winter (December through February) and summer (June through August) seasons on a global grid with a resolution of $5° \times 5°$ longitude and latitude, independently of the components selected in OPAC. More details on the archived files structure is given in Ref. [498].

5.5. GEISA interactive web distribution through Ether Products and Services Centre

The scientific input into GEISA is maintained at LMD (Ecole Polytechnique): http://ara.abct.lmd.polytechnique.fr) which involves selection and collection of new or enhanced spectroscopic data in cooperation with spectroscopy laboratories, both theory and experiment, and experts; processing of the data; software development and maintenance for the data base management and products extraction.

The GEISA on line web access and its associated maintenance are responsibility of the Ether Products and Services Centre (http://ether.ipsl.jussieu.fr), at IPSL, where the database is implemented. Ether is especially involved in distribution and generation of products of interest to the Atmospheric Chemistry Research community.

The GEISA web site is freely accessible, via the GEISA logo, through the welcome page of the Ether web site, which offers the following GEISA interrogation facilities:

- Very detailed information on the available spectroscopic data, i.e., spectroscopic parameters of the individual lines and cross-sections (IR and UV/vis), and optical and microphysical properties of atmospheric aerosols as well.
- FTP access to file data for a quick download of the database, partly or fully.
- Interactive access to the individual line spectroscopic parameters, making possible sharper search and extraction of data of interest. In this purpose, six options are available for display, histograms visualization and extractions of user's selected data information.

6. Concluding comments

The 2009 edition of GEISA exhibits important updates in spectroscopic parameters and significant addition of archived molecular species (line transitions and cross-sections sub-databases), with an associated extension of spectral ranges (especially towards near IR regions). Some specific results of this effort are especially valuable for various current research programs aiming at a better knowledge of the Earth's and planetary atmospheres, as well as climate and environmental evolution understanding. Examples of such updates, among the ones detailed above are:

(a) Within the frame work of the IASI METOP program, and ISSWG associated GEISA/IASI efforts, among the 14 molecular species selected for operational meteorological soundings, i.e., H_2O, CO_2, O_3, N_2O, CO, CH_4, O_2, NO, SO_2, NO_2, HNO_3, OCS, C_2H_2, and N_2, the spectroscopic parameters of eleven of them have been updated in the GEISA/IASI spectral range (599–3001 cm^{-1}); three of them (CO, O_2, OCS) are unchanged in this specific spectral region (however O_2 and OCS are updated elsewhere in the database). Recently, in conjunction with the 2009 update, to aid the atmospheric chemistry and climate monitoring capabilities of IASI soundings, 6 additional molecular species have been included in the GEISA/IASI archive, i.e., HCN, NH_3, HCOOH, C_2H_4, CH_3OH and H_2CO (this list is not final or complete) as well as PAN cross-sections. All these molecular species have been updated in GEISA-09 and PAN is a new cross-section entry. HCN is almost totally new in GEISA-09.

(b) Related with spectroscopy requirements for space studies of outer planets and Titan, as documented in Ref. [8], important subsequent updates have been done in GEISA-09. Data on complementary new molecular species, to those already archived in GEISA, have been included in GEISA-09, i.e., C_6H_6 (individual lines and cross-sections as well) and C_2HD; among the updated molecules are especially: C_4H_2, HC_3N, C_2H_6, C_2H_2, C_2H_4, HCN, C_3H_4, CH_3CN. Also HNC is introduced as a new molecular species. HCN and HNC molecules are of great astronomical interest. They have been observed in many galactic and extragalactic objects, ranging from circum-stellar masers through interstellar clouds to planetary atmospheres.

Even regularly updated and evolving spectroscopic databases, such as GEISA, still have their limitations and shortcomings; these have to be continuously corrected or improved upon to meet the requirements of a diverse group of users. Detailed examples, but a non-exhaustive list of these requirements was given in Ref. [8]. Among those still not met we can underline:

(a) From the "Summary Report on the Second IASI International Conference" [498]; http://smsc.cnes.fr/IASI, among the conclusions on IASI related RTM spectroscopy problems still to be solved, high priority was given to the investigation of areas mainly related to H_2O, CO_2 and CH_4, summarized as follows:
- *For H_2O (highest priority)*: Review of the accuracy of line widths (could be more important than the intensities); review of the continuum in the short wave window region (i.e., band 3; spectral range 2000–2760 cm^{-1}); measurements of widths and shifts should be made (with temperature dependence if possible).
- *For CO_2*: The inconsistency between CO_2 ν_2 and CO_2 ν_3 bands bias by improving the CO_2 spectroscopy in the ν_3 band.
- *For CH_4*: Improvement of the methane spectroscopy, introducing line mixing.

It has to be noted that, since this report and GEISA-09 have been issued, Toth et al. [499] revisited $H_2^{16}O$ line strengths in the ν_2 and $2\nu_2 - \nu_2$ bands at 6 μm. These results will be considered for the next GEISA Edition.
(b) In the frame work of space studies of outer planets and Titan: besides the 2009 updates described above, the description of data that remain to be obtained and implemented in GEISA, as given in Ref. [8], is still available.

Finally, in terms of outstanding spectroscopy issues, among the most important actions already underway, but which must be reinforced and maintained, is the necessary validation of archived spectroscopic data. This and other activities will be performed in conjunction with the recently started VAMDC European project (http://www.vamdc.eu). This project aims at building an interoperable e-Infrastructure for the exchange of atomic and molecular data [500].

Acknowledgments

Appendix A. List of acronyms

4A	Atlas Automatisé des Absorptions Atmosphériques
4A	Automatized Atmospheric Absorption Atlas
4A/OP	4A/O Perational release
ACE	Atmospheric Chemistry Experiment
AERCOMP	Aerosol Composite
AFGL	Air Force Geophysics Laboratory
AGB	Asymptotic Giant Branch
AIRS	Advanced InfraRed Sounder
ALMA	Atacama Large Millimeter/submillimeter Array
ARA	Atmospheric Radiation Analysis
BIRA/IASB	Institut d'Aéronomie Spatiale de Belgique/ Belgian Institute for Space Aeronomy
BEAMCAT	BErnese Atmospheric Meta Catalog Access Tool
CDMS	Cologne Database for Molecular Spectroscopy
CDSD	Carbon Dioxide Spectroscopic Databank
CIRS	Composite InfraRed Spectrometer
CNRS	Centre National de la Recherche Scientifique (France)
CNES	Centre National d'Etudes Spatiales (France)
CSE	Circum Stellar Envelope
CW–CRDS	Continuous Wave-Cavity Ring Down Spectroscopy
DU	Denver University
ENVISAT	ENVIronmental SATellite
EPS	European Polar System
EOS-aqua	Earth Observing System-water
EU	European Union
EUMETSAT	European Organisation for the Exploitation of Meteorological Satellites
FT	Fourier Transformed
FTIR	Fourier Transformed InfraRed spectroscopy
FTS	Fourier Transform Spectrometer
GADS	Global Aerosol Data Set
GEISA	Gestion et Etude des Informations Spectroscopiques Atmosphériques; Management and study of Atmospheric Spectroscopic Information
GOME	Global Ozone Monitoring Experiment

GOSAT	Greenhouse Observing SATellite project
GSMA	Groupe de Spectroscopie Moléculaire et Atmosphérique (France)
HITRAN	HIgh-resolution TRANsmission molecular absorption data base
HTDS	Highly spherical Top Data System
HWHM	Line Half-width at Half Maximum (line broadening)
IASI	Infrared Atmospheric Sounder Interferometer
ICB	Institut Carnot de Bourgogne
INSU	Institut National des Sciences de l'Univers (France)
IPSL	Institut Pierre Simon Laplace
ISM	Inter-Stellar Medium
IAO	Institute of Atmospheric Optics (Russia)
IR	InfraRed
IRS	InfraRed Spectrograph
ISO	Infrared Space Observatory
ISSWG	IASI Sounding Science Working Group
IUPAC	International Union of Pure and Applied Chemistry
JPL	Jet Propulsion Laboratory (USA)
LADIR	Laboratoire de Dynamique, Interaction et réactivité (France)
LESIA	Laboratoire d'Etudes Spatiales et d'Instrumentation en Astrophysique (France)
LISA	Laboratoire Inter-Universitaire des Systèmes Atmosphériques (France)
LITMS	Laboratory for Information Technologies and Mathematical Simulation (Russia)
LMD	Laboratoire de Météorologie Dynamique (France)
MIPAS	Michelson Interferometer for Passive Atmospheric Sounding
Metop	Meteorological operational satellite
MOPD	Maximum Optical Path Difference
NASA	National Aeronautics and Space Administration (USA)
NCAR	National Center for Atmospheric research (USA)
NIR	Near InfraRed
NRC	National Research Center (Canada)
NIST	National Institute of Standards and Technologies
OPAC	Optical Properties of Aerosols and Clouds
PAH	Polycyclic aromatic hydrocarbon
PAN	PeroxyAcetyl Nitrate
PNNL	Pacific Northwest National Laboratory (USA)
RTM	Radiative Transfer Modeling
SCIAMACHY	SCanning Imaging Absorption spectroMeter for Atmospheric ChartograpHY
SCISAT-1	Scientific Satellite-1
SOPHIA	Stratospheric Observatory for Infrared Astronomy
SPCAT	Spare Parts Catalog Software
S&MPO	Spectroscopy & molecular properties of Ozone
SST	Spitzer Space Telescope
UCL	Université catholique de Louvain (Belgium)
ULB	Université Libre de Bruxelles (Belgium)
UV	Ultra Violet
VAMDC	Virtual Atomic and Molecular Data Centre
VIMS	Visible and Infrared Mapping Spectrometer
VIS	Visible

Appendix B. Description of the format used for the line parameters archive in the 2009 edition of GEISA (http://ether.ipsl.jussieu.fr/etherTypo/?id=1306)

The GEISA-09 individual line list sub-database includes 31 spectroscopic line parameters corresponding to 252 characters record per entry, as described in Table 11: spectroscopic parameters symbolic field names are in the first line, and the associated field lengths and FORTRAN format descriptors in lines 2 and 3, respectively. Standard missing values, as adopted for each parameter and for the whole database, are detailed in line 4. Those values are mainly negative; blank characters correspond to missing transition quantum number identifications and to internal GEISA code as well; value "0" have been attributed to non identified field L (HITRAN isotopologue number). The description of each field is given at the bottom of the table.

Some modifications have been brought to the GEISA-03 [7–9] (http://ether.ipsl.jussieu.fr/etherTypo/?id=1072) format, i.e.,

- Lengths of fields $E1$, $E2$, $E3$, $E4$, N, O, N', O' have been extended.
- Fields P and Q, related with specific HITRAN internal information, have been suppressed. Field P, uncertainty codes for wavenumber, intensity and half-width, has been replaced in GEISA by effective values of the errors. Field Q, HITRAN indices for lookup of references for wavenumber, intensity and half-width has no correspondence in GEISA which does not include reference numbers among its line parameters.

It has to be noticed that:

- Fields K and L are HITRAN-08 [13] specific, for the users' easier possible interface between the two databases. These fields information content, i.e., molecule number (K) and isotope number (L) as in HITRAN, makes it possible to apply a biunivoque correspondence with GEISA related fields (I) and (G), respectively. It has to be noted that field (L) corresponds, in HITRAN, to the isotopologue fractional abundance code; in GEISA, field (G) represents the code associated with the isotope chemical formula; these specificities are handled in the software making it possible to convert the format of a one of the database into the one of the other.
- Value in field M is given only if directly provided by the author of the spectroscopic line file. This field has been newly appended in GEISA-09.

Detailed description of fields $E1$ and $E2$, specific of each molecule, is given on the GEISA distribution WEB site at, http://ether.ipsl.jussieu.fr, for database interactive software use facilities. The shift of the positions of certain already existing fields (such as field R), as consequence of modifications in the format of GEISA-09 since the GEISA-03 one, has to be noted.

Table 11
Fields of the format for GEISA-09 individual line list sub-database.

Parameter	A	B	C	D	E1	E2	E3	E4	F	G
Field length	12	11	6	10	25	25	15	15	4	3
FORTRAN descriptor	F12.6	1PD11.4	0PF6.4	F10.4	A25	A25	A15	A15	F4.2	I3
Undefined values	−0.999999	−9.9999D−01	−0.9999	−0.9999					−0.99	−99

Parameter	I	J	K	L	M	N	O	R	A′		B′
Field length	3	3	2	1	10	7	9	6	10		11
FORTRAN descriptor	I3	A3	I2	I1	1PE10.3	0PF7.4	F9.6	F6.4	F10.6		1PD11.4
Undefined values	−99		−9	0	−9.999E−01	−9.9999	−9.999999	−0.9999	−0.999999		−9.9999D−01

Parameter	C	F′	O′	R′	N′	S	S′	T	T′	U	U′
Field length	6	4	9	6	7	4	4	8	8	4	4
FORTRAN descriptor	0PF6.4	F4.2	F9.6	F6.4	F7.4	F4.2	F4.2	F8.6	F8.6	F4.2	F4.2
Undefined values	−0.9999	−0.99	−9.999999	−0.9999	−9.9999	−0.99	−0.99	−0.999999	−0.999999	−0.99	−0.99

A: Wavenumber of the line ν (cm^{-1}).
B: Intensity of the line I (cm^{-1}/(molecule cm^{-2})).
C: Air broadening pressure half-width α (HWHM)(cm^{-1} atm^{-1}).
D: Energy of the lower transition level E' (cm^{-1}).
E_i ($i=1,2,3,4$): Transition quantum identifications for the lower and upper state transition (unitless).
F: Temperature dependence coefficient n of the air broadening half-width (unitless).
G: Identification code for isotopologue as in GEISA (unitless).
I: Identification code for molecule as in GEISA (unitless).
J: Internal GEISA code for the data identification (unitless).
K: Molecule number as in HITRAN [13] (unitless).
L: Isotopologue number (1=most abundant, 2=second, etc.) as in HITRAN [13] (unitless).
M: Einstein A-coefficient (s^{-1}).
N: Self-broadening pressure half-width (HWHMself) (cm^{-1} atm^{-1}).
O: Air pressure shift of the line transition (cm^{-1} atm^{-1}).
R: Temperature dependence coefficient of the air pressure shift (unitless).
A': Estimated accuracy on the line position (cm^{-1}).
B': Estimated accuracy on the intensity of the line (cm^{-1}/(molecule cm^{-1})).
F': Estimated accuracy on the temperature dependence coefficient of the air broadening half-width (unitless)
O': Estimated accuracy on the air pressure shift of the line transition (cm^{-1} atm^{-1}).
R': Estimated accuracy on the temperature dependence coefficient of the air pressure shift (unitless).
N': Estimated accuracy on the self-broadened (cm^{-1} atm^{-1}).
S: Temperature dependence coefficient of the self-broadening half-width (unitless).
S': Estimated accuracy on the temperature dependence coefficient of the self-broadening half-width (unitless).
T: Self-pressure shift of the line transition (cm^{-1} atm^{-1}).
T': Estimated accuracy on the self-pressure shift (cm^{-1} atm^{-1}).
U: Temperature dependence coefficient of the self-pressure shift (unitless).
U': Estimated accuracy on the temperature dependence coefficient of the self-pressure shift (unitless).

Table 12

Complementary description of codes for new isotopologues or molecules since former GEISA editions.

Molecule	Molecule code	Isotopologue code	Formula
N_2O	4	458	$^{14}N^{14}N^{18}O$
		548	$^{15}N^{14}N^{18}O$
		556	$^{15}N^{15}N^{16}O$
CH_3D	23	312	$^{13}CH_3D$
HCN		224	$D^{12}C^{14}N$
CH_3Br	43	79	$^{12}CH_3^{79}br$
		81	$^{12}CH_3^{81}br$
CH_3OH	44	216	$^{12}CH_3^{16}OH$
NO^+	45	46	$^{14}N^{16}O^+$
HNC	46	142	$H^{14}N^{12}C$
C_6H_6	47	266	$^{12}C_6H_6$
C_2HD	48	122	$^{12}C_2HD$
CF_4	49	291	$^{12}C^{15}F_4$
CH_3CN	50	234	$^{12}CH_3^{12}C^{14}N$

Appendix C. New molecules and isotopologues in GEISA-09

Description of new molecule and isotopologue codes in GEISA-09 is given in Table 12. The molecule names and associated codes are in the two first columns; for each molecule, the isotopologue codes and the corresponding detailed formula are in columns 3 and 4, respectively.

Appendix D. Supplementary materials

Supplementary data associated with this article can be found in the online version at doi:10.1016/j.jqsrt.2011.06.004.

References

[1] McClatchey RA, Benedict WS, Clough SA, Burch DE, Calfee RF, Fox K, et al. AFCRL Atmospheric absorption line parameters compilation. AFCRL-Technical Report-0096, 1973.

[2] Garing JS, McClatchey RA. Atmospheric absorption line compilation. Appl Opt 1973;12:2545.

[3] Chédin A, Husson N, Scott NA, Jobard I, Cohen-Hallaleh I, Berroir A. La banque de données GEISA, Description et logiciel d'utilisation, Laboratoire de Météorologie Dynamique du CNRS. Internal Note 108. Ecole Polytechnique; October 1980.

[4] Chédin A, Husson N, Scott NA. Une banque de données pour l'étude des phénomènes de transfert radiatif dans les atmosphères planétaires: la banque GEISA. Bull Inform Centre Données Stellaires (France) 1982;22:121.

[5] Husson N, Chédin A, Scott NA. The GEISA spectroscopic line parameters data bank in 1984. Ann Geophys 1986;4:185–90.

[6] Husson N, Bonnet B, Scott NA, Chédin A. Management and study of spectroscopic information: the GEISA program. J Quant Spectrosc Radiat Transfer 1992;48:509–18.

[7] Jacquinet-Husson N, Arié E, Ballard J, Barbe A, Bjoraker G, Bonnet B, et al. The 1997 spectroscopic GEISA databank. J Quant Spectrosc Radiat Transfer 1999;62:205–54.

[8] Jacquinet-Husson N, Scott NA, Chédin A, Crépeau L, Armante R, Capelle V, et al. The GEISA spectroscopic database: Current and future archive for Earth and planetary atmosphere studies. J Quant Spectrosc Radiat Transfer 2008;109:1043–59.

[9] Rosenkranz Ph, Bühler S, Feist D, Hewison T, Jacquinet-Husson N, Pardo JR, et al. Thermal Microwave Radiation-Applications for Remote Sensing, Chap. 2: Emission and spectroscopy of the clear atmosphere. IEE Electromagn Waves Series (London, UK) 2006: 25–99.

[10] Jacquinet-Husson N, Scott NA, Chédin A, Garceran K, Armante R, Chursin AA, et al. The 2003 edition of the GEISA/IASI spectroscopic database. J Quant Spectrosc Radiat Transfer 2005;95: 429–67.

[11] Scott NA. A direct method of computation of transmission function of an inhomogeneous gaseous medium: description of the method and influence of various factors. J Quant Spectrosc Radiat Transfer 1974;14:691–707.

[12] Scott NA, Chédin A. A fast line-by-line method for atmospheric absorption computations: the Automatized Atmospheric Absorption Atlas. J Appl Meteor 1981;20:556–64.

[13] Rothman LS, Gordon IE, Barbe A, Benner DC, Bernath PF, Birk M, et al. The HITRAN 2008 molecular spectroscopic database. J Quant Spectrosc Radiat Transfer 2009;110:533–72;
Rothman LS, Jacquemart D, Barbe A, Chris Benner D, Birk M, Brown LR, et al. The HITRAN 2004 molecular spectroscopic database. J Quant Spectrosc Radiat Transfer 2005;96:139–204.

[14] Flaud JM, Piccolo C, Carli B. A spectroscopic database for MIPAS. in: Proceedings of the ENVISAT validation workshop, Frascati, Italy, 9–13 December 2002, ESA (August 2003), p. SP-531.

[15] Feist DG. The Bernese atmospheric multiple catalog access tool (BEAMCAT): a tool for users of popular spectral line catalogs. J Quant Spectrosc Radiat Transfer 2004;85:57–97.

[16] Pickett HM, Poynter RL, Cohen EA, Delitsky ML, Pearson JC, Muller HSP. Submillimeter, millimeter, and microwave spectral line catalog. J Quant Spectrosc Radiat Transfer 1998;60:883–90.

[17] Müller HSP, Thorwirth S, Roth DA, Winnewisser G. The Cologne Database for molecular spectroscopy, CDMS. Astron Astrophys 2001;370:L49–52;
HSP Müller, Schlöder F, Stutzki J, Winnewisser G. The Cologne Database for Molecular Spectroscopy, CDMS: a useful tool for astronomers and spectroscopists. J Mol Struct 2005;742:215–27.

[18] Matricardi M. Technical Note: An assessment of the accuracy of the RTTOV fast radiative transfer model using IASI data. Atmos Chem Phys 2009;9:6899–913.

[19] Newman SM. Report on the impact of use of different spectroscopic databases on forward modelling of IASI and ARIES spectra and associated 1d-var retrievals. Met Office internal report (Observations based research Technical Note No. 77) 2010.

[20] Coudert LH, Wagner G, Birk M, Yul Baranov, Lafferty WJ, Flaud JM. The $H_2^{16}O$ molecule: line position and line intensity analyses up to the second triad. J Mol Spectrosc 2008;251:339–57.

[21] Lanquetin R, Coudert LH, Camy-Peyret C. High-lying rotational levels of water: an analysis of the energy levels of the five first vibrational states. J Mol Spectrosc 2001;206:83–103.

[22] Toth RA. Water vapor measurements between 590 and 2582 cm^{-1}: line positions and strengths. J Mol Spectrosc 1998;190:379–96.

[23] Tolchenov RN, Tennyson J. Water line parameters from refitted spectra constrained by empirical upper state levels: study of the 9500–14,500 cm^{-1} region. J Quant Spectrosc Radiat Transfer 2008;109:559–68.

[24] Schermaul R, Learner RCM, Newnham DA, Williams RG, Ballard J, Zobov NF, et al. The water vapour spectrum in the region 8600–15,000 cm^{-1}: experimental and theoretical studies for a new spectral line database I: Laboratory measurements. J Mol Spectrosc 2001;208:32–42.

[25] Schermaul R, Brault JW, Canas AAD, Learner RCM, Polyansky OL, Zobov NF, et al. Weak line water vapour spectrum in the regions 13,200–15,000 cm^{-1}. J Mol Spectrosc 2002;211:169–78.

[26] Bykov A, Lavrentieva N, Sinitsa L. Semi-empiric approach for the line broadening and shifting calculation. Mol Phys 2004;102: 1706–12.

[27] Barber RJ, Tennyson J, Harris GJ, Tolchenov RN. A high accuracy computed water line list. Mon Not R Astron Soc 2006;368:1087–94.

[28] Bykov AD, Lavrentieva NN, Mishina TP, Sinitsa LN, Barber RJ, Tolchenov RN, et al. Water vapor line width and shift calculations with accurate vibration–rotation wave functions. J Quant Spectrosc Radiat Transfer 2008;109:1834–44.

[29] Hodges JT, Lisak D, Lavrentieva NN, Bykov A, Sinitsa L, Tennyson J, et al. Comparison between theoretical calculations and high-resolution measurements of pressure broadening for near-infrared water spectra. J Mol Spectrosc 2008;249:86–94.

[30] Bykov AD, Lavrentieva NN, Petrova TM, Sinitsa LN, Solodov AM, Barber RJ, et al. Shift of the centers of H_2O absorption lines in the region of 1.06 μm. Opt Spectrosc 2008;105:25–31.

[31] Lavrentieva NN, Osipova A, Sinitsa L, Ch Claveau, Valentin A. Shifting temperature dependence of nitrogen-broadened lines in the ν_2 band of H_2O. Mol Phys 2008;106:1261–6.

[32] Perevalov VI, Tashkun SA. CDSD-296 (Carbon Dioxide Spectroscopic Databank): updated and enlarged version for atmospheric applications. In: Proceedings of the 10th HITRAN database conference, Cambridge, MA, USA, 2008, ftp.iao.ru/pub/CDSD-2008/296.

[33] Toth RA, Brown LR, Miller CE, Devi VM, Benner DC, Miller CE. Spectroscopic database of CO_2 line parameters: 4300–7000 cm^{-1}. J Quant Spectrosc Radiat Transfer 2008;109:906–21.

[34] Tashkun SA, Perevalov VI, Teffo JL, Bykov AD, Lavrentieva NN. CDSD-296, the carbon dioxide spectroscopic databank: version for atmospheric applications. In: Proceedings of the XIV symposium on high resolution molecular spectroscopy, Krasnoyarsk, Russia, July 6–11, 2003.

[35] Ding Y, Macko P, Romanini D, Perevalov VI, Tashkun SA, Teffo JL, et al. High sensitivity cw-cavity ringdown and Fourier Transform absorption spectroscopies of $^{13}CO_2$. J Mol Spectrosc 2004;226: 146–60.

[36] André F, Perrin MY, Taine J. FTIR measurements of $^{12}C^{16}O_2$ line positions and intensities at high temperature in the 3700–3750 cm^{-1} spectral region. J Mol Spectrosc 2004;228:187–205.

[37] Amy-Klein A, Vigué H, Chardonnet C. Absolute frequency measurement of $^{12}C^{16}O_2$ laser lines with a femtosecond laser comb and new determination of the $^{12}C^{16}O_2$ molecular constants and frequency grid. J Mol Spectrosc 2004;228:206–12.

[38] Miller CE, Montgomery MA, Onorato RM, Johnstone C, McNicholas TP, Kovaric B, et al. Near infrared spectroscopy of carbon dioxide. II: $^{13}C^{16}O_2$ and $^{16}O^{13}C^{18}O$ line positions. J Mol Spectrosc 2004;228:355–74.

[39] Pouchet I, Zéninari V, Parvitte B, Durry G. Diode laser spectroscopy of CO_2 in the 1.6 μm region for the in situ sensing of the middle atmosphere. J Quant Spectrosc Radiat Transfer 2004;83:619–28.

[40] Majcherova Z, Macko P, Romanini D, Perevalov VI, Tashkun SA, Teffo JL, et al. High-sensitivity CW-cavity ringdown spectroscopy of $^{12}CO_2$ near 1.5 μm. J Mol Spectrosc 2005;230:1–21.

[41] Ding Y, Campargue A, Bertseva E, Tashkun S, Perevalov VI. Highly sensitive absorption spectroscopy of carbon dioxide by ICLAS-VeCSEL between 8800 and 9530 cm^{-1}. J Mol Spectrosc 2005;231: 117–23.

[42] Wang L, Perevalov VI, Tashkun SA, Liu AW, Hu SM. Absorption spectra of $^{12}C^{16}O_2$ and $^{13}C^{16}O_2$ near 1.05 μm. J Mol Spectrosc 2005;233:297–300.

[43] Wang L, Perevalov VI, Tashkun SA, Ding Y, Hu SM. Absolute line intensities of $^{13}C^{16}O_2$ in the 4200–8500 cm^{-1} region. J Mol Spectrosc 2005;234:84–92.

[44] Vander Auwera J, Claveau C, Teffo JL, Tashkun SA, Perevalov VI. Absolute line intensities of $^{13}C^{16}O_2$ in the 3090–3920 cm^{-1} region. J Mol Spectrosc 2006;235:77–83.

[45] Boudjaadar D, Mandin JY, Dana V, Picqué N, Guelachvili G. $^{12}C^{16}O_2$ line intensity measurements around 1.6 μm. J Mol Spectrosc 2006;236:158–67.

[46] Perevalov BV, Kassi S, Romanini D, Perevalov VI, Tashkun SA, Campargue A. CW-cavity ringdown spectroscopy of carbon dioxide isotopologues near 1.5 μm. J Mol Spectrosc 2006;238:241–55.

[47] Tanaka T, Fukabori M, Sugita T, Nakajima H, Yokota T, Watanabe T, et al. Spectral line parameters for CO_2 bands in the 4.8 to 5.3 μm region. J Mol Spectrosc 2006;239:1–10.

[48] Toth RA, Brown LR, Miller CE, Devi VM, Benner DC. Line strengths of $^{12}C^{16}O_2$: 4550–7000 cm^{-1}. J Mol Spectrosc 2006;239:221–42.

[49] Le Barbu T, Zéninari V, Parvitte B, Courtois D, Durry G. Line strengths and self-broadening coefficients of carbon dioxide isotopologues ($^{13}CO_2$ and $^{18}O^{12}C^{16}O$) near 2.04 μm for the in situ laser sensing of the Martian atmosphere. J Quant Spectrosc Radiat Transfer 2006;98:264–76.

[50] Régalia-Jarlot L, Zéninari V, Parvitte B, Grossel A, Thomas X, von der Heyden P, et al. A complete study of the line intensities of four bands of CO_2 around 1.6 and 2.0 μm: A comparison between Fourier transform and diode laser measurements. J Quant Spectrosc Radiat Transfer 2006;101:325–38.

[51] Perevalov BV, Kassi S, Romanini D, Perevalov VI, Tashkun SA, Campargue A. Global effective Hamiltonians of $^{16}O^{13}C^{17}O$ and $^{16}O^{13}C^{18}O$ improved from CW-CRDS observations in the 5900–7000 cm^{-1} region. J Mol Spectrosc 2007;241:90–100.

[52] Toth RA, Miller CE, Brown LR, Devi VM, Benner DC. Line positions and strengths of $^{16}O^{12}C^{18}O$, $^{18}O^{12}C^{18}O$ and $^{17}O^{12}C^{18}O$ between 2200 and 7000 cm^{-1}. J Mol Spectrosc 2007;243:43–61.

[53] Wang L, Perevalov VI, Tashkun SA, Song KF, Hu SM. Fourier Transform spectroscopy of $^{12}C^{18}O_2$ and $^{16}O^{12}C^{18}O$ in the 3800–8500 cm^{-1} region and the global modeling of the absorption spectrum of $^{12}C^{18}O_2$. J Mol Spectrosc 2008;247:64–85.

[54] Wilquet V, Mahieux A, Vandaele AC, Perevalov VI, Tashkun SA, Fedorova A, et al. Line parameters for the 01111–00001 band of $^{12}C^{16}O^{18}O$ from SOIR measurements of the Venus atmosphere. J Quant Spectrosc Radiat Transfer 2008;109:895–905.

[55] Perevalov BV, Deleporte T, Liu AW, Kassi S, Campargue A, Vander Auwera J, et al. Global modeling of $^{13}C^{16}O_2$ absolute line intensities from CW-CRDS and FTS measurements in the 1.6 and 2.0 micrometer regions. J Quant Spectrosc Radiat Transfer 2008;109:2009–26.

[56] Perevalov BV, Kassi S, Perevalov VI, Tashkun SA, Campargue A. High sensitivity CW-CRDS spectroscopy of $^{12}C^{16}O_2$, $^{16}O^{12}C^{17}O$ and $^{16}O^{12}C^{18}O$ between 5851 and 7045 cm^{-1}: line positions analysis and critical review of the current databases. J Mol Spectrosc 2008;252:143–59.

[57] Toth RA, Miller CE, Brown LR, Devi VM, Benner DC. Line strengths of $^{16}O^{13}C^{16}O$, $^{16}O^{13}C^{18}O$, $^{16}O^{13}C^{17}O$ and $^{17}O^{13}C^{18}O$ between 2200 and 6800 cm^{-1}. J Mol Spectrosc 2008;251:64–89.

[58] Perevalov BV, Campargue A, Gao B, Kassi S, Tashkun SA, Perevalov VI. New CW-CRDS measurements and global modeling of $^{12}C^{16}O_2$ absolute line intensities in the 1.6 μm region. J Mol Spectrosc 2008;252:190–7.

[59] Perevalov BV, Perevalov VI, Campargue AA. (nearly) complete experimental line list for $^{13}C^{16}O_2$, $^{16}O^{13}C^{18}O$, $^{16}O^{13}C^{17}O$, $^{13}C^{18}O_2$ and $^{17}O^{13}C^{18}O$ by high-sensitivity CW-CRDS spectroscopy between 5851 and 7045 cm^{-1}. J Quant Spectrosc Radiat Transfer 2008;109:2437–62.

[60] Teffo JL, Sulakshina ON, Perevalov VI. Effective Hamiltonian for rovibrational energies and line intensities of carbon dioxide. J Mol Spectrosc 1992;156:48–64.

[61] Perevalov VI, Lobodenko EI, Lyulin OM, Teffo JL. Effective dipole moment and band intensities problem for carbon dioxide. J Mol Spectrosc 1995;171:435–52.

[62] Tashkun SA, Perevalov VI, Teffo JL, Rothman LS, Tyuterev VlG. Global fitting of $^{12}C^{16}O_2$ vibration–rotation line positions using the effective Hamiltonian approach. J Quant Spectrosc Radiat Transfer 1998;60:785–801.

[63] Tashkun SA, Perevalov VI, Teffo JL, Tyuterev VlG. Global fit of $^{12}C^{16}O_2$ vibration–rotation line intensities using the effective operator approach. J Quant Spectrosc Radiat Transfer 1999;62:571–98.

[64] Campargue A, Perevalov BV. Comment on 'Spectroscopic database of CO_2 line parameters: 4300–7000 cm^{-1}'. J Quant Spectrosc Radiat Transfer 2009;109:2261–71.

[65] Rothman LS, Hawkins RL, Wattson RB, Gamache RR. Energy levels, intensities, and linewidths of atmospheric carbon dioxide bands. J Quant Spectrosc Radiat Transfer 1992;48:537–66.

[66] Toth RA, Miller CE, Devi VM, Benner DC, Brown LR. Air-broadened width and pressure shift coefficients of $^{12}C^{16}O_2$: 4700–7000 cm^{-1}. J Mol Spectrosc 2007;246:133–57.

[67] Toth RA, Brown LR, Miller CE, Devi VM, Benner DC, Dulick M. Self-broadened widths and shifts of CO_2. J Mol Spectrosc 2006;239: 243–71.

[68] Predoi-Cross A, McKellar ARW, Benner DC, Devi VM, Gamache RR, Miller CE, et al. Temperature dependences for air-broadened Lorentz half width and pressure-shift coefficients in the 30013←00001 and 30012←00001 bands of CO_2 near 1600 nm. Can J Phys 2009;87:517–35.

[69] Hartmann JM. A simple empirical model for the collisional spectral shift of air-broadened CO_2 lines. J Quant Spectrosc Radiat Transfer 2009;110:2019–26.

[70] Plateaux JJ, Barbe A, Delahaigue A. Reims high resolution Fourier transform spectrometer. Data reduction for ozone. Spectrochim Acta—Part A 1995;51:1153–69.

[71] Flaud JM, Camy-Peyret C, Devi VM, Rinsland CP, Smith MAH. The ν_1 and ν_3 bands of $^{16}O_3$: Line positions and intensities. J Mol Spectrosc 1987;124:209–17.

[72] Flaud JM, Camy-Peyret C, Rinsland CP, Smith MAH, Devi VM. Line parameters for $^{16}O_3$ bands in the 7-μm region. J Mol Spectrosc 1989;134:106–12.

[73] Mikhailenko S. IAO, Russia. Private Communication; 2000; ⟨http://smpo.iao.ru/1507x904/en/lev/par/1/4/⟩.

[74] Barbe A, Mikhailenko SN, Plateaux JJ, Tyuterev VlG. First study of the $\nu_2=3$ dyad {(130), (031)} of ozone through the analysis of hot bands in the 2300–2600 cm^{-1} region. J Mol Spectrosc 1998;187:70–4.

[75] Devi VM, Flaud J-M, Camy-Peyret C, Rinsland CP, Smith MAH. Line positions and intensities for the $\nu_1+\nu_2$ and $\nu_2+\nu_3$ bands of $^{16}O_3$. J Mol Spectrosc 1987;125:174–83.

[76] Bouazza S, Barbe A, Mikhailenko SN, Plateaux JJ. Line positions and intensities of the $\nu_1+2\nu_2+\nu_3$ and $2\nu_2+2\nu_3$ bands of $^{16}O_3$. J Mol Spectrosc 1994;166:365–71.

[77] Mikhailenko SN, Barbe A, Plateaux JJ, Tyuterev VlG. New analysis of $2v_1+v_2$, $v_1+v_2+v_3$, and v_2+2v_3 bands of ozone in the 2600–2900 cm^{-1} region. J Mol Spectrosc 1999;196:93–101.

[78] Barbe A, Plateaux J-J, Bouazza S, Sulakshina ON, Mikhailenko SN, VlG Tyuterev, et al. Experimental and theoretical study of absolute intensities of ozone spectral lines in the range 1850–2300 cm^{-1}. J Quant Spectrosc Radiat Transfer 1994;52:341–55.

[79] Mikhailenko S, Barbe A, Tyuterev VlG. Extended analysis of line positions and intensities of ozone bands in the 2900–3400 cm^{-1} region. J Mol Spectrosc 2002;215:29–41.

[80] Barbe A, Sulakshina ON, Plateaux J-J, Hamdouni A, Bouazza S. High-resolution infrared spectra of ozone in the 2300–2600 cm^{-1} region. J Mol Spectrosc 1995;170:244–50.

[81] Mikhailenko SN, Babikov YL, Tyuterev VlG, Barbe A. The databank of ozone spectroscopy on WEB (S&MPO). J Comput Technol 2002;7:64–70. ⟨http://smpo.iao.ru/1446x915/en/tran/;par/1/8-2/; http://smpo.iao.ru/1446x915/en/tran/par/1/8-3/⟩. ⟨http://ozone.univ-reims.fr/1446x915/en/tran/par/1/8-2/⟩. ⟨http://ozone.univ-reims.fr/1446x915/en/tran/par/1/8-3/⟩;
Tyuterev VlG, Barbe A, Mikhailenko SN, Babikov YL. The ozone molecule: S&MPO information system on WEB. State of art in recent studies on molecular properties and high-resolution spectroscopy. In: Proceedings of the 17th colloquium on high resolution molecular spectroscopy, Nijmegen; September 2001.

[82] Barbe A, Mikhailenko S, Plateaux JJ. First observation of the $v_2=3$ state of ozone: The (131) state through analysis of cold and hot bands. Study of v_2 behavior. J Mol Spectrosc 1997;184:448–53.

[83] Mikhailenko S, Barbe A, VlG Tyuterev, Régalia L, Plateaux JJ. Line positions and intensities of the $v_1+v_2+v_3$, $2v_2+v_3$, and $3v_1+2v_2$ bands of ozone. J Mol Spectrosc 1996;180:227–35.

[84] Bouazza S, Mikhailenko SN, Barbe A, Régalia L, VlG Tyuterev, Plateaux JJ. The $v_1+v_2+2v_3$ and v_2+3v_3 bands of $^{16}O_3$. J Mol Spectrosc 1995;174:510–9.

[85] Perrin A, Vasserot AM, Flaud JM, Camy-Peyret C, MalathyDevi VM, Smith MAH, et al. The 2.5-µm bands of ozone: line positions and intensities. J Mol Spectrosc 1991;149:519–29.

[86] Mikhailenko S, Barbe A, Tyuterev VlG, Plateaux J.J. New analysis of the (211)/(140)/(310)/(004)/(103) interacting states of ozone. In: Proceedings of the VIII joint international symposium "Atmospheric and Ocean Optics, Atmospheric Physics" June 25–29, 2001, Irkutsk, Russia; 2001.

[87] Barbe A, Plateaux J-J. Analysis of the $2v_1+2v_3$ band of ozone: line positions and intensities. J Quant Spectrosc Radiat Transfer 1996;55:449–55.

[88] Barbe A, Sulakshina ON, Plateaux JJ, Tyuterev VlG, Bouazza S. Line positions and intensities of the $3v_1+v_3$ band of ozone. J Mol Spectrosc 1996;175:296–302.

[89] Barbe A, Mikhailenko SN, VlG Tyuterev, Hamdouni A, Plateaux JJ. Analysis of the $2v_1+2v_2+v_3$ band of ozone. J Mol Spectrosc 1995;171:583–8.

[90] Barbe A, Mikhailenko SN, Plateaux JJ, Tyuterev VlG. Analysis of the $2v_1+v_2+2v_3$ band of ozone. J Mol Spectrosc 1997;182:333–41.

[91] Morville J, Romanini D, Kachanov AA, Chenevier M. Two schemes for trace detection using cavity ringdown spectroscopy. Appl Phys 2004;B78:465–76.

[92] De Backer-Barilly MR, Barbe A, VlG Tyuterev, Romanini D, Moeskops B, Campargue A. Fourier Transform and high sensitivity CW-cavity ring down absorption spectroscopies of ozone in the 6030–6130 cm^{-1} region. First observation and analysis of the $3v_1+3v_3$ and $2v_2+5v_3$ bands. J Mol Struct 2006;780–781:225–33.

[93] Barbe A, De Backer-Barilly MR, VlG Tyuterev, Campargue A, Romanini D, Kassi S. CW-cavity ring down spectroscopy of the ozone molecule in the 5980–6220 cm^{-1} region. J Mol Spectrosc 2007;242:156–75.

[94] Flaud JM, Camy-Peyret C, N'Gom A, Devi VM, Rinsland CP, Smith MAH. The v_2 bands of $^{16}O^{18}O^{16}O$ and $^{16}O^{16}O^{18}O$: line positions and intensities. J Mol Spectrosc 1989;133:217–23.

[95] Chichery A, Barbe A, VlG Tyuterev, Tashkun SA. High resolution IR spectra of ^{18}O-enriched ozone: band centers of $^{16}O^{16}O^{18}O$, $^{16}O^{18}O^{18}O$, $^{18}O^{16}O^{18}O$, and $^{16}O^{18}O^{16}O$. J Mol Spectrosc 2001;205:347–9.

[96] De Backer-Barilly MR, Barbe A, VlG Tyuterev, Chichery A, Bourgeois MT. High-resolution infrared spectra of the $^{16}O^{18}O^{16}O$ ozone isotopomer in the range 900–5000 cm^{-1}: line positions. J Mol Spectrosc 2002;216:454–64.

[97] Barbe A., De Backer-Barilly MR. Université de Reims, Reims, France. Private Communication; 2007.

[98] Toth RA. Line-list of N_2O parameters from 500 to 7500 cm^{-1}; ⟨http://mark4sun.jpl.nasa.gov/n2o.html⟩ and Refs. therein.

[99] Toth RA. Line strengths (900–3600 cm^{-1}) self-broadened line widths and frequency shifts (1800–2660 cm^{-1}) of N_2O. Appl Opt 1993;32:7326–65.

[100] Toth RA. Line positions and strengths of N_2O between 3515 and 7800 cm^{-1}. J Mol Spectrosc 1999;197:158–87.

[101] Toth RA. N_2- and air-broadened linewidths and frequency-shifts of N_2O. J Quant Spectrosc Radiat Transfer 2000;66:285–304.

[102] Drouin BJ, Maiwald FW. Extended THz measurements of nitrous oxide, N_2O. J Mol Spectrosc 2006;236:260–2.

[103] Albert S, Bauerecker A, Boudon V, Brown LR, Champion JP, Loëte M, et al. Global frequency and intensity analysis of $^{12}CH_4$ in the 0–4800 cm^{-1} region. J Chem Phys 2009;356:131–46.

[104] Wishnow EH, Orton GS, Ozier I, Gush HP. The distortion dipole rotational spectrum of CH_4: a low temperature far-infrared study. J Quant Spectrosc Radiat Transfer 2007;103:102–17.

[105] Frankenberg C, Warneke T, Butz A, Aben I, Hase F, Spietz P, et al. Methane spectroscopy in the near infrared and its implication on atmospheric retrievals. Atmos Chem Phys 2008;8:10021–55.

[106] Margolis JS. Measured line positions and strengths of methane between 5500 and 6180 cm^{-1}. Appl Opt 1988;27:4038–51.

[107] Margolis JS. Empirical values of the ground state energies for methane transitions between 5500 to 6150 cm^{-1}. Appl Opt 1990;29:2295–302.

[108] Gao B, Kassi S, Campargue A. Empirical low energy values for methane transitions in the 5852–6181 cm^{-1} region by absorption spectroscopy at 81 K. J Mol Spectrosc 2009;253:55–63.

[109] Nikitin AV, Lyulin OM, Mikhailenko SN, Perevalov VI, Filippov NN, Grigoriev IM, et al. GOSAT-2009 methane spectral line list in the 5550–6236 cm^{-1} range. J Quant Spectrosc Radiat Transfer 2010;111:2211–24.

[110] Kassi S, Gao B, Romanini D, Campargue A. The near-infrared (1.30–1.70 µm) absorption spectrum of methane down to 77 K. Phys Chem Chemic Phys (Incorporating Faraday Trans) 2008;10:4410–9.

[111] Lyulin OM, Nikitin AV, Perevalov VI, Morino I, Yokota T, Kumazawa R, et al. Measurements of N_2- and O_2-broadening and -shifting parameters of the methane spectral lines in the 5550–6236 cm^{-1} region. J Quant Spectrosc Radiat Transfer 2009;110:654–68.

[112] Nikitin AV, Mikhailenko S, Morino I, Yokota T, Kumazawa R, Watanabe T. Isotopic substitution shifts in methane and vibrational band assignment in the 5560–6200 cm^{-1} region. J Quant Spectrosc Radiat Transfer 2009;110:964–73.

[113] Campargue A, Wang L, Liu AW, Hu SM, Kassi S. Empirical line parameters of methane in the 1.63–1.48 µm transparency window by high sensitivity Cavity Ring Down Spectroscopy. Chem Phys 2010;373:203–10.

[114] Wang L, Kassi S, Liu AW, Hu SM, Campargue A. High sensitivity absorption spectroscopy of methane at 80 K in the 1.58 µm transparency window: Temperature dependence and importance of the CH_3D contribution. J Mol Spectrosc 2010;261:41–52.

[115] Campargue A, Wang L, Kassi S, Mašát M, Votava O. Temperature dependence of the absorption spectrum of CH_4 by high resolution spectroscopy at 81 K: (II) The Icosad region (1.49–1.30 µm). J Quant Spectrosc Radiat Transfer 2010;111:1141–51.

[116] Nikitin AV, Thomas X, Régalia L, Daumont L, Von der Heyden P, Tyuterev VlG, et al. Assignment of the $5v_4$ and v_2+4v_4 band systems of $^{12}CH_4$ in the 6287–6550 cm^{-1} region. J Quant Spectrosc Radiat Transfer 2011;112:28–40.

[117] Wang L, Kassi S, Campargue A. Temperature dependence of the absorption spectrum of CH_4 by high resolution spectroscopy at 81 K: (I) The region of the $2v_3$ band at 1.66 µm. J Quant Spectrosc Radiat Transfer 2010;111:1130–40.

[118] Lyulin OM, Kassi S, Sung K, Brown LR, Campargue A. Determination of the low energy values of $^{13}CH_4$ transitions in the $2v_3$ region near 1.66 µm from absorption spectra at 296 and 81 K. J Mol Spectrosc 2010;261:91–100.

[119] Brown LR, Benner DC, Champion JP, Devi VM, Fejard L, Gamache RR, et al. Methane line parameters in HITRAN. J Quant Spectrosc Radiat Transfer 2003;82:219–38.

[120] Brown LR. Empirical line parameters of methane from 1.1 to 2.1 µm. J Quant Spectrosc Radiat Transfer 2005;96:251–70.

[121] MAH Smith, Benner DC, Predoi-Cross A, Devi VM. Multispectrum analysis of $^{12}CH_4$ in the v_4 band: I, air-broadened half widths, pressure-induced shifts, temperature dependences and line mixing. J Quant Spectrosc Radiat Transfer 2009;110:639–53;
Smith MAH, Benner DC, Predoi-Cross A, Devi VM. Multispectrum analysis of $^{12}CH_4$ in the v_4 band: II, self-broadened half widths, pressure-induced shifts, temperature dependences and line

mixing. J Quant Spectrosc Radiat Transfer 2010;111:1152–66; Smith MAH, Benner DC, Predoi-Cross A, Devi VM. A multispectrum analysis of the ν_4 band of $^{13}CH_4$: widths, shifts, and line mixing coefficients. J Quant Spectrosc Radiat Transfer 2011;112:952–68.

[122] Antony BK, Niles DL, Wroblewski SB, Humphrey CM, Gabard T, Gamache RR. N_2-, O_2- and air-broadened half-widths and line shifts for transitions in the ν_3 band of methane in the 2726 to 3200 cm^{-1} spectral region. J Mol Spectrosc 2008;251:268–81.

[123] Predoi-Cross A, Brown LR, Devi VM, Brawley-Tremblay M, Benner DC. Multispectrum analysis of self-broadening and pressure-shifting coefficients of $^{12}CH_4$ from 4100 to 4635 cm^{-1}. J Mol Spectrosc 2005;232:231–46.

[124] Predoi-Cross A, Brawley-Tremblay M, Brown LR, Devi VM, Benner DC. Multispectrum analysis of $^{12}CH_4$ from 4100 to 4635 cm^{-1}: II, air-broadening coefficients (widths and shifts). J Mol Spectrosc 2006;236:201–15.

[125] Thievin J, Georges R, Carles S, Benidar A, Rowe B, Champion JP. High-temperature emission spectroscopy of methane. J Quant Spectrosc Radiat Transfer 2008;109:2027–36.

[126] Wenger C, Champion JP, Boudon V. The partition sum of methane at high temperature. J Quant Spectrosc Radiat Transfer 2008;109: 2697–706.

[127] Robichaud DJ, Hodges JT, Maslowsk P, Yeung LY, Okumura M, Miller CE, et al. High-accuracy transition frequencies for the O_2 A-band. J Mol Spectrosc 2008;251:27–37.

[128] Robichaud DJ, Hodges JT, Brown LR, Lisak D, Maslowsk P, Yeung LY, et al. Experimental intensity and line-shape parameters of the oxygen A-band using frequency-stabilized cavity ring-down spectroscopy. J Mol Spectrosc 2008;248:1–13.

[129] Robichaud DJ, Hodges JT, Lisak D, Miller CE, Okumura M. High-precision pressure shifting measurement technique using frequency-stabilized cavity ring-down spectroscopy. J Quant Spectrosc Radiat Transfer 2008;109:435–44.

[130] Robichaud DJ, Yeung LY, Long DA, Havey DK, Hodges JT, Lisak D, et al. Experimental line parameters of the $b^1\Sigma_g^+ \leftarrow X^3\Sigma_g^-$ band of oxygen isotopologues at 760 nm using frequency-stabilized cavity ring-down spectroscopy. J Phys Chem A 2009;113:13089–99.

[131] Falke S, Tiemann E, Lisdat C, Schnatz H, Grosche G. Transition frequencies of the D lines of K-39, K-40, and K-41 measured with a femtosecond laser frequency comb. Phys Rev 2006;A 74 (art. no.-032503).

[132] Babcock HD, Herzberg L. Fine structure of the red system of atmospheric oxygen bands. Astrophys J 1948;108:167–90.

[133] Yang Z, Wennberg PO, Cageao RP, Pongetti TJ, Toon GC, Sander SP. Ground-based photon path measurements from solar absorption spectra of the O_2 A-band. J Quant Spectrosc Radiat Transfer 2005;90:309–21.

[134] Predoi-Cross A, Hambrook K, Keller R, Povey C, Schofield I, Hurt-mans D, et al. Spectroscopic line shape study of the self-perturbed oxygen A-band. J Mol Spectrosc 2008;248:85–110.

[135] Predoi-Cross A, Holladay C, Heung H, Bouanich J-P, GCh Mellau, et al. Nitrogen-broadened line shapes in the oxygen A-band: experimental results and theoretical calculations. J Mol Spectrosc 2008;251:159–75.

[136] Brown LR, Plymate C. Experimental line parameters of the Oxygen A band at 760 nm. J Mol Spectrosc 2000;199:166–79.

[137] Tran H, Hartmann JM. An improved O_2 A band absorption model and its consequences for retrievals of photon paths and surface pressures. J Geophys Res 2008;113:D18104, doi:10.1029/2008JD010011.

[138] Goldman A. DU, USA. Private Communication; 2008.

[139] Goldman A, Brown LR, Schoenfeld WG, Spencer MN, Chackerian Jr. C, Giver LP, et al. Nitric oxide line parameters: review of 1996 HITRAN update and new results. J Quant Spectrosc Radiat Transfer 1998;60: 825–38.

[140] Belayev D, Fedorova A, Korablev O, Vandaele AC, Mahieux A, Neefs E, et al. SO_2 detection in the Venus mesosphere with the SOIR spectrometer on board Venus Express. J Geophys Res 2008. doi:10.1029/2008JE003143.

[141] Bertaux J-L, Widemann T, Hauchecorne A, Moroz VI, Ekonomov AP. VEGA 1 and VEGA 2 entry probes: an investigation of local UV absorption (220–400 nm) in the atmosphere of Venus (SO_2, aerosols, cloud structure). J Geophys Res 1996;101:12709–46.

[142] Barker ES. Detection of SO_2 in the UV Spectrum of Venus. Geophys Res Lett 1979;6:117–20.

[143] Esposito LW, Copley M, Eckert R, Gates L, Stewart AIF, Worden H. Sulfur dioxide at the Venus cloud tops, 1978–1986. J Geophys Res 1988;93:5267–76.

[144] Esposito LW, Winick JR, Stewart AI. Sulfur dioxide in the Venus atmosphere: distribution and implications. Geophys Res Lett 1979;6:601–4.

[145] Jessup KL, Spencer J, Yelle R. Sulfur volcanism on Io. Icarus 2007;192:24–40.

[146] Bertaux JL, Belton MJS. Evidence of SO_2 on Io from UV observations. Nature 1979;282:813–5.

[147] Ballester GE, Mcgrath MA, Strobel DF, Zhu X, Feldman PD, Moos HW. Detection of the SO_2 atmosphere on Io with the Hubble Space Telescope. Icarus 1994;111:2–17.

[148] McGrath MA, Belton M, Spencer J, Sartoretti P. Spatially resolved spectroscopy of Io's Pele plume and SO_2 atmosphere. Icarus 2000;146:476–93.

[149] Kim SJ, A'Hearn MF. Upper limits of SO and SO_2 in Comets. Icarus 1991;90:79–95.

[150] Kim SJ, Bockelée-Morvan D, Crovisier J, Biver N. Abundances of SO and SO_2 in Comet Hale–Bopp (C/1995 O1). Earth Moon Planets 1997;78:65–6.

[151] Despois D. Radio line observations of molecular and isotopic species in Comet C/1995 O1 (Hale-Bopp). Earth Moon Planets 1997;79:103–24.

[152] Bockelée-Morvan D, Crovisier J. Lessons of Comet Hale-Bopp for coma chemistry: observations and theory. Earth Moon Planets 2002;89:53–71.

[153] Camy-Peyret C, Bergquist B, Galle B, Carleer M, Clerbaux C, Colin R, et al. Intercomparison of instruments for troposheric measurements using differential optical absorption spectroscopy. J Atmos Chem 1996;23:51–80.

[154] Möhler O, Arnold F. Gaseous sulfuric acid and sulfur dioxide measurements in the arctic troposphere and lower stratosphere: implications for hydroxyl radical abundances. Geophys Res Lett 1992;19:1763–6.

[155] Vandaele AC, Tsouli A, Carleer M, Colin R. UV Fourier transform measurements of tropospheric O_3, NO_2, SO_2, benzene, and toluene. Environ Pollut 2002;116:193–201.

[156] Sagawa E, Itoh T. Mass spectrometric observation of SO_2 in the stratosphere. Geophys Res Lett 1977;4:29–32.

[157] Jaeschke W, Schmitt R, Georgii HW. Preliminary results of strato-spheric SO_2 measurements. Geophys Res Lett 1976;3:517–9.

[158] Lellouch E, Th Encrenaz, Belton M, de Pater I, Gulkis S. Io's atmosphere from microwave detection SO_2. Nature 1990;346: 639–41;
Spencer JR, Lellouch E, Richter MJ, Lopez-Valverde MA, Jessup KL, et al. Mid-infrared detection of large longitudinal asymmetries in Io's SO_2 atmosphere. Icarus 2005;176:283–304.

[159] Chu PM, Wetzel SJ, Lafferty WJ, Perrin A, Flaud JM, Arcas Ph, et al. Line intensities for the 8 μm bands of SO_2. J Mol Spectrosc 1998;189:55–63.

[160] Flaud JM, Perrin A, Salah LM, Lafferty WJ, Guelachvili G. A reanalysis of the (0 1 0), (0 2 0), (1 0 0) and (0 0 1) rotational levels of $^{12}S^{16}O_2$. J Mol Spectrosc 1993;160:272–8.

[161] Henningsen J, Barbe A, De Backer-Barilly MR. Revised molecular parameters for $^{32}SO_2$ and $^{34}SO_2$ from high resolution study of the infrared spectrum in the 7–8 μm wavelength region. J Quant Spectrosc Radiat Transfer 2008;109:2491–510.

[162] Lafferty WJ, Pine AS, Hilpert G, Sams RL, Flaud JM. The $\nu_1+\nu_3$ and $2\nu_1+\nu_3$ band systems of SO_2: line positions and intensities. J Mol Spectrosc 1996;176:280–6.

[163] Lafferty WJ, Flaud JM, Sams RL, Ngom EHA. High resolution analysis of the rotational levels of the (0 0 0), (0 1 0), (1 0 0), (0 0 1), (0 2 0), (1 1 0) and (0 1 1) vibrational states of $^{34}S^{16}O_2$. J Mol Spectrosc 2008;252:72–6.

[164] Lafferty WJ, Flaud JM, Ngom EHA, Sams RL. $^{34}S^{16}O_2$: high resolution analysis of the (0 3 0), (1 0 1), (1 1 1), (0 0 2) and (2 0 1) vibrational states: determination of equilibrium rotational constants for sulfur dioxide and anharmonic vibrational constants. J Mol Spectrosc 2009;253:51–4.

[165] Flaud JM, Lafferty WJ, Sams RL. Line intensities for the ν_1, ν_3 and $\nu_1+\nu_3$ bands of $^{34}SO_2$. J Quant Spectrosc Radiat Transfer 2009;110:669–74.

[166] Müller HSP, Brünken S. Accurate rotational spectroscopy of sulfur dioxide, SO_2, in its ground vibrational and first excited bending states, $\nu_2=0$, 1, up to 2 THz. J Mol Spectrosc 2005;232:213–22.

[167] Perrin A, Flaud JM, Goldman A, Camy-Peyret C, Lafferty WJ, Arcas Ph, et al. NO_2 and SO_2 line parameters: 1996 HITRAN update and new results. J Quant Spectrosc Radiat Transfer 1998;60:839–50.

[168] Benner DC, Blake TA, Brown LR, Devi VM, Smith MAH, Toth RA. Air-broadening parameters in the ν_3 band of $^{14}N^{16}O_2$ using a multispectrum fitting technique. J Mol Spectrosc 2004;228: 593–619.

[169] Kleiner I, Brown LR. LISA, France, and JPL, USA, private communication, 2003.

[170] Kleiner I, Tarrago G, Cottaz C, Sagui L, Brown LR, Poynter RL, et al. NH₃ and PH₃ line parameters: 2000 HITRAN update and new results. J Quant Spectrosc Radiat Transfer 2003;82:293–312.

[171] Burgdorf MJ, Orton GS, Encrenaz T, Davis GR, Sidher SD, Lellouch E, et al. The FIR spectrum of Jupiter and Saturn. Planet Space Sci 2004;52:379–83.

[172] Noll KS, Larson HP. The spectrum of Saturn from 1990 to 2230 cm⁻¹: abundances of AsH₃, CH₃D, CO, GeH₄, NH₃, and PH₃. Icarus 1991;89:168–89.

[173] Beer R, Taylor FW. Phosphine absorption in the 5-micron window of Jupiter. Icarus 1979;40:189–92.

[174] Larson HP, Fink U, Smith MHA, Davis DS. The middle-infrared spectrum of Saturn: evidence for phosphine and upper limits to other trace atmospheric constituents. Astrophys J 1980;240:327–37.

[175] Kim JH, Kim SJ, Geballe TR, Kim SS, Brown LR. High-resolution spectroscopy of Saturn at 3 microns: CH₄, CH₃D, C₂H₂, C₂H₆, PH₃, clouds and haze. Icarus 2006;185:476–86.

[176] Capaccioni F, Coradini A, Cerroni P, Amici S. Imaging spectroscopy of Saturn and its satellites: VIMS-V onboard Cassini. Planet Space Sci 1998;46:1263–76.

[177] Butler RAH, Sagui S, Kleiner I, Brown LR. The absorption spectrum of phosphine (PH₃) between 2.8 and 3.7 microns: line positions, intensities, and assignments. J Mol Spectrosc 2006;238:178–92.

[178] Nikitin AV, Champion JP, Butler RAH, Brown LR, Kleiner I. Global modeling of the lower three polyads of PH₃: preliminary result. J Mol Spectrosc 2009;216:4–16;
Nikitin AV, Holka F, Tyuterev VG, Fremont J. Vibration energy levels of the PH₃, PH₂D, and PHD₂ molecules calculated from high order potential energy surface. J Chem Phys 2009. doi:10.1063/1.3156311.

[179] Perrin A. LISA, France. Private Communication; 2008.

[180] Petkie DT. Wright State University, USA. Private Communication; 2008.

[181] Flaud JM, Brizzi G, Carlotti M, Perrin A, Ridolfi M. MIPAS database: validation of HNO₃ line parameters using MIPAS satellite measurements. Atmos Chem Phys 2006;6:1–12.

[182] Gomez L, Tran H, Perrin A, Gamache RR, Laraia A, Orphal O, et al. Some improvements of the HNO₃ spectroscopic parameters in the spectral region from 600 to 950 cm⁻¹. J Quant Spectrosc Radiat Transfer 2009;110:675–86.

[183] Perrin A, Orphal J, Flaud JM, Klee S, Mellau G, Mäder H, et al. New analysis of the ν₅ and 2ν₉ bands of HNO₃ by infrared and millimeter wave techniques: line positions and intensities. J Mol Spectrosc 2004;228:375–91.

[184] Chackerian Ch Sharpe SW, Blake TA. Anhydrous nitric acid integrated absorption cross sections: 820–5300 cm⁻¹. J Quant Spectrosc Radiat Transfer 2003;82:429–41.

[185] Laraia A, Gamache RR, Hartmann JM, Perrin A, Gomez L. Theoretical calculations of N₂-broadened half-widths of ν₅ transitions of HNO₃. J Quant Spectrosc Radiat Transfer 2009;110:687–99.

[186] Mencaraglia F, Bianchini G, Boscaleri A, Carli B, Ceccherini S, Raspollini P, et al. Validation of MIPAS satellite measurements of HNO₃ using comparison of rotational and vibrational spectroscopy. J Geophys Res 2006;111:D19305, doi:10.1029/2005JD006099.

[187] Tran H, Brizzi G, Gomez L, Perrin A, Hase F, Ridolfi M, et al. Validation of HNO₃ spectroscopic parameters using atmospheric absorption and emission measurements. J Quant Spectrosc Radiat Transfer 2009;110:109–17.

[188] Perrin A, Lado-Bordowski O, Valentin A. The ν₃ and ν₄ interacting bands of HNO₃. Mol Phys 1989;67:249–70.

[189] Petkie DT, Goyette TM, Helminger P, Pickett HM, De Lucia FC. The energy levels of the ν₅/2ν₉ dyad of HNO₃ from millimeter and submillimeter rotational spectroscopy. J Mol Spectrosc 2001;208:121–35.

[190] Petkie DT, Helminger P, Butler RAH, Albert S, De Lucia FC. The millimeter and submillimeter spectra of the ground state and excited ν₉, ν₈, ν₇, and ν₆ vibrational states of HNO₃. J Mol Spectrosc 2003;218:127–30.

[191] Petkie DT, Helminger P, Winnewisser BP, Winnewisser M, Butler RAH, Jucks KW, et al. The simulation of infrared bands from the analyses of rotational spectra: the 2ν₉–ν₉ and ν₅–ν₉ hot bands of HNO₃. J Quant Spectrosc Radiat Transfer 2005;92:129–41.

[192] Pickett HM. The fitting and prediction of vibration–rotation spectra with spin interactions. J Mol Spectrosc 1991;148:371–7.

[193] Sirota JM, Weber M, Reuter DC, Perrin A. HNO₃: absolute line intensities for the ν₉ fundamental. J Mol Spectrosc 1997;184:140–4.

[194] Goldman A, Burkholder JB, Howard CJ, Escribano R, Maki AG. Spectroscopic constants for the ν₉ infrared band of HNO₃. J Mol Spectrosc 1988;131:195–200.

[195] Perrin A, Flaud JM, Camy-Peyret C, Winnewisser BP, Klee S, Goldman A, et al. First analysis of the 3ν₉–ν₉, 3ν₉–ν₅, and 3ν₉–2ν₉ bands of HNO₃: torsional splitting in the 3ν₉–ν₉ vibrational-mode. J Mol Spectrosc 1994;166:224–43.

[196] Naim S, Fayt A, Bredohl H, Blavier J-F, Dubois I. Fourier transform spectroscopy of carbonyl sulfide from 3700 to 4800 cm⁻¹ and selection of a line-point program. J Mol Spectrosc 1998;192:91–101.

[197] Fayt A, Vandenhaute R, Lahaye J-G. Global rovibrational analysis of carbonyl sulfide. J Mol Spectrosc 1986;119:233–66.

[198] Lahaye J-G, Vandenhaute R, Fayt A. CO₂ laser saturation Stark spectra and global rovibrational analysis of the main isotopic species of carbonyl sulfide (OC³⁴S, O¹³CS, and ¹⁸OCS). J Mol Spectrosc 1987;123:48–83.

[199] Masukidi LS, Lahaye J-G, Fayt A. Intracavity CO and CO₂ laser Stark spectroscopy of the isotopomers of carbonyl sulfide. J Mol Spectrosc 1992;154:137–62.

[200] Strugariu T, Naim S, Bredohl H, Blavier J-F, Dubois I. Fourier transform spectroscopy of ¹⁸O-enriched carbonyl sulfide from 1825 to 2700 cm⁻¹. J Mol Spectrosc 1998;89:206–19.

[201] Sung K, Toth RA, Brown LR, Crawford TJ. Line strength measurements of Carbonyl Sulfide (¹⁶O¹²C³²S) in the 2ν₃, ν₁+2ν₂+ν₃, and 4ν₂+ν₃ bands. J Quant Spectrosc Radiat Transfer 2009;110:2082–101.

[202] Toth RA, Sung K, Brown LR, Crawford TJ. Line positions and strengths of 41 bands including 10 OCS isotopologues in the 3850–4200 cm⁻¹ region. J Quant Spectrosc Radiat Transfer 2010;111:1193–2008.

[203] Bermejo D, Domenech JL, Bouanich J-P, Blanquet G. Absolute line intensities in the 2ν₃ band of ¹⁶O¹²C³²S. J Mol Spectrosc 1997;185:26–30.

[204] Mouchet A, Blanquet G, Herbin P, Walrand J, Courtoy CP. Diode laser measurements of N₂-broadened linewidths in the ν₁ band of OCS. Can J Phys 1985;63:527–31.

[205] Bouanich JP, Walrand J, Alberty S, Blanquet G. Diode laser measurements of oxygen-broadened linewidths in the ν₁ band of OCS. J Mol Spectrosc 1987;123:37–47.

[206] Bouanich JP, Blanquet G. Pressure broadening of CO and OCS spectral lines. J Quant Spectrosc Radiat Transfer 1988;40:205–20.

[207] Bouanich JP, Blanquet G, Walrand J, Courtoy CP. Diode laser measurements of line strengths and collisional half-widths in the ν₁ band of OCS at 298 and 200 K. J Quant Spectrosc Radiat Transfer 1986;36:295–306.

[208] Koshelev MA, Tretyakov MY. Collisional broadening and shifting of OCS rotational spectrum lines. J Quant Spectrosc Radiat Transfer 2009;110:118–28.

[209] Domenech JL, Bermejo D, Bouanich JP. Pressure lineshift and broadening coefficients in the 2ν₃ band of OCS. J Mol Spectrosc 2000;200:266–76.

[210] Bouanich J-P, Campers C, Blanquet G, Walrand J. Diode-laser measurements of Ar- and CO₂-broadened linewidths in the ν₁ band of OCS. J Quant Spectrosc Radiat Transfer 1988;39:353–65.

[211] Steck T, Glatthor N, von Clarmann T, Fischer H, Flaud JM, Funke B, et al. Retrieval of global upper tropospheric and stratospheric formaldehyde (H₂CO) distributions from high-resolution MIPAS-ENVISAT spectra. Atmos Chem Phys 2008;8:463–70.

[212] Dufour G, Szopa S, Barkley MP, Boone CD, Perrin A, Palmer P, et al. Global upper tropospheric formaldehyde seasonal cycles investigated through ACE-FTS space borne observations. Atmos Chem Phys 2009;9:3893–910.

[213] Perrin A, Jacquemart D, Kwabia Tchana F, Lacome N. Absolute line intensities measurements and calculations for the 5.7 and 3.6 μm bands of formaldehyde. J Quant Spectrosc Radiat Transfer 2009;110:700–16.

[214] Kwabia Tchana F, Perrin A, Lacome N. New analysis of the ν₂ band of formaldehyde (H₂¹⁶O). J Mol Spectrosc 2007;245:141–4;
Kwabia Tchana F, Perrin A, Lacome N. Corrigendum to "New analysis of the ν₂ band of formaldehyde (H₂¹²C¹⁶O): line positions for the ν₂, ν₃, ν₄ and ν₆ interacting bands. J Mol Spectrosc 2008;250:57;
Margulés L, Perrin A, Janeckovà R, Bailleux S, Endres CP, Giesen TF, et al. Rotational transitions within the ν₂, ν₃, ν₄ and ν₆ bands of formaldehyde H₂¹²C¹⁶O. Can J Phys 2009;87:425–35.

[215] Perrin A, Valentin A, Daumont L. New analysis of the ν₁, ν₅, 2ν₄, ν₄+ν₆, 2ν₆, ν₃+ν₄, ν₃+ν₆, ν₂+ν₄, 2ν₃, ν₂+ν₆, and ν₂+ν₃ bands of formaldehyde H₂CO. Line positions and intensities in the 3.6 μm spectral region. J Mol Struct 2006;780–782:28–44.

[216] Jacquemart D, Kwabia Tchana F, Lacome N, Perrin A, Laraia A, Gamache RR. Formaldehyde around 3.5 and 5.7-μm: measurement and calculation of broadening coefficients. J Quant Spectrosc Radiat Transfer 2010;111:1209–22.

[217] Daunt SJ, Atakan AK, Blass WE, Halsey GW, Jennings DE, Reuter DC, et al. The 12 micron band of ethane: high-resolution laboratory analysis with candidate lines for infrared heterodyne searches. Astrophys J 1984;280:921–36.

[218] Weber M, Reuter DC, Sirota JM, Blass WE, Hillman JJ. Fourier Transform infrared and tunable diode laser spectra of the $^{13}C^{12}CH_6$ ν_{12} torsion-vibration–rotation band: frequencies, intensities, and barriers to internal rotation. J Chem Phys 1994;100:8681–8.

[219] Weber M, Reuter DC, Sirota JM. A spectral atlas of the ν_{12} fundamental of $^{13}C^{12}C_6$ in the 12 μm region. NASA Technical memorandum 104601, Greenbelt; 1994.

[220] Vander Auwera J, Moazzen-Ahmadi N, Flaud JM. Toward an accurate database for the 12 μm region of the ethane spectrum. Astrophys J 2007;662:750–7.

[221] Sharpe SW, Johnson TJ, Sams RL, Chu PM, Rhoderick GC, Johnson PA. Gas-phase databases for quantitative infrared spectroscopy. Appl Spectrosc 2004;58:1452–61.

[222] Cooper JR, Moazzen-Ahmadi N. Global fit analysis including the $\nu_9 + \nu_4 - \nu_4$ hot band of ethane: evidence of an interaction with the ν_{12} fundamental. J Mol Spectrosc 2006;239:51–8.

[223] Blass WE, Halsey GW, Jennings DE. Self- and foreign-gas broadening of ethane lines determined from diode laser measurements at 12 μm. J Quant Spectrosc Radiat Transfer 1987;38:183–4.

[224] Pine AS, Stone SC. Torsional tunneling and A_1–A_2 splittings and air broadening of the $^rQ_0$ and $^PQ_3$ sub-branches of the ν_7 band of ethane. J Mol Spectrosc 1996;175:21–30.

[225] Nixon CA, Achterberg RK, Vinatier S, Bézard B, Coustenis A, Irwin PGJ, et al. The $^{12}C/^{13}C$ isotopic ratio in Titan hydrocarbons from Cassini/CIRS infrared spectra. Icarus 2008;195:778–91.

[226] Coustenis A, Jennings DE, Nixon CA, Achterbergh RK, Lavvas P, Vinatier S, et al. Titan trace gaseous composition from CIRS at the end of the Cassini–Huygens prime mission. Icarus 2010;207:461–76.

[227] Wilson EH, Atreya SK. J Phys Chem A 2009;113:11221–6.

[228] Hougen JT. Perturbations in the vibration–rotation–torsion energy levels of an ethane molecule exhibiting internal rotation splittings. J Mol Spectrosc 1980;82:92–116.

[229] Devi VM, Rinsland CP, Benner DC, Sams RL, Blake TA. Multi-spectrum analysis of the ν_9 band of $^{12}C_2H_6$: positions, intensities, self- and N_2-broadened half-width coefficients. J Quant Spectrosc Radiat Transfer 2010;111:1234–51;
Devi VM, Benner DC, Rinsland CP, Smith MAH, Sams RL, Blake TA, et al. Multispectrum measurements of spectral line parameters including temperature dependences of N_2- and self-broadened half-width coefficients in the region of the ν_9 band $^{12}C_2H_6$. J Quant Spectrosc Radiat Transfer 2010;111:2481–504.

[230] Pine AS, Rinsland CP. The role of torsional hot bands in modeling atmospheric ethane. J Quant Spectrosc Radiat Transfer 1999;62:445–58.

[231] Dang-Nhu M, Goldman A. Line parameters for C_2H_6 in the 3000 cm^{-1} region. J Quant Spectrosc Radiat Transfer 1987;38:159–61.

[232] Goldman A, Dang-Nhu M, Bouanich JP. Ethane 3 μm spectral clusters of atmospheric interest. J Quant Spectrosc Radiat Transfer 1989;41:17–21.

[233] Harrison JJ, Nicholas DCA, Bernath PF. Infrared absorption cross sections for ethane (C_2H_6) in the 3 μm region. J Quant Spectrosc Radiat Transfer 2010;111:357–63.

[234] Toon GC. Private Communication, and website ⟨http://mark4sun.jpl.nasa.gov⟩.

[235] Di Lauro C, Lattanzi F, Brown LR, Sung K, Vander Auwera J, Mantz AW, et al. High resolution investigation of the 7 μm region of the ethane spectrum. Planet Space Sci 2011. doi:10.1016/j.pss.2011.01.008.

[236] Lattanzi F, di Lauro C, Vander Auwera J. Toward the understanding of the high resolution infrared spectrum of C_2H_6 near 3.3 μm. J Mol Spectrosc 2011. doi:10.1016/j.jms.2011.02.003.

[237] Lattanzi V, Walters A, Pearson JC, Drouin BJ. THz spectrum of monodeuterated methane. J Quant Spectrosc Radiat Transfer 2008;109:580–6.

[238] Bézard B, Nixon CA, Kleiner I, Jennings DE. Detection of $^{13}CH_3D$ on Titan. Icarus 2007;191:397–400.

[239] Ulenikov ON, Onopenko GA, Tyabaev NE, Anttila R, Alanko S, Schroderus J. Rotational analysis of the ground state and the lowest fundamentals ν_3, ν_5, and ν_6 of $^{13}CH_3D$. J Mol Spectrosc 2000;201:9–17.

[240] Brown LR, Nikitin A, Benner DC, Devi VM, Smith MAH, Fejard L, et al. Line intensities of CH_3D in the Triad region: 6–10 μm. J Mol Struct 2004;695–696:181–8.

[241] Seo H, Kim SJ, Kim JH, Geballe TR, Courtin R, Brown LR. Titan at 3 microns: Newly identified spectral features and an improved analysis of haze opacity. Icarus 2009;199:449–57.

[242] Kim JH, Kim SJ, Geballe TR, Kim SS, Brown LR. High-resolution spectroscopy of Saturn at 3 microns: CH_4, CH_3D, C_2H_2, C_2H_6, PH_3, clouds, and haze. Icarus 2006;185:476–86.

[243] Nikitin A, Champion JP, Brown LR. Preliminary analysis of CH_3D from 3250 to 3700 cm^{-1}. J Mol Spectrosc 2006;240:14–25.

[244] Boussin C, Lutz BL, De Bergh C, Hamdouni A. Line intensities and self-broadening coefficients for the $3\nu_2$ band of monodeuterated methane. J Quant Spectrosc Radiat Transfer 1998;60:501–14 (and private communication DeBergh C).

[245] Devi VM, Benner DC, Smith MAH, Rinsland C, Brown LR. Self- and nitrogen-broadening, pressure induced shift and line mixing coefficients in the ν_5 of $^{12}CH_3D$ using a multi-spectrum fitting procedure. J Quant Spectrosc Radiat Transfer 2002;74:1–41.

[246] El Hachtouki R, Vander Auwera J. Absolute line intensities in acetylene: the 1.5 μm region. J Quant Spectrosc Radiat Transfer 2002;216:355–62.

[247] Jacquemart D, Lacome N, Mandin JY, Dana D, Tran H, Gueye FK, et al. The IR spectrum of $^{12}C_2H_2$: line intensity measurements in the 1.4 μm region and update of the databases. J Quant Spectrosc Radiat Transfer 2009;110:717–32.

[248] Jacquemart D, Lacome N, Mandin JY. Line intensities of $^{12}C_2H_2$ in the 1.3, 1.2, and 1 μm spectral regions. J Quant Spectrosc Radiat Transfer 2009;110:733–42.

[249] Kou Q, Guelachvili G, Abbouti Temsamani M, Herman M. The absorption spectrum of C_2H_2 around $\nu_1 + \nu_3$: energy standards in the 1.5 μm region and vibrational clustering. Can J Phys 1994;72:1241–50.

[250] Lyulin OM, Perevalov VI, Mandin JY, Dana V, Gueye F, Thomas X, et al. Line intensities of acetylene: measurements in the 2.5 μm spectral region and global modeling in the $\Delta p = 4$ and 6 series. J Quant Spectrosc Radiat Transfer 2007;103:496–523.

[251] Jacquemart D, Lacome N, Mandin JY, Dana V, Lyulin OM, Perevalov VI. Multispectrum fitting of line parameters for $^{12}C_2H_2$ in the 3.8 μm spectral region. J Quant Spectrosc Radiat Transfer 2007;103:478–95.

[252] Kabbadj Y, Herman M, Di Lonardo G, Fusina L, Johns JWC. The bending energy levels of C_2H_2. J Mol Spectrosc 1991;150:535–65.

[253] Gomez L, Jacquemart D, Lacome N, Mandin J-Y. Line intensities of $^{12}C_2H_2$ in the 7.7 μm spectral region. J Quant Spectrosc Radiat Transfer 2009;110:1223–33;
Gomez L, Jacquemart D, Lacome N, Mandin J-Y. New line intensity measurements for $^{12}C_2H_2$ around 7.7 μm and HITRAN format line list for applications. J Quant Spectrosc Radiat Transfer 2010;111:2256–64.

[254] Matsuura M, Wood PR, Sloan GC, Zijlstra AA. Spitzer observations of acetylene bands in carbon-rich asymptotic giant branch stars in the Large Magellanic Cloud. Mon Not R Astron Soc 2006;371:415–20.

[255] Vander Auwera J. Absolute intensities measurements in the $(\nu_4 + \nu_5)$ band of $^{12}C_2H_2$: analysis of Herman–Wallis effects and forbidden transitions. J Mol Spectrosc 2000;201:143–50.

[256] Rotger M, Boudon V, Vander Auwera J. Line positions and intensities in the ν_{12} band of ethylene near 1450 cm^{-1}: an experimental and theoretical study. J Quant Spectrosc Radiat Transfer 2008;109:952–62.

[257] Blanquet G, Bouanich JP, Walrand J, Lepère M. Self-broadening coefficients in the ν_7 band of ethylene at room and low temperatures. J Mol Spectrosc 2003;222:284–90.

[258] Brannon JF, Varanasi P. Tunable diode laser measurements on the 951.7393 cm^{-1} line of $^{12}C_2H_4$ at planetary atmospheric temperatures. J Quant Spectrosc Radiat Transfer 1992;47:237–42.

[259] Reuter DC, Sirota JM. Absolute intensities and foreign gas broadening coefficients of the $11_{1,10} \leftarrow 11_{2,10}$ and $18_{0,18} \leftarrow 18_{1,18}$ lines in the ν_7 band of C_2H_4. J Quant Spectrosc Radiat Transfer 1993;50:477–82.

[260] Blanquet G, Walrand J, Bouanich JP. Diode-laser measurements of N_2-broadening coefficients in the ν_7 band of C_2H_4. J Mol Spectrosc 2000;201:56–61.

[261] Harris GJ. University College London, London, UK. Private Communication; 2008.

[262] Maki A. Mill Creak, WA 98012, USA. Private Communication; 2008.

[263] Harris GJ, Polyansky OL, Tennyson J. Opacity data for HCN and HNC from a new ab initio line-list. Astrophys J 2002;578:657–63.

[264] Lecoutre M, Rohart F, Huet TR, Maki AG. Photoacoustic detection of new bands of HCN between 11390 and 13028 cm^{-1}. J Mol Spectrosc 2000;203:158–64.

[265] Maki A, Quapp W, Klee S, GCh Mellau, Albert S. Infrared transitions of $H^{12}C^{14}N$ and $H^{12}C^{15}N$ between 500 and 10,000 cm^{-1}. J Mol Spectrosc 1996;180:323–36.

[266] Maki AG, Mellau GC, Klee S, Winnewisser M, Quapp W. High temperature infrared measurements in the region of the bending fundamental of $H^{12}C^{14}N$, $H^{12}C^{15}N$, and $H^{13}C^{14}N$. J Mol Spectrosc 2000;202:67–82.

[267] Maki AG, Mellau GC. High-temperature infrared emission measurements on HNC. J Mol Spectrosc 2001;206:47–52.

[268] Smith AM, Jørgensen UG, Lehmann KK. The intensities of HCN overtone transitions from 12600–18400 cm^{-1}. J Chem Phys 1987;87:5649–56.

[269] Smith AM, Coy SL, Klemperer W, Lehmann KK. Fourier transform spectra of overtone bands of HCN from 5400 to 15100 cm^{-1}. J Mol Spectrosc 1989;134:134–53.

[270] Smith AM, Klemperer W, Lehmann KK. The intensity of the 105–000 transition of HCN. J Chem Phys 1989;90:4633–4.

[271] Harris GJ, Tennyson J, Kaminsky BM, YaV Pavlenko, Jones HRA. Improved HCN/HNC line-list, model atmospheres synthetic spectra for WZ Cas. Mon Not R Astron Soc 2006;367:400–6.

[272] Maki A, Quapp W, Klee S. Intensities of hot-band transitions: HCN hot bands. J Mol Spectrosc 1995;171:420–32.

[273] Maki A, Quapp W, Klee S, GCh Mellau, Albert S. The CN mode of HCN: a comparative study of the variation of the transition dipole and Herman–Wallis constants for seven isotopomers and the influence of vibration–rotation interaction. J Mol Spectrosc 1995;174:365–78.

[274] Maki AG. Microwave spectra of molecules of astrophysical interest, VI carbonyl sulfide and hydrogen cyanide. J Phys Chem Ref Data 1974;3:221–44.

[275] Preusser J, Maki AG. Millimeter-wave measurements of vibrationally excited states of the HCN isotopomers $H^{13}C^{14}N$, $H^{12}C^{15}N$, $H^{13}C^{15}N$, $D^{12}C^{14}N$, $D^{13}C^{14}N$, $D^{12}C^{15}N$, and $D^{13}C^{15}N$. J Mol Spectrosc 1993;162:484–97.

[276] Maiwald F, Lewen F, Ahrens V, Beaky M, Gendriesch R, Koroliev AN, et al. Pure rotational spectrum of HCN in the terahertz region: use of a new planar Schottky diode multiplier. J Mol Spectrosc 2000;202:166–8.

[277] Thorwirth S, Müller HSP, Lewen F, Brünken S, Ahrens V, Winnewisser G. A concise new look at the *l*-type spectrum of $H^{12}C^{14}N$. Astrophys J Lett 2003;585:L163–5.

[278] Ahrens V, Lewen F, Takano S, Winnewisser G, Urban S, Negirev AA, et al. Sub-Doppler saturation spectroscopy of HCN up to 1 THz and detection of $J=3\rightarrow2$ $(4\rightarrow3)$ emission from TMC1. Z Naturforsch 2002;57a:669–81.

[279] Zelinger Z, Amano T, Ahrens V, Brünken S, Lewen F, Müller HSP, et al. Submillimeter-wave spectroscopy of HCN in excited vibrational states. J Mol Spectrosc 2003;220:223–33.

[280] Brünken S, Fuchs U, Lewen F, Urban S, Giesen T, Sub-Doppler Winnewisser G. and Doppler spectroscopy of DCN isotopomers in the terahertz region: ground and first excited bending states $(v_1v_2v_3)=(0\ 1^{ef}\ 0)$. J Mol Spectrosc 2004;225:152–62.

[281] Cazzoli G, Puzzarini C. The Lamb-dip spectrum of the $J+1\leftarrow J$ ($J=0$, 1, 3–8) transitions of $H^{13}CN$: the nuclear hyperfine structure due to H, ^{13}C, and ^{14}N. J Mol Spectrosc 2005;233:280–9.

[282] Freund SM, Maki AG. Laser Stark spectroscopy of DCN and $DC^{15}N$. J Mol Spectrosc 1982;93:433–7.

[283] Möllmann E, Maki AG, Winnewisser M, Winnewisser BP, Quapp W. High-temperature infrared emission spectra of $D^{12}C^{14}N$ and $D^{13}C^{14}N$. J Mol Spectrosc 2002;212:22–31.

[284] Tomasevich GR. PhD thesis. Cambridge, MA: Harvard University; 1970.

[285] De Leon RJ, Muenter JS. The vibrational dipole moment function of HCN. J Chem Phys 1984;80:3992–9.

[286] Ebenstein WL, Muenter JS. Dipole moment and hyperfine properties of the ground state and the C–H excited vibrational state of HCN. J Chem Phys 1984;80:3989–91.

[287] Devi VM, Benner DC, Smith MAH, Rinsland CP, Predoi-Cross A, Sharpe SW, et al. A multispectrum analysis of the v_2 band of $H^{12}C^{14}N$: Part I, intensities, broadening, and shift coefficients. J Mol Spectrosc 2005;231:66–84.

[288] Devi VM, Benner DC, Smith MAH, Rinsland CP, Sharpe SW, Sams RL. A multispectrum analysis of the $2v_2$ spectral region of $H^{12}C^{14}N$: intensities, broadening, and pressure-shift coefficients. J Quant Spectrosc Radiat Transfer 2004;87:339–66.

[289] Maki A, Quapp W, Klee S, GCh Mellau, Albert S. Intensity measurements of $\Delta l>1$ transitions of several isotopomers of HCN. J Mol Spectrosc 1997;185:356–69.

[290] Devi VM, Benner DC, Smith MAH, Rinsland CP, Sharpe SW, Sams RL. A multispectrum analysis of the v_1 band of $H^{12}C^{14}N$: Part I, intensities, self-broadening, and self-shift coefficients. J Quant Spectrosc Radiat Transfer 2003;82:319–41.

[291] Rinsland CP, Devi VM, Smith MAH, Benner DC, Sharpe SW, Sams RL. A multispectrum analysis of the v_1 band of $H^{12}C^{14}N$: Part II, air- and N_2-broadening, shifts and their temperature dependences. J Quant Spectrosc Radiat Transfer 2003;82:343–62.

[292] Smith MAH. NASA Langley Research Center, USA. Private Communication; 2007.

[293] Flaud JM. LISA, France. Private Communication; 2007.

[294] Giver LP, Varanasi P, Valero FPJ. Propane absorption band intensities and band model parameters from 680 to 1580 cm^{-1} at 296 and 200 K. J Quant Spectrosc Radiat Transfer 1984;31:203–13.

[295] Nixon CA, Jennings DE, Flaud JM, Bezard B, Teanby NA, Irwin PGJ, et al. Titan's prolific propane: The Cassini CIRS perspective. Planet Space Sci 2009;57:1573–85.

[296] Nadler S, Jennings DE. Foreign-gas pressure broadening parameters of propane near 748 cm^{-1}. J Quant Spectrosc Radiat Transfer 1989;42:399–403.

[297] Hillman J, Reuter DC, Jennings DE, Bjoraker GL. Extraterrestrial spectroscopy: foreign-gas broadening of propane as it applies to the atmosphere of Titan. Spectrochim Acta 1992;48A:1249–55.

[298] Flaud JM, Kwabia Tchana F, Lafferty WJ, Nixon CA. High resolution analysis of the v_{26} and $2v_9-v_9$ bands of propane: modeling of Titan's infrared spectrum at 13.4 μm. Mol Phys 2010;108:699–704.

[299] Grecu JC, Winnewisser BP, Winewisser M. Absolute rovibrational line intensities in the v_5 band system of cyanogen NCCN. J Mol Spectrosc 1993;159:551–71.

[300] Kim K, King WTJ. Integrated infrared intensities in cyanogens. J Chem Phys 1979;70:4577–82.

[301] Grecu JC, Winnewisser BP, Winewisser M. High-resolution Fourier transform infrared spectrum of the v_5 band system of cyanogen, NCCN. J Mol Spectrosc 1993;159:534–50.

[302] Jolly A, Fayt A, Benilan Y, Jacquemart D, Nixon CA, Jennings DE. The v_8 bending mode of diacetylene: from laboratory spectroscopy to the detection of ^{13}C isotopologues in Titan's atmosphere. Astrophys J 2010;714:852–9.

[303] Fayt A, Vigouroux C, Willaert F, Margules L, Constantin F-L, Demaison J, et al. Global analysis of high resolution infrared and rotational spectra of $HCCC^{15}N$ up to 1335 cm^{-1}. J Mol Struct 2004;695–696:295–311.

[304] Arié E, Johns JWC. The bending energy levels of C_4H_2. J Mol Spectrosc 1992;155:195–204.

[305] Guelachvili G, Craig AM, Ramsay DA. High-resolution Fourier studies of diacetylene in the regions of the v_4 and v_5 fundamentals. J Mol. Spectrosc 1984;105:156–92.

[306] McNaughton D, Bruget DN. The high resolution infrared spectrum of diacetylene. J Mol Struct 1992;273:11–25.

[307] Matsumura K, Etoh T, Tanaka T. Microwave spectroscopy of the v_8-v_6 band of diacetylene. J Mol Spectrosc 1981;90:106–15.

[308] Koops T, Visser T, Smit WMA. The harmonic force field and absolute infrared intensities of diacetylene. J Mol Struct 1984;125:179–96.

[309] Kim SJ, Caldwell J, Rivolo AR, Wagener R, Orton GS. Infrared polar brightening on Jupiter III. Spectrometry from the Voyager 1 IRIS experiment. Icarus 1985;64:233–48.

[310] Kunde VG, Aikin AC, Hanel RA, Jennings DE, Maguire WC, C_4H_2 Samuelson RE. HC_3N and C_2N_2 in Titan's Atmosphere. Nature 1981;292:686–8.

[311] Coustenis A, Salama A, Schulz B, Ott S, Lellouch E, Encrenaz T, et al. Titan's atmosphere from ISO mid-infrared spectroscopy. Icarus 2003;161:383–403.

[312] Coustenis A, Achterberg RK, Conrath BJ, Jennings DE, Marten A, Gautier D, et al. The composition of Titan's stratosphere from Cassini/CIRS mid-infrared spectra. Icarus 2007;189:35–62.

[313] Burgdorf MJ, Orton GS, Van Cleve J, Meadows VS, Houck J. Detection of new hydrocarbons in Uranus' atmosphere by infrared spectroscopy. Icarus 2006;184:634–7.

[314] Meadows VS, Orton GS, Line M, Liang M-C, Yung YL, Van Cleve J, et al. First Spitzer observations of Neptune: detection of new hydrocarbons. Icarus 2008;197:585–9.

[315] Cernicharo J, Heras A, Pardo J, Tielens A, Guelin M, Dartois E, et al. Methylpolyynes and small hydrocarbons in CRL 618. Astrophys J 2001;546:127–30.

[316] Goldman A. DU, USA. Private Communication; 1980.

[317] Arié E, Dang Nhu M, Arcas Ph, Graner G, Bürger H, Pawelke G, et al. Analysis of cyanoacetylene spectra in the mid-infrared. J Mol Spectrosc 1990;143:318–26.

[318] Jolly A, Benilan Y, Fayt A. New infrared integrated band intensities for HC_3N and extensive line list for the v_5 and v_6 bending modes. J Mol Spectrosc 2007;242:46–54.

[319] Jennings DE, Nixon CA, Jolly A, Bézard B, Coustenis A, Vinatier S, et al. Isotopic ratios in Titan's atmosphere from Cassini CIRS limb sounding: HC_3N in the north. Astrophys Jl 2008;681:L109–11.

[320] Goldman A. DU, USA. Private Communication; 2007.

[321] Goldman A, Tipping RH, Ma Q, Boone CD, Bernath PF, Demoulin P, et al. On the line parameters for the $X^1S_g^+$ (1–0) infrared quadrupolar transitions of $^{14}N_2$. J Quant Spectrosc Radiat Transfer 2007;103:168–74.

[322] Li H, Le Roy RJ. Quadrupole moment function and absolute infrared quadrupolar intensities for N_2. J Chem Phys 2007;126: 224301–9.

[323] Chackerian C, Brown LR, Lacome N, Tarrago G. Methyl chloride ν_5 region line shape parameters and rotational constants for the ν_2, ν_5 and $2\nu_3$ vibrational bands. J Mol Spectrosc 1998;191:148–57.

[324] Brown LR. JPL, USA. Private Communication; 2007.

[325] Perrin A, Valentin A, Flaud JM, Camy-Peyret C, Schriver L, Schriver A. Arcas Ph. The 7.9-μm Band of Hydrogen peroxide: Line Positions and Intensities. J Mol Spectrosc 1995;171:358–73.

[326] Klee S, Winnewisser M, Perrin A, Flaud JM. Absolute line intensities for the ν_6 band of H_2O_2. J Mol Spectrosc 1999;195:154–61.

[327] Sumpf B, Meusel I, Kronfeldt HD. Self- and air-broadening in the ν_1 and ν_3 bands of H_2S. J Mol Spectrosc 1996;177:143–5.

[328] Kissel A, Kurtz O, Kronfeldt HD, Sumpf B. Quantum number and perturber dependence of pressure-induced line shift and line broadening in the $2\nu_2$, ν_1, and ν_3 bands of H_2S. In: Proceedings of the 15th international conference on high resolution molecular spectroscopy, Prague, Czech Republic; August 30–September 3, 1998.

[329] Kissel A, Sumpf B, Kronfeldt HD, Tikhomirov BA, Ponomarev YN. Molecular-gas-pressure-induced line-shift and line-broadening in the ν_2-band of H_2S. J Mol Spectrosc 2002;216:345–54.

[330] Waschull J, Kuhnemann F, Sumpf B. Self-, air- and helium broadening of the ν_2 band of H_2S. J Mol Spectrosc 1994;165:150–8.

[331] Sumpf B. Experimental investigation of the self-broadening coefficients in the $\nu_1 + \nu_3$ band of SO_2 and the $2\nu_2$ band of H_2S. J Mol Spectrosc 1997;181:160–7.

[332] Goldman A, Gillis JR. Line parameters and line calculation for molecules of stratospheric interest. Technical report. Department of Physics, University of Denver; 1984.

[333] Vander Auwera J. High-resolution investigation of the far-infrared spectrum of formic acid. J Mol Spectrosc 1992;155:136–42.

[334] Willemot E, Dangoisse D, Monnanteuil N, Bellet J. Microwave spectra of molecules of astrophysical interest. XVIII. Formic acid. J Phys Chem Ref Data 1980;9:59–160.

[335] Chardon JC, Genty C, Guichon D, Theobald JG. RF spectrum and hyperfine structure of formic acid. J Chem Phys 1976;64:1437–41.

[336] Belov SP, Burenin AV, Kazarov VP, Karyakin EN, Krupnov AF. Microwave gas spectroscopy in the 200–870 GHz range. JETP Lett Engl Transl 1973;18:167–9.

[337] Weber WH, Maker PD, Johns JWC, Weinberg E. Sub-Doppler laser-Stark and high-resolution Fourier transform spectroscopy of the ν_3 band of formic acid. J Mol Spectrosc 1987;121:243–60.

[338] Winnewisser M, Winnewisser BP, Stein M, Birk M, Wagner G, Winnewisser G, et al. I. Rotational spectra of cis-HCOOH, trans-HCOOH, and trans-H^{13}COOH. J Mol Spectrosc 2002;216:259–65.

[339] Vander Auwera J, Didriche K, Perrin A, Keller F. Absolute line intensities for formic acid and dissociation constant of the dimer. J Chem Phys 2007;126:124311/1–9.

[340] Perrin A, Vander Auwera J. An improved database for the 9 μm region of the formic acid spectrum. J Quant Spectrosc Radiat Transfer 2007;108:363–70.

[341] Notholt J, Cappellani F, Roesdahl H, Restelli G. Absolute infrared band intensities and air broadening coefficient for spectroscopic measurements of formic acid in air. Spectrochim Acta Part A 1991;47:477–83.

[342] Perrin A, Vander Auwera J, Zelinger Z. High-resolution Fourier transform study of the ν_3 fundamental band of trans-formic acid. J Quant Spectrosc Radiat Transfer 2009;110:743–55.

[343] Geller LS, Elkins JW, Lobert JM, Clarke AD, Hurst DF, Butler JH, et al. Tropospheric SF_6: Observed latitudinal distribution and trends, derived emissions and interhemispheric exchange time. Geophys Res Lett 1997;24:675–8.

[344] Boudon V, Pierre G. Rovibrational spectroscopy of sulphur hexafluoride: a review. In: Pandalai SG, editor. Recent research developments in molecular spectroscopy, vol. 1. Trivandrum, India. ISBN: 81-7895-026-X. p. 25–55.

[345] Boudon V, Pierre G, Burger H. High resolution spectroscopy and analysis of the ν_4 bending region of SF_6 near 615 cm^{-1}. J Mol Spectrosc 2001;205:304–11.

[346] Kim KC, Person WB, Seitz D, Krohn BJ. Analysis of the ν_4 (615 cm^{-1}) region of the Fourier transform and diode laser spectra of SF_6. J Mol Spectrosc 1979;76:322–40.

[347] Person WB, Krohn BJ. Coriolis intensity perturbations of the ν_4 band of SF_6. J Mol Spectrosc 1983;98:229–57.

[348] Wenger Ch Boudon V, Champion JP, Pierre G. Highly-Spherical Top Data System (HTDS) Software for the spectrum simulation of octahedral XY_6 molecules. J Quant Spectrosc Radiat Transfer 2000;66:1–16 See also: ⟨http://icb.u-bourgogne.fr/OMR/SMA/SHTDS⟩.

[349] Pekkala K, Graner G, Wlodarczak G, Demaison J, Koput J. A global treatment of the $\nu_9=1$ and $\nu_{10}=2$ vibrational levels of propyne. J Mol Spectrosc 1991;149:214–29.

[350] Blanquet G, Walrand J, Dang-Nhu M. Absolute line intensities of the ν_9 band of propyne at 15.5 μm. Spectrochim Acta 1992;48: 1231–3.

[351] Horneman V-M, Graner G, Fakour H, Tarrago G. Propyne at 30 μm: a line by line simulation of the ν_{10} band. J Mol Spectrosc 1989;137:1–8.

[352] Graner G, Wagner G. High-resolution infrared spectrum of propyne: the 30 μm region. J Mol Spectrosc 1990;144:389–415.

[353] Pekkala K. The ν_9 band of propyne. J Mol Spectrosc 1990;144: 416–28.

[354] Coustenis A, Encrenaz Th, Bézard B, Bjoraker GL, Graner G, Dang-Nhu M, et al. Modeling Titan's thermal infrared spectrum for high-resolution space observations. Icarus 1993;102:240–60.

[355] Müller HSP, Pracna P, Horneman VM. The $\nu_{10}=1$ level of propyne, H_3CCCH, and its interactions with $\nu_9=1$ and $\nu_{10}=2$. J Mol Spectrosc 2002;216:397–407.

[356] Pracna P, Müller HSP, Klee S, Horneman VM. Interactions in symmetric top molecules between vibrational polyads: rotational and rovibrational spectroscopy of low-lying states of propyne, H_3C–C≡CH. Mol Phys 2004;102:1555–68.

[357] Pracna P, Müller HSP, Urban Š, Horneman VM, Klee S. Interactions between vibrational polyads of propyne, H_3C–C≡CH: rotational and rovibrational spectroscopy of the levels around 1000 cm^{-1}. J Mol Spectrosc 2009;256:152–62.

[358] Butler RAH, Petkie DT, Helminger P, De Lucia FC, Bialkowska-Jaworska E, Kisiel Z. The millimeter-wave spectrum of chlorine nitrate ($ClONO_2$): the ν_6 vibrational state. J Mol Spectrosc 2007;244:113–6.

[359] Butler RAH, Petkie DT, Helminger P, De Lucia FC, Kisiel Z. The rotational spectrum of chlorine nitrate ($ClONO_2$): the $\nu_5/\nu_6\nu_9$ dyad. J Mol Spectrosc 2007;243:1–9.

[360] Müller HSP, Helminger P, Young SH. Millimeter and submillimeter spectroscopy of chlorine nitrate: the Cl quadrupole tensor and the harmonic force field. J Mol Spectrosc 1997;181:363–78.

[361] Šimečková M, Jacquemart D, Rothman LS, Gamache RR, Goldman A. Einstein A-coefficients and statistical weights for molecular absorption transitions in the HITRAN database. J Quant Spectrosc Radiat Transfer 2006;98:130–55.

[362] Goldman A, Gamache RR, Perrin A, Flaud JM, Rinsland CP, Rothman LS. HITRAN partition functions and weighted transition-moments squared. J Quant Spectrosc Radiat Transfer 2000;66: 455–86.

[363] McElroy MB, Salawitch RJ, Wofsy SC, Logan JA. Reductions of atlantic ozone due to synergistic interactions of chlorine and bromine. Lett Nat 1986;321:759–62.

[364] Kurylo MJ, Rodriguez JM, Andreae MO, Atlas EL, Blake DR, Butler JM, et al. Short-lived ozone-related compounds. In: Albritton DL, Aucamp PJ, Megie G, Watson RT, editors. Scientific assessment of ozone depletion: 1998. WMO; 1999. p. 2.1–56.

[365] Jacquemart D, Kwabia Tchana F, Lacome N, Kleiner I. A complete set of line parameters for CH_3Br in the 10-μm spectral region. J Quant Spectrosc Radiat Transfer 2007;105:264–302.

[366] Jacquemart D, Tran H. Temperature dependence of self- and N_2-broadening coefficients for CH_3Br in the 10-μm spectral region. J Quant Spectrosc Radiat Transfer 2008;109:569–79.

[367] Kwabia Tchana F, Kleiner I, Orphal J, Lacome N, Bouba$_{79}$O. New analysis of the Coriolis-interacting ν_2 and ν_5 bands of CH$_3^{81}$Br and CH$_3^{79}$Br. J Mol Spectrosc 2004;228:441–52.

[368] Kwabia Tchana F, Jacquemart D, Lacome N, Kleiner I, Orphal J. Absolute line intensities in methyl bromide: the 7 μm region. J Mol Spectrosc 2006;235:132–43.

[369] Benedict WS, Kaplan LD. Calculation of line widths in H_2O–H_2O and H_2O–O_2 collisions. J Quant Spectrosc Radiat Transfer 1964;4: 453–69.

[370] Toth RA, Brown LR. Oxygen broadening parameters of water vapour: 1212–2136 cm^{-1}. J Mol Spectrosc 2003;218:133–50.

[371] Rothman LS, Gamache RR, Goldman A, Brown LR, Toth RA, Pickett HM, et al. The HITRAN database: 1986 edition. Appl Opt 1987;26: 4058–97.

[372] Bouanich JP, Blanquet G, Walrand J. Theoretical O_2- and N_2-broadening coefficients of CH_3Cl spectral lines. J Mol Spectrosc 1993;161:416–26.

[373] Colmont JM, Rohart F, Wlodarczak G, Bouanich JP. *K*-dependence and temperature dependence of N_2- and O_2-broadening coefficients for the $J=14$–13 transition of methyl chloride $CH_3^{35}Cl$. J Mol Spectrosc 2006;780–781:268–76.

[374] Gamache RR, Davies RW. Theoretical N_2-, O_2-, and air-broadened halfwidths of $^{16}O_3$ calculated by quantum Fourier transform theory with realistic collision dynamics. J Mol Spectrosc 1985;109:283–99.

[375] Tran H, Jacquemart D, Mandin JY, Lacome N. Line-mixing in the ν_6 Q branches of methyl bromide broadened by nitrogen: experiment and modeling. J Quant Spectrosc Radiat Transfer 2008;109: 119–31.

[376] Gomez L, Tran H, Jacquemart D. Line-mixing in the ν_6 Q branches of nitrogen-broadened methyl bromide at low temperatures. J Mol Spectrosc 2009;256:35–40.

[377] Rosenkranz PW. Shape of the 5 mm oxygen band in the atmosphere. IEEE Trans Antennas Propag 1975;AP-23:498–506.

[378] Ball JA, Gottlieb CA, Lilley AE, Radford HE. Detection of methyl alcohol in Sagittarius. Astrophys J Lett 1970;1962:L203.

[379] Worden H, Beer R, Rinsland CP. Airborne infrared spectroscopy of 1994 western wildfires. J Geophys Res 1997;102:1287–99.

[380] Dufour G, Szopa S, Hauglustaine DA, Boone CD, Rinsland CP, Bernath PF. The influence of biogenic emissions on upper-tropospheric methanol as revealed from space. Atmos Chem Phys 2007;7:6119–29.

[381] Yokelson RJ, Goode JG, Ward DE, Susott RA, Babbitt RE, Wade DD, et al. Emissions of formaldehyde, acetic acid, methanol and other trace gases from biomass fires in North Carolina measured by airborne Fourier transform infrared spectroscopy (AFTIR). J Geophys Res—Atmos 1999;104:30109–25.

[382] Mumma MJ, McLean IS, DiSanti MA, Larkin JE, Dello Russo N, Magee-Sauer K, et al. The Startling Organic Composition of C/ 1999 S4 (Linear): a comet formed near Jupiter? Astrophys J 2001;546:1183–93.

[383] Reuter DC. The contribution of methanol to the 3.4 µm emission feature in comets. Astrophys J 1992;386:330–5.

[384] Gibb EL, Whittet DCB, Schutte WA, Boogert ACA, Chiar JE, Ehrenfreund P. at al. An inventory of interstellar ices toward the embedded protostar W33A. Astrophys J 2000;536:347–56.

[385] Bockelée-Morvan D, Lis DC, Wink JE, Despois D, Crovisier J, Bachiller R, et al. New molecules found in comet C/1995 O1 (Hale–Bopp)—investigating the link between cometary and interstellar material. Astron Astrophys 2000;353:1101–14.

[386] Xu LH, Hougen JT. Global fit of rotational transitions in the ground and first excited torsional states of methanol. J Mol Spectrosc 1995;173:540–51.

[387] Xu LH, Lovas FJ. Microwave spectra of molecules of astrophysical interest XXIV: methanol (CH_3OH and $^{13}CH_3OH$). J Phys Chem Ref Data 1997;26:17–56.

[388] Xu LH, Fisher J, Lees RM, Shi HY, Hougen JT, Pearson JC, et al. Torsion–rotation global analysis of the first three torsional states ($\nu_t=0$, 1, 2) and terahertz database for methanol. J Mol Spectrosc 2008;251:305–13.

[389] Xu LH, Lees RM, Wang P, Brown LR, Kleiner I, Johns JWC. New assignments, line intensities and HITRAN database for CH_3OH at 10 µm. J Mol Spectrosc 2004;228:453–70.

[390] Rothman LS, Rinsland CP, Goldman A, Massie ST, Edwards DP, Flaud JM, et al. The HITRAN molecular spectroscopic database and HAWKS (HITRAN atmospheric workstation) 1996 edition. J Quant Spectrosc Radiat Transfer 1998;60:665–710;
Werner HJ, Rosmus P. Ab initio calculations of radiative transition probabilities in the $X^1\Sigma^+$ ground state of the NO^+ ion. J Mol Spectrosc 1982;96:362–7.

[391] Lopez-Puertas M, Flaud JM, Peralta-Calvillo J, Funke B, Gil-Lopez S. NO^+ fundamental and first hot rovibrational line frequencies from MIPAS/ENVISAT atmospheric spectra. J Mol Spectrosc 2006;237:218–24;
Flaud JM, Ridolfi M. Spectral line parameters for C_2H_6 and NO^+. Deliverable of the ESA-ESRIN Contract 17580/03/I-OL. Project title: support to MIPAS level 2 product validation Issue 1; July 2007;
Flaud J.M. LISA, France. Private Communication; 2008.

[392] Van Mourik T, Harris GJ, Ol Polyansky, Tennyson J, Csaszar AG, Knowles PJ. Ab initio global potential, dipole, adiabatic and relativistic correction surfaces for the HCN/HNC system. J Chem Phys 2001;115:3706–18.

[393] Hirota T, Yamamoto S, Mikami H, Ohishi M. Abundances of HCN and HNC in dark cloud cores. Astrophys J 1998;503:717–28.

[394] Barber RJ, Harris GJ, Tennyson J. Temperature dependent partition functions and equilibrium constant for HCN and HNC. J Chem Phys 2002;117:11239–43.

[395] Harris GJ, Pavlenko YV, Jones HRA, Tennyson J. The identification of HCN and HNC in carbon stars: model atmospheres, synthetic spectra and fits to observations in the 2.7–4.0 µm region. Mon Not R Astron Soc 2003;344:1107–18.

[396] Northrup FJ, Bethardy GA, Macdonald RG. Infrared absorption spectroscopy of HNC in the region 2.6 to 3.1 µm. J Mol Spectrosc 1997;186:349–62.

[397] Nezu M, Amano T, Kawaguchi K. Transition dipole moments for the vibrational fundamentals of HNC determined from the Herman–Wallis effect. J Mol Spectrosc 1998;192:41–6;
Nezu M, Amano T, Kawaguchi K. On "Transition dipole moments for the vibrational fundamentals of HNC determined from the Herman–Wallis effect". J Mol Spectrosc 1999;198:186.

[398] Mellau GC. Complete experimental rovibrational eigenenergies of HNC up to 3743 cm^{-1} above the ground state. J Chem Phys 2010;133:164303.

[399] Mellau GC. The ν_1 band system of HNC. J Mol Spectrosc 2010;264: 2–9.

[400] Thorwirth S, Muller HSP, Lewen F, Gendriesch R, Winnewisser G. The submillimeter-wave spectrum of hydrogenisocyanide, HNC, in its (0,0,0) and (0,1,0) vibrational states up to 2 THz. Astron Astrophys 2001;363:L367–9.

[401] Amano T, Zelinger Z. Submillimeter-wave spectroscopy of HNC produced in an extended negative glow discharge. J Mol Spectrosc 2002;211:273–8.

[402] Bézard B, Drossart P, Encrenaz T, Feuchtgruber H. Benzene on the giant planets. Icarus 2001;154:492–500.

[403] Dang-Nhu M, Plíva J. Intensities in the ν_4, ν_{12}, ν_{13}, and ν_{14} bands of benzene. J Mol Spectrosc 1989;138:423–9.

[404] Dang-Nhu M, Blanquet G, Walrand J, Raulin F. Spectral intensities in the ν_4 band of benzene at 15 µm. J Mol Spectrosc 1989;134: 237–9.

[405] Raulin F, Accaoui B, Razaghi A, Dang-Nhu M, Coustenis A, Gautier D. Infrared spectra of gaseous organics: application to the atmosphere of Titan. II C_4 alkanenitriles and benzene. Spectrochim Acta 1990;46: 671–83.

[406] Coustenis A, Jennings DE, Jolly A, Bénilan Y, Conor AN, Vinatier S, et al. Detection of C_2HD and the D/H ratio on Titan. Icarus 2008;197:539–48.

[407] Jolly A, Benilan Y, Cané E, Fusina L, Tamassia F, Fayt A, et al. Measured integrated band intensities and simulated line-by-line spectra for C_2HD between 25 and 2.5 µm, and new global vibration rotation parameters for the bending vibrations. J Quant Spectrosc Radiat Transfer 2008;109:2846–56.

[408] Fayt A, Vigouroux C, Willaert F, Margules L, Lucian Florin Constantin LF, et al. Global analysis of high resolution infrared and rotational spectra of $HCCC^{15}N$ up to 1335 cm^{-1}. J Mol Struct 2004;695–696:295–311.

[409] Fayt A, Vigouroux C, Winther F. Analysis of the ν_9 band complex of dicyanoacetylene and application of a theory of relative intensities to all sub-bands. J Mol Spectrosc 2004;224:114–30.

[410] Brown LR, Farmer CB, Rinsland CP, Toth RA. Molecular line parameters for the Atmospheric Trace Molecule Spectroscopy (ATMOS) experiment. Appl Opt 1987;26:5154–82.

[411] Worton DR, Sturges WT, Gohar LK, Shine KP, Martinerie P, Oram DE, et al. Atmospheric trends and radiative forcings of CF_4 and C_2F_6 inferred from firn air. Environ Sci Technol 2007;41:2184–9.

[412] Cicerone RJ. Atmospheric carbon tetrafluoride: a nearly inert gas. Science 1979;206:59–61.

[413] Zander R, Solomon S, Mahieu E, Goldman A, Rinsland CP, Gunson MR, et al. Increase of stratospheric carbon tetrafluoride (CF_4) based on ATMOS observations from space. Geophys Res Lett 1996;23:2353–6.

[414] Rinsland CP, Mahieu E, Zander R, Nassar R, Bernath P, Boone C, et al. Long-term stratospheric carbon tetrafluoride (CF_4) increase inferred from 1985 to 2004 infrared space-based solar occultation measurements. Geophys Res Lett 2006;33: L02808, doi:10.1029/2005GL024709.

[415] Goldman A, Murcray DG, Murcray FJ, Cook GR, van Allen JW, Bonomo FS, et al. Identification of the ν_3 vibration–rotation band

of CF₄ in infrared balloon-borne solar spectra. Geophys Res Lett 1979;6:609–12.

[416] Gabard T, Pierre G, Takami M. Study of the ν_3 and $2\nu_4$ interacting states of $^{12}CF_4$. Mol Phys 1995;85:735–44.

[417] Wenger C, Boudon V, Rotger M, Sanzharov M, Champion JP. XTDS and SPVIEW: graphical tools for the analysis and simulation of high-resolution molecular spectra. J Mol Spectrosc 2008;251: 102–13.

[418] Papoušek D, Papouskova Z, Chong DP. Density functional computations of the dipole moment derivatives for halogenated methanes. J Phys Chem 1995;99:15387–95.

[419] Boudon V, Domanskaya A, Maul C, Georges R, Mitchell J, Harter WG. High-resolution spectroscopy and analysis of the $2\nu_4/\nu_3$ dyad of CF4, J Quant Spectrosc Radiat Transfer, submitted.

[420] Höjer S, May RD. Air-broadening coefficients for the ν_3 band of CF₄. J Mol Spectrosc 1996;178:139–42.

[421] Marten A, Hidayat T, Biraud Y, Moreno R. New millimeter heterodyne observations of Titan: vertical distributions of nitriles HCN, HC₃N, CH₃CN, and the isotopic ratio $^{15}N^{14}N$ in its atmosphere. Icarus 2002;158:532–44.

[422] Teanby NA, Irwin PGJ, Kok R, Nixon CA, Coustenis A, Bézard B. Latitudinal variations of HCN, HC₃N and C₂N₂ in Titan's stratosphere derived from Cassini CIRS data. Icarus 2006;181:243–55.

[423] Crovisier J. Physics and chemistry of comets: recent results from comets Hyakutake and Hale-Bopp. Faraday Discuss 1998;109: 437–52.

[424] Watson C, Churchwell E, Pankonin V, Bieging JH. Arc second images of CH₃CN toward W75N. Astrophys J 2002;577:260–4.

[425] Bange HW, Williams J. New directions: acetonitrile in atmospheric and. biogeochemical cycles. Atmos Environ 2000;34: 4959–60.

[426] Livesey NJ, Waters JW, Rhosvari R, Brasseur GB, Tyndall TS, Read W. Stratospheric CH₃CN from the UARS microwave limb sounder. Geophys Res Lett 2001;28:779–82.

[427] Livesey NJ, Fromm MD, Waters JW, Manney GL, Santee ML, Read WG. Enhancements in lower stratospheric CH₃CN observed by the upper atmosphere research satellite microwave limb sounder following boreal forest fires. J Geophys Res 2004:109 (Paper No. 10.1029.2003JD004055).

[428] Kleinböhl A, Toon GC, Sen B, Blavier J-F, Weisenstein DK, Wennberg PO. Infrared measurements of atmospheric CH₃CN. Geophys Res Lett 2005;32:L23807, doi:10.1029/2005GL024283 Paper No..

[429] Rinsland CP, Devi VM, Benner DC, Blake TA, Sams RL, Brown LR, et al. Multispectrum analysis of the ν_4 band of CH₃CN: Positions, intensities, self- and N₂-broadening and pressure-induced shifts. J Quant Spectrosc Radiat Transfer 2008;109:974–94.

[430] Colmont JM, Rohart F, Wlodarczak Boyanich JP. K-Dependence and temperature dependence of N₂-, H₂- and He-broadening coefficients for the $J=12–11$ transition of acetonitrile CH₃C^{14}N located near 220.7 GHz. J Mol Spectrosc 2006;238:87–107.

[431] Toon GC. JPL pseudo line list: 〈http://mark4sun.jpl.nasa.gov/data/spec/Pseudo/Readme〉.

[432] Rinsland CP, Sharpe SW, Sams RL. Temperature-dependent infrared absorption cross sections of methyl cyanide (acetonitrile). J Quant Spectrosc Radiat Transfer 2005;96:271–80.

[433] Rinsland CP, Sharpe SW, Sams RL. Temperature-dependent cross-sections in the thermal infrared bands of SF₅CF₃. J Quant Spectrosc Radiat Transfer 2003;82:483–90.

[434] Scientific assessment of ozone depletion, 1988. Global ozone research and monitoring project, report 44. Geneva: World Meteorological Organization; 1999.

[435] Rinsland CP, Devi VM, Blake TA, Sams RL, Sharpe S, Chiou LS. Quantitative measurement of integrated band intensities of benzene vapor in the mid-infrared at 278, 298, and 323 K. J Quant Spectrosc Radiat Transfer 2008;109:2511–22.

[436] Stephens ER, Hanst PL, Doerr RC, Scott WE. Reactions of nitrogen dioxide and organic compounds in air. Ind Eng Chem 1956;48: 1498–504.

[437] Remedios JJ, Allen G, Waterfall AM, Oelhaf H, Kleinert A, Moore DP. Detection of organic compound signatures in infra-red, limb mission spectra observed by the MIPAS-B2 balloon instrument. Atmos Chem Phys 2007;7:1599–613.

[438] Allen G. The infrared remote sensing of peroxyacetyl nitrate in the upper troposphere. PhD thesis. University of Leicester; 2005.

[439] Coheur PF, Herbin H, Clerbaux C, Hurtmans D, Wespes C, Carleer M, et al. ACE-FTS observation of a young biomass burning plume:first reported measurements of C₂H₄, C₃H₆O, H₂CO and PAN by infrared occultation from space. Atmos Chem Phys 2007;7:5437–46.

[440] Allen G, Remedios JJ, Newnham DA, Smith KM, Monks PS. Improved mid-infrared cross-sections for peroxyacetylnitrate (PAN) vapour. Atmos Chem Phys 2005;5:47–56.

[441] Allen G, Remedios JJ, Smith KM. Low temperature mid-infrared cross-sections for peroxyacetyl nitrate (PAN) vapour. Atmos Chem Phys 2005;5:3153–8.

[442] Gaffney JS, Fajer R, Senum GI. An improved procedure for high purity gaseous peroxyacetyl nitrate production: use of heavy lipid solvents. Atmos Environ 1984;18:215–8.

[443] Bruckmann PW, Willner H. Infrared spectroscopic study of peroxyacetyl nitrate (PAN) and its decomposition products. Environ Sci Technol 1983;17:352–7.

444] Wang WF, Stevenson A, Reuter DC, Sirota JM. Absolute band intensities in the ν_{19}/ν_{23} (530 cm^{-1}) and ν_7 (777 cm^{-1}) bands of acetone ((CH₃)₂CO) from 232 to 295 K. Spectrochim Acta Part A 2000;56:1111–6.

[445] Waterfall AM, Remedios JJ, Allen G, Sembhi H. Infrared remote sensing of organic compounds in the upper troposphere. Proceedings of the ENVISAT Symposium 2004. Salzburg, Austria, ESA SP-572, ESA Publications Division, European Space Agency, Noordwijk, The Netherlands; 2004.

[446] Waterfall A. Measurement of organic compounds in the upper troposphere. PhD thesis. University of Oxford; 2003.

[447] Wang WF, Stevenson A, Reuter DC, Sirota JM. Absolute band intensities of acetone ((CH₃)₂CO) in the infrared region of 830–3200 cm^{-1} at low and room temperatures. Spectrochim Acta Part A 2001;57:1603–10.

[448] Orphal J. A critical review of the absorption cross-sections of O₃ and NO₂ in the ultraviolet and visible. J Photochem Photobiol 2003;157:185–209;
Orphal J, Fellows CE, Flaud PM. The visible absorption spectrum of NO₃ measured by high-resolution Fourier transform spectroscopy. J Geophys Res 2003;108:4077, doi:10.1029/2002JD002489.

[449] Vandaele AC, Hermans C, Fally S, Carleer M, Colin R, Mérienne MF, et al. High-resolution Fourier transform measurement of the NO₂ visible and near-infrared absorption cross sections: temperature and pressure effects. J Geophys Res 2002;107:43–8.

[450] Voigt S, Orphal J, Burrows JP. The temperature and pressure dependence of the absorption cross-sections of NO₂ in the 250–800 nm region measured by Fourier-transform spectroscopy. J Photochem Photobiol 2002;149:1–7.

[451] Yoshino K, Esmond JR, Parkinson WH. High-resolution absorption cross section measurements of NO₂ in the UV and visible region. Chem Phys 1997;221:169–74.

[452] Harder JW, Brault JW, Johnston PV, Mount GH. Temperature dependent NO₂ cross sections at high spectral resolution. J Geophys Res D 1997;102:3861–79.

[453] Frost GJ, Goss LM, Vaida V. High resolution UV–VIS absorption cross sections of NO₂ at stratospheric temperatures. J Geophys Res 1996;101:3869–77.

[454] Burrows JP, Richter A, Dehn A, Deters B, Himmelmann S, Voigt S, et al. Atmospheric remote -sensing reference data from GOME-2: temperature-dependent absorption cross sections of O₃ in the 231–7 94 nm range. J Quant Spectrosc Radiat Transfer 1999;61: 509–17.Burrows JP, Dehn A, Deters B, Himmelmann S, Richter A, Voigt S, et al. Atmospheric remote-sensing reference data from GOME: Part 1, temperature-dependent absorption cross-sections of NO₂ in the 231–794 nm range. J Quant Spectrosc Radiat Transfer 1998;60:1025–31.

[455] Bogumil K, Orphal J, Homann T, Voigt S, Spietz P, Fleischmann OC, et al. Measurements of molecular absorption spectra with the SCIAMACHY pre-flight model: instrument characterization and reference data for atmospheric remote-sensing in the 230–2380 nm region. J Photochem Photobiol 2003;157:167–84.

[456] Vandaele AC, De Mazière M, Hermans C, Carleer M, Clerbaux C, Coheur P, et al. UV–visible and near-IR spectroscopy of atmospheric species. Recent Res Devel Chem Phys 2003;4:325–44.

[457] Brion J, Daumont D, Malicet J. New measurements of the absolute absorption cross-sections of ozone at 294 and 223 K in the 310–350 nm spectral range. J Phys (Paris) Lett 1984;45:L57–60;
Brion J, Chakir A, Daumont D, Malicet J, Parisse C. High-resolution laboratory absorption cross section of O₃: temperature effect. Chem Phys Lett 1993;213:610–2;
Daumont D, Brion J, Charbonnier J, Malicet J. Ozone UV spectroscopy I: absorption cross-sections at room temperature. J Atmos Chem 1992;15:145–55;
Brion J, Chakir A, Charbonnier J, Daumont D, Parisse C, Malicet J. Absorption spectra measurements for the ozone molecule in the 350–830 nm region. J Atmos Chem 1998;30:291–9.

[458] Bass AM, Paur RJ. The ultraviolet cross-sections of ozone, Part I, the measurements. In: Zerefos CS, Ghazi A, Reidel D, editors. Atmospheric ozone. MA, USA: Norwell; 1985. p. 606–10; Paur RJ, Bass AM. The ultraviolet cross-sections of ozone, Part II, result and temperature dependence. In: Zerefos CS, Ghazi A, Reidel D, editors. Atmospheric ozone. MA, USA: Norwell; 1985. p. 611–6.

[459] Voigt S, Orphal J, Bogumil K, Burrows JP. The temperature dependence (203–293 K) of the absorption cross sections of O_3 in the 230–850 nm region measured by Fourier-transform spectroscopy. J Photochem Photobiol 2001;143:1–9.

[460] Hamada Y, Merer AJ. Rotational structure at the long wavelength end of the 2900 Å system of SO_2. Can J Phys 1974;52:1443–57.

[461] Hillier IH, Saunders VR. A theoretical interpretation of the bonding, and the photoelectron and ultra-violet spectra of sulphur dioxide. Mol Phys 1971;22:193–201.

[462] Brand JCD, Hardwick JL, Humphrey DR, Hamada Y, Merer AJ. Zeeman effects in the $A^1A_2 \leftarrow A^1A_2$ band system of sulfur dioxide. Can J Phys 1976;54:186–96.

[463] Vandaele AC, Hermans C, Fally S. Fourier Transform measurements of SO_2 absorption cross sections: II, temperature dependence in the 29000–44000 cm^{-1} (227–345 nm) region. J Quant Spectrosc Radiat Transfer 2009;110:2115–26.

[464] Hermans C, Vandaele AC, Fally S. Fourier transform measurements of SO_2 absorption cross sections: I, temperature dependence in the 24000–29000 cm^{-1} (345–420 nm) region. J Quant Spectrosc Radiat Transfer 2009;110:756–65.

[465] Vandaele AC, Simon PC, Guilmot JM, Carleer M, Colin R. SO_2 absorption cross section measurement in the UV using a Fourier transform spectrometer. J Geophys Res 1994;99(D12):25599–605.

[466] Rufus J, Stark G, Smith PL, Pickering JC, Thorne AP. High-resolution photoabsorption cross section measurements of SO_2, 2: 220 to 325 nm at 295 K. J Geophys Res 2003. doi:10.1029/2002JE001931.

[467] Greenblatt GD, Orlando JJ, Burkholder JB, Ravishankara AR. Absorption measurements of oxygen between 330 and 1140 nm. J Geophys Res 1990;95:18577–82.

[468] Newnham DA, Ballard J. Visible absorption cross sections and integrated absorption intensities of molecular oxygen (O_2 and O_4). J Geophys Res 1998;103D:28801–16.

[469] Kromminga H, Orphal J, Spietz P, Voigt S, Burrows JP. New measurements of OClO absorption cross-sections in the 325–435 nm region and their temperature dependence between 213 and 293 K. J Photochem Photobiol 2003;157:149–60.

[470] Wahner A, Tyndall GS, Ravishankara AR. Absorption cross-sections for OClO as a function of temperature in the wavelength range 240–480 nm. J Phys Chem 1987;91:2734–8.

[471] Gratien A, Picquet-Varrault B, Orphal J, Doussin JF, Flaud JM. Laboratory intercomparison of the formaldehyde absorption cross-sections in the infrared (1660–1820 cm^{-1}) and ultraviolet (300–360 nm) spectral regions. J Geophys Res D 2007;112:D05305, doi:10.1029/2006JD007201.

[472] Meller R, Moortgat GK. Temperature dependence of the absorption cross-sections of formaldehyde between 223 and 323 K in the wavelength range 225–375 nm. J Geophys Res 2000;105:7089–101.

[473] Fleischmann OC, Meyer-Arnek J, Burrows JP, Orphal J. The visible absorption spectrum of OBrO, investigated by Fourier transform spectroscopy. J Phys Chem 2005;109:5093–103.

[474] Wilmouth DM, Hanisco TF, Donahue NM, Anderson JG. Fourier transform ultraviolet spectroscopy of the $A^2\Pi_{3/2} \leftarrow X^2\Pi_{1/2}$ transition of BrO. J Phys Chem 1999;103:8935–45.

[475] Fleischmann OC, Burrows JP, Hartmann M, Orphal J. New ultraviolet absorption cross-sections of BrO at atmospheric temperatures measured by time-windowing Fourier transform spectroscopy. J Photochem Photobiol 2004;168:117–32.

[476] Wahner A, Ravishankara AR, Sander SP, Friedl RR. Absorption cross-section of BrO between 312 and 385 nm at 298 and 223 K. Chem Phys Lett 1988;152:507–12.

[477] Yokelson RJ, Burkholder JB, Fox RW, Talukdar RK, Ravishankara AR. Temperature dependence of the NO_3 absorption spectrum. J Phys Chem 1994;98:13144–50.

[478] Gratien A, Lefort M, Picquet-Varrault B, Orphal J, Doussin J-F, Flaud JM. Experimental intercomparison of the absorption cross-sections of nitrous acid (HONO) in the ultraviolet and mid-infrared spectral regions. J Quant Spectrosc Radiat Transfer 2009;110:256–63.

[479] Bongartz A, Kames J, Welter F, Schurath U. Near-UV absorption cross sections and trans/cis equilibrium of nitrous acid. J Phys Chem 1991;95:1076–82.

[480] Stutz J, Kim ES, Platt U, Bruno P, Perrino C, Febo A. UV–visible absorption cross-sections of nitrous acid. J Geophys Res 2000;105:14585–92.

[481] Volkamer R, Spietz P, Burrows JH, Platt U. High-resolution absorption cross-section of glyoxal in the UV/VIS and IR spectral ranges. J Photochem Photobiol 2005;175:35–46.

[482] Spietz P, Gómez Martín JC, Burrows JP. Spectroscopic studies of the I_2/O_3 photochemistry, Part 2: improved spectra of iodine oxides and analysis of the IO absorption spectrum. J Photochem Photobiol 2005;176:50–67.

[483] Himmelmann S, Orphal J, Bovensmann H, Richter A, Ladstätter-Weissenmayer A, Burrows JP. First observation of the OIO molecule by time-resolved flash photolysis absorption spectroscopy. Chem Phys Lett 1996;251:330–4.

[484] Gómez-Martín JC, Spietz P, Burrows JP. Spectroscopic studies of the I_2/O_3 photochemistry: part 1: determination of the absolute absorption cross-sections of iodine oxides of atmospheric relevance. J Photochem Photobiol 2005;176:15–38.

[485] Volkamer R, Etzkorn T, Geyer A, Platt U. Correction of the oxygen interference with UV spectroscopic (DOAS) measurements of monocyclic aromatic hydrocarbons in the atmosphere. Atmos Environ 1998;32:3731–47.

[486] Finlayson-Pitts BJ, Pitts Jr. JN. Tropospheric air pollution: ozone, airborne toxics, polycyclic aromatic hydrocarbons, and particles. Science 1997;276:1045–51.

[487] Bruston P, Khlifi M, Bénilan Y, Raulin F. Laboratory studies of organic chemistry in planetary atmospheres: from simulation experiments to spectroscopic determinations. J Geophys Res 1994;99:19047–62, doi:10.1029/94JE01086.

[488] Fally S, Carleer M, Vandaele AC. UV Fourier transform absorption cross sections of benzene, toluene, meta-, ortho-, and para-xylene. J Quant Spectrosc Radiat Transfer 2009;110:766–82.

[489] Etzkorn T, Klotz B, Sorensen S, Patroescu IV, Barnes I, Becker KH, et al. Gas-phase absorption cross sections of 24 monocyclic aromatic hydrocarbons in the UV and IR spectral ranges. Atmos Environ 1999;33:525–40.

[490] Suto M, Wang X, Shan J, Lee LC. Quantitative photoabsorption and fluorescence spectroscopy of benzene, naphtalene, and some derivatives at 106–295 nm. J Quant Spectrosc Radiat Transfer 1992;48:79–89.

[491] Trost B, Stutz J, Platt U. UV-absorption cross sections of a series of monocyclic aromatic compounds. Atmos Environ 1997;31:3999–4008.

[492] Massie ST. Indices of refraction for the HITRAN compilation. J Quant Spectrosc Radiat Transfer 1994;52:501–13.

[493] Massie ST, Goldman A. The infrared absorption cross-section and refractive-index data in HITRAN. J Quant Spectrosc Radiat Transfer 2003;82:413–28.

[494] Massie ST. NCAR, USA. Private Communication; 2004.

[495] Rublev AN. Algorithms and calculations of aerosol phase functions. Internal note IAE-5715/16 of the Russian Research Center. Kurchatov Institute; 1994. 51 p. (in Russian).

[496] Hess M, Koepke P, Schult I. Optical properties of aerosols and clouds: the software package OPAC. BAMS 1998;79:831–44.

[497] Köpke P, Hess M, Schult I, Shettle EP. Global aerosol dataset. Report no. 243, Max-Plank-Institut für Meteorologie. Hamburg; 1997. 44 p.

[498] Report on the Second International IASI Conference (CNES, EUMETSAT, CNRS/INSU), Sevrier. France; 25–29 January 2010.

[499] Toth RA, Sung K, Brown LR. H_2O line strengths revisited: ν_2 and $2\nu_2 - \nu_2$ at 6 μm. J Mol Spec 2011;265:59–68.

[500] Dubernet ML, Boudon V, Culhane JL, Dimitrijevic MS, Fazliev AZ, Joblin C, et al. Virtual Atomic and Molecular Data Centre. J Quant Spectrosc Radiat Transfer 2010;111:2151–9.